MALDI-MS ANALYSIS OF BIOMARKERS IN PHYTOPLANKTON

Luis Miguel Díaz Sánchez

Chemist, Master in Science

Thesis submitted in partial fulfillment of the requirements for the degree of Doctor of Philosophy in Chemistry

Centro de Estudios e Investigaciones Ambientales-CEIAM

Universidad Industrial de Santander

Facultad de Ciencias

Escuela de Química

Bucaramanga

2025

MALDI-MS ANALYSIS OF BIOMARKERS IN PHYTOPLANKTON

Luis Miguel Díaz Sánchez

Chemist, Master in Science

Thesis submitted in partial fulfillment of the requirements for the degree of Doctor of Philosophy in Chemistry

Advisor:

Marianny Y. Combariza Montañez, Ph.D. in Chemistry

Co-advisor:

Cristian Blanco Tirado, Ph.D. in Chemistry

Centro de Estudios e Investigaciones Ambientales-CEIAM

Universidad Industrial de Santander

Facultad de Ciencias

Escuela de Química

2025

TABLE OF CONTENTS **Pag**

LIST OF FIGURES

detected in the phytoplankton sample collected in June at Boca de La Barra, using MALDI FT-ICR MS. Colors indicate different compound classes. Inset shows two toxins that vary in -CH_2 in their structures and derivatives of anatoxin ($C_{11}H_{17}NO$) that vary by one oxygen atom.

LIST OF TABLES

LIST OF APPENDIXES

ABSTRACT

Title: MALDI-MS ANALYSIS OF BIOMARKERS IN PHYTOPLANKTON

Author: Luis Miguel Díaz Sánchez, Chemist, MSc

Keywords: Photoprotective pigments; Photosynthetic pigments; Microalgae; Chlorophylls; Carotenoids; Toxins; Cyanobacteria; Electron transfer ionization; Matrix-assisted laser desorption/ionization; MALDI; Mass spectrometry; Ultra-high-resolution; FT-ICR MS.

Phytoplankton, a group of autotrophic aquatic microorganisms, plays a crucial role in marine and freshwater ecosystems by fixing nearly 40% of atmospheric CO_2 and generating a significant portion of the Earth's molecular oxygen. These communities are fundamental to both the carbon cycle and the aquatic food web, making their monitoring essential for assessing ecosystem health and the availability of food at higher trophic levels.

While established methods exist for analyzing phytoplankton extracts, many studies agree that lengthy analytical procedures can lead to biomarker degradation, failure to detect compounds present in low concentrations, and co-elution of compounds in separation techniques such as chromatography. This doctoral thesis addressed these issues by utilizing electron transfer (ET) processes in MALDI mass spectrometry. ET processes in MALDI ensure the survival of gas-phase molecular ions of labile and thermally unstable molecules with low ionization energy (Ei) values, compared to the Ei of the matrix used (DCTB, Ei: 8.54 eV), such as chlorophyll- and carotenoid-type pigments (Ei: 6.2 – 7.2 eV), which serve as phytoplankton biomarkers.

The research developed a methodology for analyzing pigments in phytoplankton extracts using ET-MALDI-MS. This method allows for efficient biomarker detection in a significantly shorter time, reducing data acquisition from approximately 60 minutes to just a few seconds while also lowering solvent consumption compared to established techniques such as HPLC.

Additionally, the study examined the influence of extraction techniques on the pigment profile obtained via MALDI-MS, evaluating intact cells and isolated chloroplasts from model microalgae, as well as extracts obtained with different polarities. It was found that the MALDI methodology enables the measurement of the phytoplankton pigment profile even without prior treatment. This not only provides a more efficient and sensitive approach but also opens possibilities for chemotaxonomic identification and biomarker monitoring in aquatic ecosystems, contributing to their understanding and conservation.

The research also investigated the impact of different mass analyzers (TOF and 21-Tesla FT-ICR) on the pigment profile of the model microalga Chlorella vulgaris. According to the scientific literature reviewed, this is the first report of C. vulgaris pigments using ultra-high-resolution (UHR) FT-ICR MS. Experiments with 21T FT-ICR allowed for the identification of all ionizable species present in the sample. A total of 2,992 different compounds were identified, highlighting nitrogenated species N4Oo (o=0-6) and oxygenated species Oo (o=2-7), which were attributed to the presence of chlorophylls, carotenoids, and lipids in the cells.

Finally, the doctoral thesis evaluated the effectiveness of the MALDI-MS methodology for identifying biomarkers in real phytoplankton samples collected from the Ciénaga Grande de Santa Marta (CGSM). The study included samples from different sampling stations and seasons, allowing for a broad evaluation of molecular composition in freshwater environments and connection points with the Caribbean Sea. The use of MALDI-MS enabled the identification of

specific biomarkers correlated with oceanographic variables measured at the sampling points and the detection of cyanotoxins such as anabaenopeptins and micropeptins, characteristic of Anabaena and Microcystis cyanobacteria, previously reported in the CGSM through taxonomic analysis. Phytoplankton pigment profiles provide valuable insights into community adaptation to environmental changes, offering a robust tool for environmental monitoring and contributing to the sustainable management of aquatic ecosystems.

RESUMEN

Título: ANÁLISIS MALDI-MS DE BIOMARCADORES EN FITOPLANCTON

Autor: Luis Miguel Díaz Sánchez, Químico, MSc

Palabras clave: Pigmentos fotoprotectores; Pigmentos fotosintéticos; Microalgas; Clorofilas; Carotenoides; Toxinas; Cianobacterias; Ionización por transferencia de electrones; Desorción-ionización láser asistida por matriz; MALDI; Espectrometría de masas; Ultra-Alta-Resolución; FT-ICR MS.

El fitoplancton, conjunto de microorganismos acuáticos autótrofos, desempeña un papel crucial en los ecosistemas marinos y de agua dulce al fijar casi el 40% del CO_2 atmosférico y generar gran parte del oxígeno molecular terrestre. Estas comunidades son fundamentales tanto para el ciclo del carbono como para la red trófica acuática, y su monitoreo es esencial para evaluar la salud de los ecosistemas y la disponibilidad de alimento en los niveles tróficos superiores.
Si bien existen métodos establecidos para analizar extractos de fitoplancton, muchos estudios concuerdan que los largos procedimientos analíticos pueden provocar la descomposición de los biomarcadores, la no detección de compuestos presentes en bajas concentraciones y la co-elución de compuestos en técnicas se separación como la cromatografía. La tesis doctoral abordó estos problemas mediante el uso de procesos de transferencia electrónica (ET) en espectrometría de masas MALDI. Los procesos de ET en MALDI garantizan la sobrevivencia de los iones moleculares en fase gaseosa de moléculas lábiles y termoinestables con bajos valores de energía de ionización, comparados con la Ei de la matriz empleada (DCTB, Ei: 8.54 eV) como pigmentos de tipo clorofila y carotenoide (Ei: 6.2 – 7.2 eV), biomarcadores de fitoplancton.
En la investigación se desarrolló una metodología para analizar pigmentos en extractos de fitoplancton utilizando ET-MALDI-MS. Este método permite la detección eficiente de biomarcadores en un tiempo significativamente más corto, de ca., 60 min a tan solo unos segundos para la toma de datos y con un menor consumo de solventes en comparación con técnicas establecidas como HPLC.

Además, se determinó la influencia de las técnicas de extracción sobre el perfil pigmentario obtenido en MALDI-MS, evaluando células intactas y cloroplastos aislados de microalgas modelo, junto con extractos obtenidos con diferente polaridad. Se encontró que la metodología MALDI permite medir el perfil pigmentario de las células de fitoplancton incluso sin tratamiento previo. Esto no solo ofrece un enfoque más eficiente y sensible, sino que también abre posibilidades para la identificación quimiotaxonómica y el monitoreo de biomarcadores en ecosistemas acuáticos, contribuyendo a su comprensión y conservación.

La investigación también estudió la influencia de distintos analizadores de masas (TOF y FT-ICR de 21 Teslas) sobre el perfil de pigmentos de la microalga modelo Chorella vulgaris. De acuerdo con la bibliografía científica consultada, este es el primer reporte de pigmentos de C. vulgaris mediante ultra alta resolución (UHR) FT-ICR MS. Los experimentos con 21T FT-ICR permitieron identificar todas las especies ionizables presentes en la muestra. Se identificaron 2992 compuestos diferentes, destacándose especies nitrogenadas N4Oo (o=0-6) y oxigenadas Oo (o=2-7), atribuidas a la presencia clorofilas, carotenoides y lípidos en las células.

Finalmente, la tesis doctoral evaluó la eficacia de la metodología MALDI-MS para identificar biomarcadores en muestras reales de fitoplancton colectadas en la Ciénaga Grande de Santa Marta (CGSM). La investigación incluyó muestras de diferentes estaciones de muestreo y epocas del año, permitiendo una evaluación amplia de la composición molecular en entornos de agua dulce y puntos de conexión con el mar Caribe. El uso de MALDI-MS permitió identificar

biomarcadores específicos que fueron correlacionados con las variables oceanográficas medidas en los puntos de muestro, y detectar cianotoxinas como anabaenopeptinas y micropeptinas, propias de cianobacterias Anabaena y Microcystis, reportadas previamente en la CGSM mediante análisis taxonómico. Los perfiles pigmentarios del fitoplancton brindan información valiosa sobre la adaptación de sus comunidades a cambios ambientales, proporcionando una herramienta robusta para el monitoreo ambiental y contribuyendo a la gestión sostenible de ecosistemas acuáticos.

INTRODUCTION

Phytoplankton comprises a multitude of microorganisms deemed as primary producers in marine and freshwater environments. These organisms, integral to the aquatic food web, serve as a biological pump, fixing nearly 40% of atmospheric CO_2 and generating a substantial portion of terrestrial molecular oxygen. Monitoring phytoplankton biomass in water bodies worldwide provides insight into food availability for secondary and tertiary consumers. Typically, this monitoring involves optical microscopy, taxonomic key-based identification, and chemotaxonomy relying on specific or general pigments unique to each microorganism species. Chlorophylls and carotenoids, commonly used for phytoplankton monitoring, possess molecular structures capable of capturing solar energy. Some of these pigments are indicative of particular phytoplanktonic microorganisms. Characterizing these pigments conventionally involves chromatographic separations and UV-Vis spectroscopy analysis, entailing extensive sample preparation, solvent consumption, and time. However, direct, and detailed molecular characterization of phytoplankton pigments without chromatography remains limited.

Matrix-Assisted Laser Desorption/Ionization (MALDI), introduced in 1989 by professors Michael Karas and Franz Hillenkamp, emerged as a robust tool for analyzing non-volatile, labile, and high molecular weight compounds like polymers, proteins, oligosaccharides, peptides, and amino acids. Its versatility extends to analyzing labile and thermally unstable compounds of moderate to low molecular weight due to its soft ionization mechanism. MALDI's analytical flexibility lies in utilizing various matrices—organic and inorganic—that control ionization pathways, enhancing selectivity with target compounds. Ionization in MALDI occurs through proton or cation transfer reactions between the analyte and the matrix, as well as secondary electron-transfer (ET) reactions from neutral analytes to the matrix's primary ions. Proton or cation transfer reactions yield ions like $[A + M]^+$ or $[A - H]^-$, where M can be H^+, Na^+, K^+, Ag^+, among others, while charge-transfer reactions predominantly produce radical species like $[M]^{+\bullet}$ and $[M]^{-\bullet}$. Fig. 1 shows a general scheme of the doctoral thesis.

Chapter 1 presents a methodology for pigment analysis from microalgae/phytoplankton extracts using electron-transfer Matrix-Assisted Laser Desorption Ionization Mass Spectrometry (ET MALDI MS). Traditional pigment analysis methods are resource -and time- intensive due to the broad polarity range of target analytes. ET MALDI MS offers a rapid screening alternative for detecting pigments in microalgae extracts. Results obtained from ET MALDI MS were compared with those from traditional techniques such as HPLC analysis of pigment extracts and optical microscopy analysis of phytoplankton samples.

Chapter 2 explores the molecular composition of microalgal *Chlorella vulgaris* by comparing pigment profiles obtained through MALDI-MS of *C. vulgaris* cells, extracts, and intact chloroplasts. Utilizing ultrasound-assisted and supercritical fluid extraction methods, comprehensive extracts rich in polar and non-polar compounds were obtained. MALDI-MS reveals distinct compositional differences, emphasizing the impact of extraction protocols on microalgal pigment identification. Additionally, MALDI enables the identification of specific lipids within chloroplast membranes and other organelles of microalgae.

Chapter 3 investigates the influence of different mass analyzers, specifically Time-of-Flight (TOF) and 21-Tesla Fourier Transform Ion Cyclotron Resonance (FT-ICR), on MALDI pigment profiling of microalgae *C. vulgaris* extracts. The study assesses mass accuracy, isotopic patterns, and the number of detected signals with each analyzer. While MALDI TOF enables accurate molecular assignments, FT-ICR offers a comprehensive characterization of ionizable species, making it promising for identifying new biomarkers in microalgae.

Chapter 4 evaluates the MALDI MS methodology's efficacy in detecting pigment biomarkers of microalgae/phytoplankton in real samples collected from the Ciénaga Grande de Santa Marta (CGSM) in collaboration with the technical team of the Instituto de Investigaciones Marinas y Costeras José Benito Vives de Andréis (INVEMAR). Samples were collected from contrasting points within CGSM during different seasons, allowing for a comprehensive assessment of molecular composition in both freshwater and Caribbean-connected environments. Understanding these pigments and biomarkers is crucial for deciphering ecological roles and physiological responses of phytoplankton communities to environmental changes, offering insights for conservation and sustainable management.

Finally, chapters 5 and 6 provide general conclusions of the research and offer some recommendations for future studies, respectively. Chapter 5 summarizes the key findings and insights gained from the analysis conducted in preceding chapters, while chapter 6 outlines potential avenues for further research to build upon the current study's findings and address some remaining questions or areas for exploration.

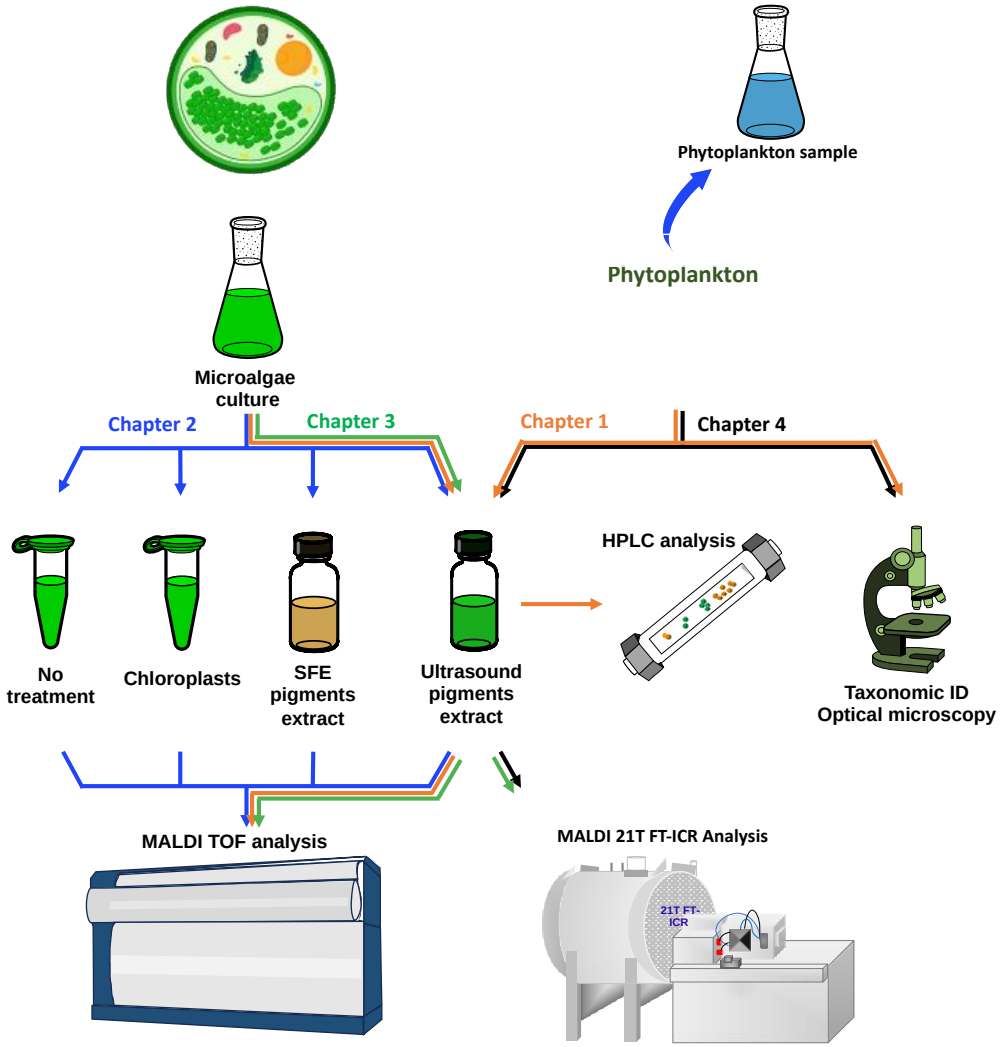

Fig. 1 General scheme of the doctoral thesis.

Chapter 1.

Electron-transfer MALDI MS methodology for microalgae/phytoplankton pigments analysis

Edited from: Luis M. Díaz-Sánchez, Cristian Blanco-Tirado, Marianny Y. Combariza, MethodsX. 10. 2023. 102140. (https://doi.org/10.1016/j.mex.2023.102140).

Keywords
Photoprotective pigments; Photosynthetic pigments; Microalgae; Chlorophylls; Carotenoids; Electron transfer ionization; Matrix Assisted Laser Desorption Ionization; MALDI; Mass Spectrometry.

Abstract
The method describes pigment analysis from microalgae/phytoplankton extracts using electron-transfer Matrix-Assisted Laser Desorption Ionization Mass Spectrometry (ET MALDI MS). Current microalgae/phytoplankton pigment analysis requires resource- and time-intensive chromatographic methods due to the broad polarity range of the target analytes. On the other hand, traditional MALDI MS chlorophyll analysis, using proton-transfer matrices such as 2,5-dihydroxybenzoic acid (DHB) or α-cyano-4-hydroxycinnamic acid (CHCA), results in central metal loss and phytol–ester cleavage. ET MALDI MS is an alternative for the rapid screening and detection of pigments in microalgae extracts.

- MALDI matrices with ionization energies above 8.0 eV guarantee electron-transfer processes from photosynthetic and photoprotective pigments whose ionization energies lay below 7.5 eV.
- ET MALDI MS pigment analysis agrees with data gathered from conventional chromatographic techniques (HPLC) and optical microscopy for pigment extracts from *C. vulgaris* cultures and freshwater phytoplankton samples.
- The ET MALDI MS method allows fast and reliable detection of pigments in microalgae cultures and freshwater phytoplankton samples.

Graphical abstract

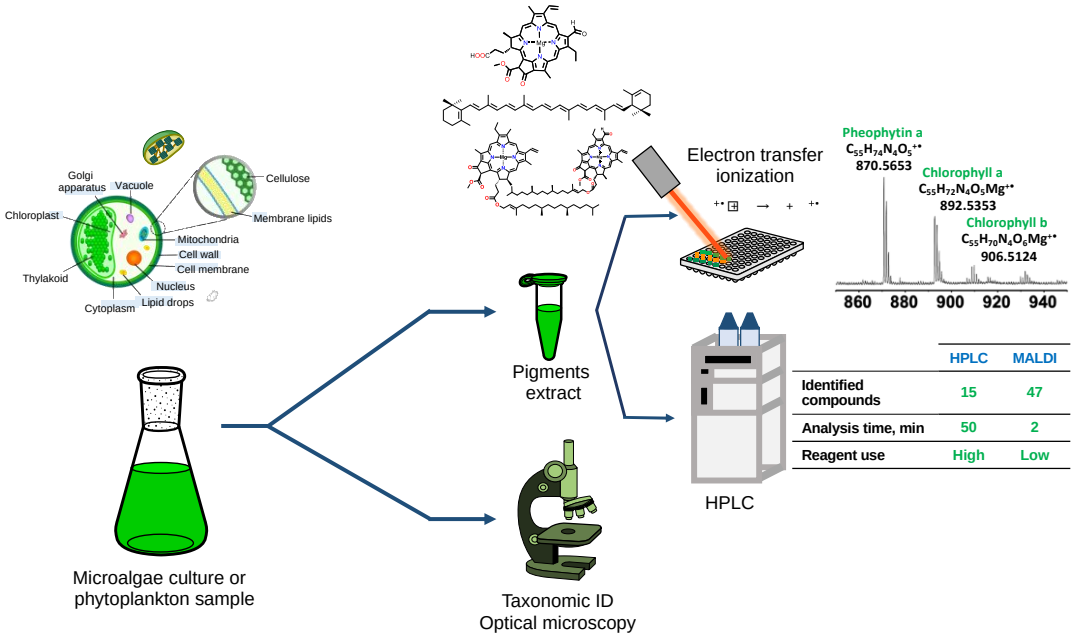

Specifications table

Subject area	Chemistry.
More specific subject area	*Pigment analysis by Electron-Transfer MALDI MS.*
Name of your method	*Electron-transfer MALDI MS methodology for microalgae pigments analysis.*
Name and reference of original method	*N/A.*
Resource availability	*Flexcontrol manual (Software used for data collection)* *https://researchservices.pitt.edu/sites/default/files/flexControl%20User%20Manual.pdf* *Flexanalysis manual (Software used for data analysis)* *https://researchservices.pitt.edu/sites/default/files/flexAnalysis%20User%20Manual.pdf* *Certified standards* *https://c14.dhigroup.com/productdescriptions/mixedphytoplanktonpigments* *https://c14.dhigroup.com/productdescriptions/phytoplanktonpigmentstandards*

Method details

Chlorella vulgaris culturing and freshwater phytoplankton sampling

1 The handling and manipulation of *Chlorella vulgaris* cultures and freshwater phytoplankton samples should be carried out in a laminar flow hood (Class-2 Biohazard safety cabinet, BSL-2) to avoid bacterial and fungi contamination.

2 *Chlorella vulgaris* were cultured under intermittent lighting (12 V white LED, 12 h of light, and 12 h of darkness) using the BBM medium. The process starts with $1.4x10^6$ cells/mL in 100 mL of culture medium (Fig 1).

3 Freshwater samples -for phytoplankton isolation- were collected using a bottle sampler by gently scooping surface water from a shallow artificial lake located on the main campus of the Universidad Industrial de Santander, Bucaramanga, Colombia (7°8'28.271'' N, 73°7'14.731'' W, 1009 mamsl).

4 *Chlorella vulgaris* and phytoplankton, from culture media and freshwater samples, were collected in 50 mL sterile Falcon tubes filled to 3/4 with the liquid samples. The samples were centrifuged at 8000 rpm, at 4 ºC, for 15 min (avoid tightly closing the Falcon tube lid), the supernatant was discarded, and the resulting pellet -containing biomass- was stored at -80 ºC until extraction (Fig 1). At this point, it is advisable to divide the pellet into several small fractions - and individually store them in amber vials- to avoid thawing the whole pellet when minute samples are required for pigment extraction.

Microscopy analysis

1 Optical microscopy analysis of phytoplankton and *Chlorella vulgaris* cells was performed on an OLYMPUS BX53 optical microscope. Place a 10 µL aliquot of *Chlorella vulgaris* culture or phytoplankton sample on a glass microscope slide previously cleaned with isopropyl alcohol and dried at room temperature.

2 Place a clean and dry coverslip over the liquid sample. Set the slide on the microscope stage and secure it with the stage clips. The sample is ready to observe using a 10x eyepiece and a 40x objective. Microorganisms found in the samples can be photographed with a Canon Professional Digital EOS 5DSR camera in an autofocus setting.

Pigment extraction protocol

1 The microalgae/phytoplankton biomass pellets manipulation should be performed in amber vials under a fume hood with dimmed light to avoid pigment photooxidation.

2 Weigh 2 mg of a previously thawed microalgae/phytoplankton pellet in a 1.5 mL amber vial and add 1 mL of analytical grade acetone at room temperature (avoid thawing large amounts of biomass).

3 Cell lysis was performed under ultrasonic radiation using an ultrasound bath (40 kHz, Branson Ultrasonics™ CPX, Danbury, CT, USA) for 25 min. Cell lysis time depends on microorganism type [1], [2] (Fig 1).

4 Filter the extraction mixture using a 0.45 µm PTFE membrane filter. Store the liquid extracts in amber vials below 4 ºC until analysis. It is preferable to perform the analysis immediately after the extraction to avoid pigment decomposition.

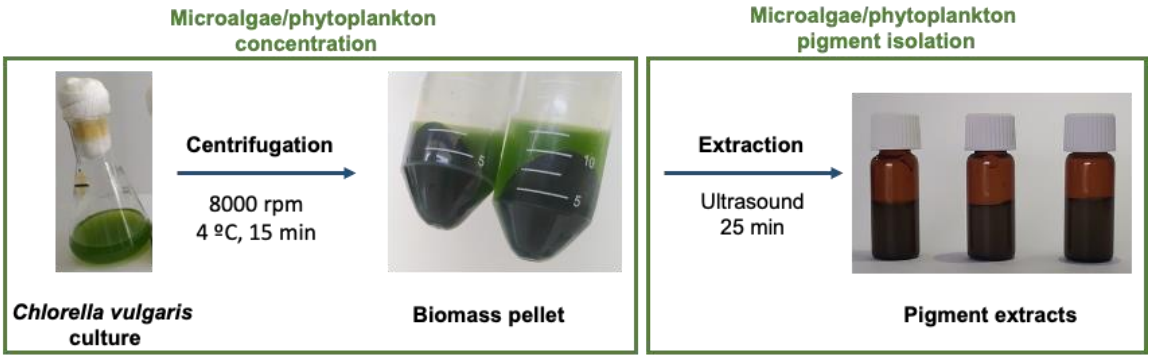

Figure 1. Microalgae/phytoplankton concentration and pigment extraction.

Electron-transfer Matrix-Assisted Laser Desorption Ionization (ET MALDI MS)

1 Prepare a 4 mM (1 mg) solution of *trans*-2-[3-(4-tert-butylphenyl)-2-methyl-2-propenylidene] malononitrile (DCTB), MALDI matrix Sigma-Aldrich (St Louis-MO) in 1 mL of acetonitrile (ACN gradient grade for HPLC). If necessary, use an ultrasound bath -for two minutes- to completely dissolve the solid (40 kHz, Branson UltrasonicsTM CPX, Danbury, CT, USA).

2 Prepare a calibration sample using a pigment standard (chlorophyll a, chlorophyll b, **β**-carotene, diadinoxanthin, and astaxanthin) and the MALDI matrix solution to reach an analyte-to-matrix (A:M) ratio of 1:1000. Use a vortex at 1000 rpm for two minutes to ensure proper mixing. The standard was purchased from DHI (Horsholm, Denmark) with known amounts of individual pigments.

3 Mix the *Chlorella vulgaris*/phytoplankton pigment extracts with the MALDI matrix solution using a vortex at 1000 rpm as described above to reach an A:M ratio of 1:1000. The ratio was calculated using literature reports of chlorophyll-a concentration in *Chlorella vulgaris*. Alternatively, an approximate chlorophyll-a concentration can be derived using UV-vis measurements [3].

4 Using the dried droplet method, seed the mixture (1 µL) on a polished steel MALDI target at room temperature and allow it to dry. Place at least three spots per sample to improve data reproducibility and reduce sample-to-sample variations due to sweet spots. Also, we recommend using only freshly prepared matrix solutions for the MALDI experiments. Test the matrix purity and stability by taking an LDI spectrum before performing any MALDI experiments. Purify the matrix, by recrystallization or sublimation, in case of degradation.

5 Prepare a saturated solution of **α**-cyano-4-hydroxycinnamic acid (**α**-CHCA) in 30:70 v/v acetonitrile: 0.1% trifluoroacetic acid (TFA) in water. Prepare a 200 ppb solution of standard peptides (leu-enkephalin, bradykinin, bombesin, and renin substrate) in water, mixing with a vortex at 1000 rpm for one minute. Mix the two solutions prepared above in 1:1 v/v proportions, and deposit 1 µL of the mixture on a polished steel MALDI target. Run at least five spots of the calibrants to improve data reproducibility and reduce sample-to-sample variations due to sweet spots.

6 Insert the polished steel MALDI target in the ionization source of an Ultraflextreme MALDI-TOF/TOF mass spectrometer (Bruker Daltonics, Billerica, MA, USA). Wait until the source reaches a working pressure (set point: 3.0x10-6 mbar). Start by analyzing the calibration mixture using the following conditions (note that these conditions may vary depending on instrument type and years of use, particularly parameters related to the laser energy-per-pulse): PIE (pulsed ion extraction) 100 ns, laser spot size 100 µm, laser attenuation 40%, laser frequency 1000 s-1, source voltage 20 kV. Accumulate a total of 3000 spectra corresponding to three shots per spot. The TOF mass analyzer was operated in reflectron mode (25 kV).

7 The laser energy per pulse was varied from 0.15 to 2.74 μJ using the instrument's attenuation setting. The actual laser's energy output was measured using a PowerMax-USB UV/Vis Wand (Coherent, Santa Clara, USA); all laser energy-per-pulse measurements were performed in triplicate. However, if there is no means of measuring the laser energy-per-pulse, use the instrument attenuation setting to obtain reproducible signals with high S/N ratios and resolution. Use the following α-CHCA related ions for calibrating the spectrum low mass region: $[M + H]^+$ at *m/z* 190.04987, $[M + Na]^+$ at *m/z* 212.03181, $[2M + H]^+$ at *m/z* 379.09246, $[2M + Na]^+$ at *m/z* 401.07048, and $[3M + H]^+$ at *m/z* 568.13506. Use the $[M + H]^+$ peptide signals at *m/z* 556.27657, 1060.56868, 1619.82234, and 1758.93260 for leu-enkephalin, bradykinin, bombesin, and renin substrate, respectively, to calibrate the medium and high mass range. Note that pigments are low-molecular-weight metabolites by MALDI-TOF standards; thus, the mass range for the MS method should be set to *m/z* 3000.

8 Calibrate the instrument using the standard internal calibration protocol (see Resource availability section, FlexControl 3.4 User Manual section 3.7.6). Once internal calibration was performed, start running the pigment standards and the pigment extracts using the same conditions described above for the calibration samples. If necessary, adjust (increase or decrease) the laser attenuation to improve signal descriptors (abundance/relative intensity, S/N, resolution). Check the signal abundance in different parts of the spot (you can use the auto setting in the instrument). We recommend building a table including expected charged species such as chlorophyll a ($C_{55}H_{72}O_5N_4Mg$, $M^{+\bullet}$ *m/z* 892.5353), chlorophyll b ($C_{55}H_{70}O_6N_4Mg$, $M^{+\bullet}$ *m/z* 906.5145), and derivatives such as pheophytin a ($C_{55}H_{74}N_4O_5$, $M^{+\bullet}$ *m/z* 870.5659), chlorophyllide a ($C_{35}H_{34}N_4O_5Mg$, $M^{+\bullet}$ *m/z* 614.2379), and chlorophyllide b ($C_{35}H_{32}N_4O_6Mg$, $M^{+\bullet}$ *m/z* 628.2172), and the MALDI matrix DCTB ($C_{17}H_{18}N_2$, $M^{+\bullet}$ *m/z* 250.1470). See Table 1 for an example.

Table 1. Suggested pigment signals for checking instrument calibration and sample behavior.

Peak label	Ref *m/z*
Chlorophyll a, $M^{+\bullet}$	892.53531
Chlorophyll b, $M^{+\bullet}$	906.51457
Pheophytin a, $M^{+\bullet}$	870.56592
Chlorophyllide a, $M^{+\bullet}$	614.23796
Chlorophyllide b, $M^{+\bullet}$	628.21722
DCTB, $M^{+\bullet}$	250.14700

Beware: DCTB is primarily an electron-transfer matrix: thus, radial cations are the species expected in the MALDI experiment. However, DCTB has an acidic b-H and can produce protonated molecules even when using aprotic solvents for sample preparation.

9 Store the data using a consecutive code; these files can be used, compressed, or exported for data processing.

10 Data analysis was performed using the Flex Analysis software (Bruker Daltonics, Billerica MA, USA). After external calibration, use the peak finding setting for an automatic report of ion abundances, S/N ratios, resolution, peak area, and monoisotopic masses. Mass spectra were not smoothed, or baseline corrected before analysis.

11 Pigment identification involved comparing the *m/z* values of the signals detected in the extracts to the standard mixture of pigments and a database previously built by our research group from literature reports of pigments identified in microalgae using other analytical techniques. Furthermore, experimental, and theoretical isotope patterns, calculated with ChemCalc [4], were compared to verify compound identification. Establishing a minimum

relative intensity threshold (0.01%) for assigning signals in the mass spectrum is suggested. The mass spectra were plotted in Origin Pro 9.0 64-bit.

Method validation

Optical microscopy analysis of Chlorella vulgaris cultures and freshwater phytoplankton.

Chlorella's studies-initiated algae research in the 1950s. *Chlorella vulgaris* is a green, spherical (2-10 μm), unicellular microalgae belonging to the *Chlorellaceae* family, *Chlorophyta* taxon. Commonly found in freshwater, *C vulgaris* has a high nutritional value due to its pigments (chlorophyll and carotenoid, 1-2 wt%) and protein (42-58 wt%) contents [5]. In addition, *Chlorella vulgaris* presents an interesting lipid composition (structural and signaling lipids) ranging between 5 and 40 wt% depending on the medium and culture conditions such as pH, temperature, nutrient availability, and light exposure. Figure 2A shows an optical microscopy image of *Chlorella vulgaris* cells. We observe *Chlorella vulgaris* as spherical cells with diameters from 5 to 10 μm, a nucleus of about 2.1 μm, and a chloroplast occupying a third or, in some cases, half of the cell. The morphological characteristics reported above agree with previous literature reports [5], [6]. *C. vulgaris* cells are much smaller than other phytoplankton microalgae, such as the ones in Figure 2B.

On the other hand, phytoplankton is a diverse community of autotrophic organisms that live in freshwater and marine bodies. There is a consensus that phytoplankton communities are composed of eukaryotic algae, such as diatoms, dinoflagellates, and prokaryotic cyanobacteria. Phytoplankton communities are the first link in the trophic chains that make up aquatic ecosystems and serve as food for primary consumers such as zooplankton [2], [7], [8]. The photosynthetic organisms of phytoplankton are biological pumps that capture up to 40% of atmospheric CO_2, fixing inorganic carbon in the form of organic matter. Additionally, because of photosynthetic reactions, more than 50% of atmospheric oxygen is produced by phytoplankton [9]–[11]. Due to the fundamental role of these organisms in the carbon, water, and oxygen cycles, monitoring their activity and composition is vital in oceanographic, ecosystemic, and climate change studies. We identified seven specimens in freshwater phytoplankton samples using morphological observations from optical microscopy and taxonomic keys available in the literature [12]–[14]. Four specimens were identified up to the genus taxonomic level and the other three up to subclass (*Bacillariophycidae* and *Fragilariophycidae* subclasses). The identified species were *Phacus salinus* cf., *Tetradesmus lagerheimii* cf., *Stauridium tetras* cf., and *Pediastrum duplex* cf. Figure 2B show optical microscopy images of some of the observed specimens.

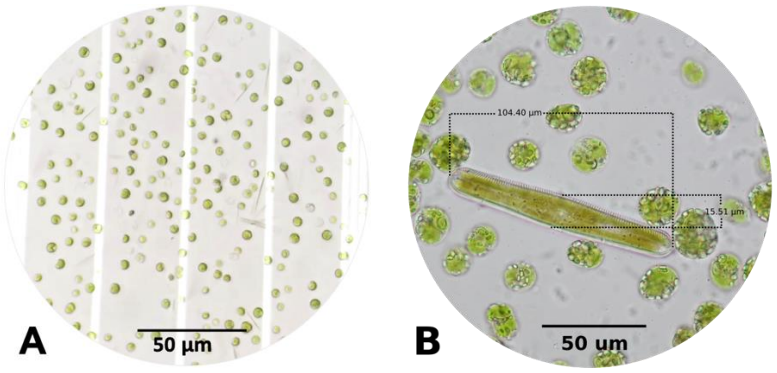

Figure 2. Optical *microscopy* of microalgae/phytoplanktonic species in liquid samples*,* magnification *1000x*. **A**-*Chlorella vulgaris* cells in BBM culture media. **B**-Specimen of the genus *Phacus*, with a clear eyespot and a conical tail, and specimen of diatom *Bacillariophyceae* subclass showing the frustule: a rigid cell wall made of opaline silica characteristic of diatoms**.**

HPLC analysis of pigment standards and phytoplankton pigment extracts

HPLC is the "gold standard" employed to perform chemotaxonomical analysis of phytoplankton populations using pigments as biomarkers [15]–[17]. Qualitative and quantitative HPLC data is used, together with oceanographic/aquatic variables such as dissolved oxygen, temperature, pH, salinity, and conductivity, to feed algorithms that allow estimating phytoplankton class abundances from chemical markers.

We performed HPLC analysis of pigment standards and microalgae pigment extracts using the method reported by Heukelem et al. [15]. The pigment standard sample, used as a reference compound to identify pigments in freshwater phytoplankton extracts, contains chlorophyll a, chlorophyll b, **β**-carotene, diadinoxanthin, and astaxanthin. In short, an Eclipse XD8 C18 column (150 × 3.9 mm) was used for pigment separation with gradient elution involving solution A (0.001% formic acid in H_2O) and solution B (0.001% formic acid in MeOH) at a flow rate of 1 mL·min−1 as follows: 0–0.5 min, 95% B; 0.5–3.00 min, 95%–100% B; 3.00–50.00 min, 100% B. Colum equilibration, before sample injection, was achieved by flushing with MeOH for 15 min and pigment detection was performed using a DAD (λ= 450 nm). Figure 3 shows the chromatographic trace and identity of the pigments in the freshwater phytoplankton sample.

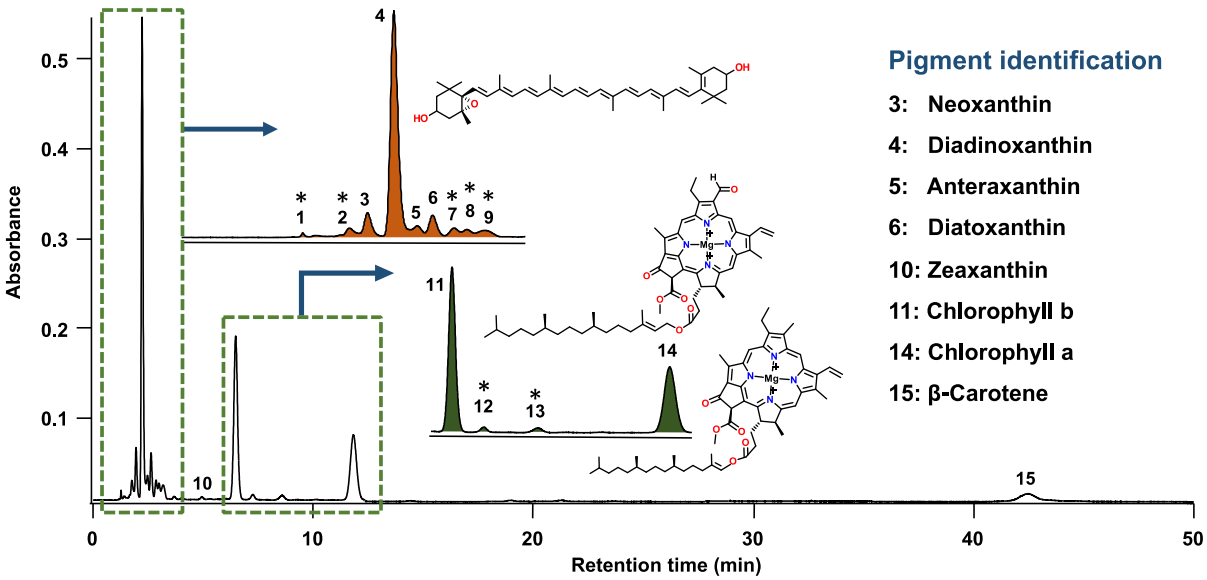

Figure 3. HPLC chromatogram of the pigments extracted from a freshwater phytoplankton sample. Eclipse XD8 C18 column (150 × 3.9 mm). Peaks marked with an asterisk (*) were not identified.

Four of fifteen signals detected in the phytoplankton pigment sample were identified using certified standards (diadinoxanthin, chlorophyll a, chlorophyll b, and **β**-carotene), and four by comparison with retention times reported in the literature (neoxanthin, antheraxanthin, diatoxanthin and zeaxanthin). The remaining chromatographic peaks were not identified; however, with lower retention times than chlorophyll a and b, these may correspond to polar derivatives, e.g., chlorophyllide and pheophorbide. The results shown in Figure 3 are consistent with Brotas & Plante-Cuny [18], who reported the presence of diadinoxanthin, antheraxanthin, and diatoxanthin, in methanolic extracts of *Euglena* sp grown under controlled conditions of temperature and sunlight. *Euglena* sp. is a microalga typically found in freshwater. The authors also reported chlorophyllide b and pheophytin b in *Euglena* sp. Additionally, other authors have identified carotenoid pigments such as neoxanthin, diadinoxanthin, diatoxanthin, α-carotene, and β-carotene in freshwater microalgae, *e.g.*, *Euglena gracilis* [11], [19]. In this work, we identified neoxanthin, diadinoxanthin, diatoxanthin, and β-carotene by HPLC.

Regarding analytical resources, the pigment extract HPLC analysis took over 50 minutes, from running the standard mix to assigning individual retention times. Also, the volume of solvents used in the HPLC analysis was close to 60 mL per sample after column and detector stabilization. These facts highlight the resources required for analyzing a phytoplankton pigment extract by HPLC. However, despite the operational costs involved in HPLC analysis, separating all pigments in the mixture remains an analytical challenge.

ET MALDI MS analysis of a pigment standard and microalgae/phytoplankton pigment extracts

Several charging schemes are viable in MALDI MS. Proton transfer/abstraction and cation exchanges are typically used for biomolecule analysis. However, using proton-transfer matrices like **α**-CHCA, 2,5-DHB, and SA is not recommended for pigment analysis because acid matrices provoke chlorophyll demetallation and phytol hydrolysis [20]. On the other hand, electron transfer (ET) in MALDI MS is predominantly used in material analysis applications where proton or cation exchanges are challenging [21]. ET begins with the formation of primary matrix ions through a "pooling" mechanism - as described in the CPCD model (Coupled Physical and Chemical Dynamics) [22], [23]. Once formed, the matrix ions ($M^{+\bullet}$) can abstract an electron from

a neutral analyte (A) to form a secondary ion ($A^{+\bullet}$). This reaction is only possible if the analyte ionization energy $E_{i(A)}$ is lower than the matrix $E_{i(M)}$ [24]–[26]. The ET reactions proceed according to the following mechanism:

$$M + nhv \rightarrow M^{+\bullet}$$
$$M^{+\bullet} + A \rightarrow M + A^{+\bullet}$$
$$E_{i(Matrix)} > E_{i(Analyte)} \therefore \Delta E_i > 0.5\ eV$$

Previously, various researchers reported using the ET MALDI approach to detect chlorin-type pigments such as bacteriochlorophyll a, chlorophyll a, and carotenoids in microorganisms and food. For these analyses DAN and DCTB exhibited the best performance as ET matrices [27]–[29]. During the method development we also tested **α**-cyanophenylenevinylenes (**α**-CNPVs) derivatives, reported by our research group as efficient ET-MALDI matrices for nanoparticle, polymer, petroporphyrin, and fullerene analysis [30]–[33]. Unlike DCTB, **α**-CNPVs exhibit high vacuum stability meaning a low vapor pressure under the MALDI source conditions, which is an advantage for imaging applications. However, we observed that the vacuum instability of DCTB is beneficial for intact chlorophyll desorption since a very low laser pulse energy (0.42 µJ) is required to transfer this labile molecule to the gas phase. On the other hand, chlorophyll ionization with **α**-CNPV matrices requires higher laser pulse energy (> 0.5 µJ) than with DCTB which ultimately causes decomposition.

ET ionization is a valuable strategy for the selective ionization of structurally related compounds with similar ionization energies, such as detecting petroporphyrins in complex mixtures, as previously reported [30]–[33]. In microalgae, photosynthetic (chlorine derivatives) and photoprotective (isoprenoid derivatives) pigments share common architectures, and consequently, their ionization energies (amongst the members of each group) are similar. Thus, we selected the commercially-available electron transfer matrix (DCTB) with an ionization energy of 8.54 eV to perform the ionization step [34][31]–[33]. According to literature reports and our calculations, the E_i values of photosynthetic and photoprotective phytoplankton pigments range between 6.2 to 7.1 eV; thus, electron transfer from neutral analytes to primary matrix ions is thermodynamically feasible according to the mechanism shown above [35]. Considering the scope of this method, which is to detect a wide range of chlorophylls, carotenoids, and xanthophylls in a single run, DCTB is the most suitable electron-transfer matrix.

Figure 4 shows the ET MALDI TOF mass spectra of pigment extracts from *C vulgaris* and freshwater phytoplankton, using DCTB as a matrix, with an A:M ratio of 1:1000, 0.42 µJ of laser energy, and 3000 shots per spot. We observe two distinct regions in the MS; photoprotective pigments -carotenoids- are distributed between *m/z* 500 and *m/z* 600, while intact photosynthetic pigments -chlorophylls- signals occur between *m/z* 850 and *m/z* 1000. Pigment molecules readily form radical cations under the MALDI conditions used. Signal clustering at different spectral regions facilitates data interpretation. However, keep in mind that some pigments are labile -particularly chlorophylls- and even under MALDI's soft ionization conditions, fragments can be formed and detected at low *m/z* values. In the chlorophyll region, typical ions correspond to chlorophyll a ($C_{55}H_{72}O_5N_4Mg$, *m/z* 892.535), chlorophyll b ($C_{55}H_{70}O_6N_4Mg$, *m/z* 906.514), and derivatives such as chlorophyllide a ($C_{35}H_{34}N_4O_5Mg$, *m/z* 614.237), chlorophyllide b ($C_{35}H_{32}N_4O_6Mg$, *m/z* 628.217), and pheophytin a ($C_{55}H_{74}N_4O_5$, *m/z* 870.565). Interestingly, the identification of chlorophyll derivatives (chlorophyllides and pheophorbides) could not only be associated with the breakdown of the chlorophyll molecule during the extraction or purification process but also with a biological response. Chlorophyll derivatives are naturally present in water bodies as by-products of metabolism in fish; they are vital indicators of ecosystemic processes connected to the functioning of trophic chains. Also, using mutant photosynthetic microorganisms, Vavilin et al. found that chlorophyllide and pheophorbide are products of

chlorophyll degradation in the photosystems I and II [36]. We observed chlorophyll a ($C_{55}H_{72}O_5N_4Mg$-K) and -b ($C_{55}H_{70}O_6N_4Mg$-K) adducts at *m/z* 931.499 and 945.478, respectively. Some authors have previously reported the affinity of chlorophylls with different cations [37]–[40].

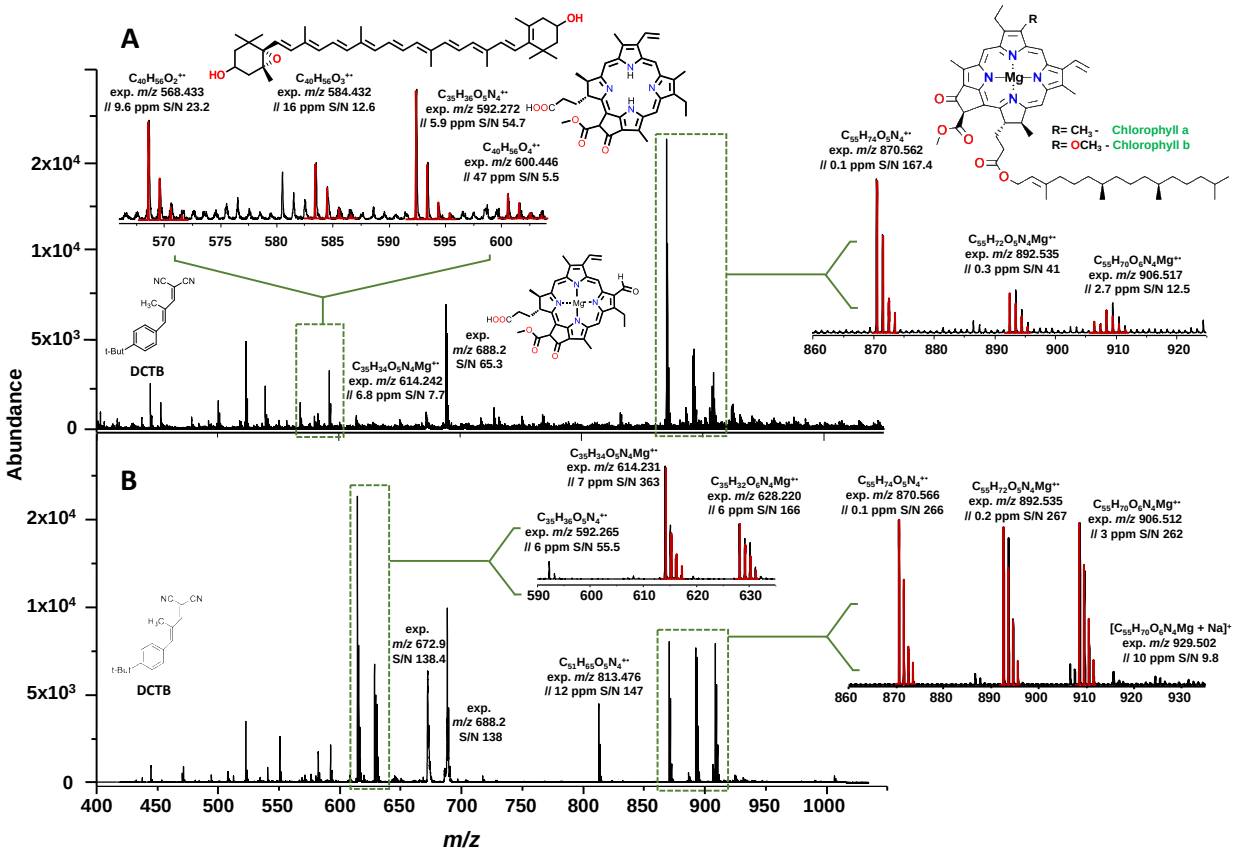

Figure 4. ET MALDI MS mass spectra of **A**, *Chlorella vulgaris* cells pigment extract and **B**, freshwater phytoplankton pigment extract. Insets show molecular formula, experimental mass, mass accuracy, signal/noise ratio, and theoretical/experimental isotopic pattern for the identified pigments.

Chlorophyll a experiences fragmentation reactions resulting in the fragments at *m/z* 614.237, *m/z* 555.147, and *m/z* 481.098. Pheophytin also undergoes fragmentation resulting in the species at *m/z* 592.578, *m/z* 533.165, and *m/z* 459.157 [41]. Also, some chlorophyll b fragments are detected at *m/z* 553.256 (loss of –(phytyl-H)OCH_3-CO_2), *m/z* 495.146 (loss of -CHO-COOphytyl-$COOCH_3$), *m/z* 476.128 (loss of -CHO-CH_2CH_2COOphytyl-$COOCH_3$) [42]. In MALDI MS approaches, the number and type of fragments detected from chlorophyll depend on the measurement conditions and sample treatment. In this work, electron-transfer matrix used (DCTB, 8.54 eV, low vapor pressure $9.09x10^{-7}$ mm Hg at 25 °C [43]) reduces chlorophyll fragmentation during the MALDI process by facilitating the desorption of labile intact species. We believe some unidentified signals in the spectrum may be due to acyl glycerides. Identifying and quantifying pigments, such as chlorophyll a and chlorophyll b, is vital to calculate parameters like Net Primary Production (NPP) in water bodies essential to determine the health of the trophic chain in aquatic ecosystems [44].

The carotenoid ET MALDI spectral region includes signals in the form of radical cations from diadinoxanthin ($C_{40}H_{54}O_3$, *m/z* 582.407), neoxanthin ($C_{40}H_{56}O_4$, *m/z* 600.417), diatoxanthin ($C_{40}H_{54}O_2$, *m/z* 566.412), **β**-e-carotene ($C_{40}H_{56}$, *m/z* 536.438), zeaxanthin ($C_{40}H_{56}O_2$, *m/z* 568.428), and antheraxanthin ($C_{40}H_{56}O_3$, *m/z* 584.422). We detected an astaxanthin ($C_{40}H_{52}O_4$) sodium adduct $[M + Na]^+$ at *m/z* 619.376. Among these compounds, diadinoxanthin ($C_{40}H_{54}O_3$,

m/z 582.407) belongs to the xanthophyll cycle, a critical enzymatic cycle that serves as an indicator of a photosynthetic organism's physiological condition. In phytoplanktonic microorganisms, diadinoxanthin is transformed into diatoxanthin (in the case of diatoms) or dinoxanthin (for dinoflagellates) [45]. Using HPLC, other authors have reported the same pigments we identified via our ET MALDI MS methodology in *Chlorella vulgaris* [46], and in phytoplankton from freshwater samples, we also identified these pigments using HPLC. The compounds identified are characteristic biomarkers of algae belonging to the Haptophyte, Chlorophyta, and Euglenophyta phyla [7]. This work offers a rapid methodology for detecting photosynthetic and photoprotective pigments in a single assay, with comparable results to other analytical techniques [46]. For instance, microalgae growth is typically monitored via UV-vis spectroscopy [47]. We have successfully applied ET MALDI to investigate how *Chlorella vulgaris* growth affects pigment profiles (data not shown). Overall, this methodology has the potential to provide valuable insights into the growth status of microalgae and their response to changing environmental factors.

We use isotopic pattern coincidence as an additional criterion for compound identification besides mass accuracy. Figure 4 includes theoretical/experimental isotopic pattern comparisons using information from the Compass Isotope Pattern software (Bruker Daltonics), and the experimental data from the ET MALDI assays. Isotope patterns correspond to a group of signals related to ions with the same chemical formula but containing different isotopes, also known as isotopologues. Therefore, the isotopic pattern is vital in identifying ionic species in mass spectrometry [48].

The ET MALDI experiments also resulted in metastable ion detection (Figure 4). Metastable ions are vibrationally excited species that can emerge from the MALDI plume. These ions fragment after the ionization source and typically exhibit broad signals with an apparent mass different from the original ion's. Baldas and Porter [49] reported metastable ions in carotenoids and chlorophylls MALDI studies. Using HRMS, a characteristic M-80 signal was assigned to C_6H_8 loss in carotenoids analysis. Brown and Wilkins [50] indicate that metastable chlorophyll ions arise from excess energy supplied during desorption. Several parameters can influence MALDI's metastable ion formation, such as energy absorption directly from the laser, collision with matrix molecules, ion acceleration through the source's electrical field, and exothermic reactions in the MALDI plume [48], [51], [52]. The metastable ion at *m/z* 672.9 (Figure 4) could have a likely structure $[M + 2K - H - (phytyl - H) - H_2O]^+$ [53].

Conclusions

Electron-transfer reactions allow selective ionization of compound families sharing similar architectures (chlorins and carotenoids) with ionization energies below the matrix ionization energy. Compared with the gold standard (HPLC), ET MALDI provides valuable chemical information. HPLC separates pigments based on differential interactions between the analytes, mobile, and stationary phases. Although robust, reliable, and easily adapted, the technique requires excessive sample handling, long run times, and high reagent consumption. For pigment analysis, issues with coelution, complex workouts for low-abundance pigments, and artifact formation are still unresolved.

Electron-transfer MALDI-TOF MS, on the other hand, selectively ionizes groups of compounds and separates them by mass. Complete analysis of pigment extracts can be completed in minutes. In addition to a speedy analysis, ET MALDI has advantages such as high sensitivity, selectivity, tolerance to impurities and contaminants, broad applicability, and the capability of complex mixture analysis [54]–[56]. Also, the technique's high sensitivity (pico to femtomole levels [48] of the extract on the sample holder) and selectivity allows for detecting low-abundance compounds in the extract. Recent reports show the importance of ultra-low-abundance pigments as vital biomarkers for identifying threatened/valuable/key organisms in phytoplankton communities. On the other hand, tolerance to contaminants is an attractive

advantage for microalgae/phytoplankton analysis in MALDI MS, due to the presence of dissolved organic matter in these habitats and the micro and macronutrient requirements for microalgae growth. Finally, we believe ET MALDI can become a robust strategy for pigment analysis paving the way to phytoplankton chemotaxonomic identification using mass spectrometry.

Acknowledgments

The authors acknowledge funding from MINCIENCIAS (Grant 2019000100020). They also thank Guatiguará Technology Park and the Central Research Laboratory Facility at Universidad Industrial de Santander (UIS) for infrastructural support. In addition, we acknowledge the Vice Chancellor for Research Office (VIE-UIS) project 2815-2021. The authors thank the In-silico Research Group at Universidad de Sucre, Colombia, especially Dr. Aldo Combariza, and BSc Carlos Padilla, for the taxonomic identification of the freshwater phytoplankton samples.

References

[1] H. Begum, F. Yusoff, S. Banerjee, H. Khatoon, and M. Shariff, "Availability and Utilization of Pigments from Microalgae," *Crit Rev Food Sci Nutr*, vol. 56, no. 13, pp. 2209–2222, Oct. 2016.

[2] Porra Robert, Oster Ulrike, and Scheer Hugo, "2. Recent advances in chlorophyll and bacteriochlorophyll biosynthesis," in *PHYTOPLANKTON PIGMENTS: Characterization, Chemotaxonomy and Applications in Oceanography*, First Edit., S. Roy, C. Llewellyng, E. Skarstad, and G. Jhonsen, Eds. United Kingdom: Cambridge University Press, 2011, pp. 78–112.

[3] H. Lichtenthaler and A. Wellburn, "Determinations of total carotenoids and chlorophylls a and b of leaf extracts in different solvents," *Biochem Soc Trans*, vol. 11, pp. 591–592, 1983.

[4] L. Patiny and A. Borel, "ChemCalc: A Building Block for Tomorrow's Chemical Infrastructure.," *J Chem Inf Model*, vol. 53, pp. 1223–1250, 2013.

[5] S. Weber, P. Grande, L. Blank, and H. Klose, "Insights into cell wall disintegration of Chlorella vulgaris," *PLoS One*, vol. 17, no. 1, pp. 1–14, Jan. 2022.

[6] J. Liu and F. Chen, "Biology and industrial applications of Chlorella: Advances and prospects," *Adv Biochem Eng Biotechnol*, vol. 153, pp. 1–35, Dec. 2016.

[7] S. Wright and S. Jeffrey, "Pigment Markers for Phytoplankton Production," *Hdb. Env. Chem.*, vol. 2, pp. 71–104, 2006.

[8] R. Wetzel and G. Likens, *Composition and Biomass of Phytoplankton*, Primera., vol. First Edit. N.Y., 2000.

[9] J. Capblancq and J. Catalan, "Phytoplankton: which, and how much?," pp. 9–30, 1994.

[10] D. Boyce, M. Lewis, and B. Worm, "Global phytoplankton decline over the past century," *Nature*, vol. 466, pp. 591–596, 2010.

[11] S. Jeffrey, R. Mantoura, and S. Wright, *Phytoplankton pigments in oceanography: guidelines to modern methods*, Primera., vol. 48. Paris, 1997.

[12] E. Cupp, *Marine Plankton Diatoms of the West Coast of North America*, vol. 5. 1943.

[13] L. Vidal and M. Carbonell, “Diatomeas y dinoflagelados de la Bahía de Cartagena,” Tesis de grado de Biología Marina, Bogota, Jorge Tadeo Lozano, 1977.

[14] C. D’Agrosa, O. Vidal, and W. Graham, “Mortality of the vaquita (Phocoena sinus) in gillnet fisheries during 1993-94.,” *Reports-international whal comm spec issues*, vol. 94, pp. 283–294, 1995.

[15] L. Heukelem and C. Thomas, “Computer-assisted high-performance liquid chromatography method development with applications to the isolation and analysis of phytoplankton pigments.,” *J Chromatogr A*, vol. 910, no. 1, pp. 31–49, 2001.

[16] L. Van-Heukelem, A. Lewitus, T. Kana, and N. Craft, “Improved separations of phytoplankton pigments using temperature-controlled high performance liquid chromatography,” *Oceanographic Literature Review*, vol. 5, pp. 369–376, 1995.

[17] L. Van-Heukelem, A. Lewitus, T. Kana, and N. Craft, “High-Performance Liquid Chromatography of Phyto- plankton Pigments Using a Polymeric Reversed-Phase C18 Column.,” *J Phycol*, vol. 28, pp. 867–872, 1992.

[18] V. Brotas and M. Plante-cuny, “The use of HPLC pigment analysis to study microphytobenthos communities,” *Acta Oecologica*, vol. 24, pp. 109–115, 2003.

[19] M. Zapata and J. Garrido, “La diversidad pigmentaria del fitoplancton marino: implicaciones ecológicas,” *Biotecnología y Aplicaciones de Microorganismos Pigmentados*, vol. 2, pp. 75–94, 2000.

[20] T. Suzuki, H. Midonoya, and Y. Shioi, “Analysis of chlorophylls and their derivatives by matrix-assisted laser desorption/ionization–time-of-flight mass spectrometry,” *Anal Biochem*, vol. 390, no. 1, pp. 57–62, 2009.

[21] T. Mccarley, R. L. Mccarley, and P. A. Limbach, “Electron-Transfer Ionization in Matrix-Assisted Laser Desorption/Ionization Mass Spectrometry,” *Anal Chem*, vol. 70, pp. 4376–4379, 1998.

[22] R. Knochenmuss and R. Zenobi, “MALDI ionization: The role of in-plume processes,” *Chem Rev*, vol. 103, pp. 441–452, 2003.

[23] R. Knochenmuss, “MALDI mechanisms: wavelength and matrix dependence of the coupled photophysical and chemical dynamics model,” *Analyst*, vol. 139, no. 1, pp. 147–156, 2014.

[24] R. Knochenmuss, “Ion formation mechanisms in UV-MALDI,” *Analyst*, vol. 131, no. 9, pp. 966–986, 2006.

[25] R. Knochenmuss, “MALDI ionization mechanisms: The coupled photophysical and chemical dynamics model correctly predicts ’temperature’-selected spectra,” *Journal of Mass Spectrometry*, 2013.

[26] R. Zenobi and R. Knochenmuss, “Ion formation in MALDI Mass Spectrometry,” *Mass Spectrom Rev*, vol. 17, pp. 337–366, 1999.

[27] C. Calvano, G. Ventura, M. Trotta, G. Bianco, T. Cataldi, and F. Palmisano, “Electron-Transfer secondary reaction matrices for MALDI MS analysis of Bacteriochlorophyll a in Rhodobacter sphaeroides and its zinc and copper analogue pigments,” *J Am Soc Mass Spectrom*, vol. 28, no. 1, pp. 125–135, 2017.

[28] C. Calvano, G. Ventura, T. Cataldi, and F. Palmisano, “Improvement of chlorophyll identification in foodstuffs by MALDI ToF/ToF mass spectrometry using 1,5-diaminonaphthalene electron transfer secondary reaction matrix,” *Anal Bioanal Chem*, vol. 407, no. 21, pp. 6369–6379, 2015.

[29] N. Boutaghou and R. Cole, “9,10-Diphenylanthracene as a matrix for MALDI-MS electron transfer secondary reactions,” *Journal of Mass Spectrometry*, vol. 47, no. 8, pp. 995–1003, Aug. 2012.

[30] L. Castellanos-García *et al.*, “Oligo p-Phenylenevinylene Derivatives as Electron Transfer Matrices for UV-MALDI,” *J Am Soc Mass Spectrom*, vol. 28, pp. 2548–2560, 2017.

[31] J. S. Ramírez-Pradilla, C. Blanco-Tirado, and M. Y. Combariza, “Electron-Transfer Ionization of Nanoparticles, Polymers, Porphyrins, and Fullerenes Using Synthetically Tunable α-Cyanophenylenevinylenes as UV MALDI-MS Matrices,” *ACS Appl Mater Interfaces*, vol. 11, no. 11, pp. 10975–10987, 2019.

[32] J. S. Ramírez-Pradilla, C. Blanco-Tirado, M. Hubert-Roux, P. Giusti, C. Afonso, and M. Y. Combariza, “Comprehensive Petroporphyrin Identification in Crude Oils Using Highly Selective Electron Transfer Reactions in MALDI-FTICR-MS,” *Energy and Fuels*, vol. 33, no. 5, pp. 3899–3907, 2019.

[33] D. Giraldo-Dávila, M. L. Chacón-Patiño, J. S. Ramirez-Pradilla, C. Blanco-Tirado, and M. Y. Combariza, “Selective ionization by electron-transfer MALDI-MS of vanadyl porphyrins from crude oils,” *Fuel*, vol. 226, pp. 103–111, 2018.

[34] Y. Vasil, O. Khvostenko, A. Streletskii, O. Boltalina, S. Kotsiris, and T. Drewello, “Electron Transfer Reactivity in Matrix-Assisted Laser Desorption / Ionization (MALDI): Ionization Energy , Electron Affinity and Performance of the DCTB Matrix within the Thermochemical Framework,” *The Journal of Physical chemistry A Letters*, vol. 110, pp. 5967–5972, 2006.

[35] C. Padilla Jaramillo, L. Díaz Sánchez, M. Combariza Montañez, C. Blanco Tirado, and A. Combariza Montañez, “Photon Harvesting Molecules: Ionization Potential from Quantum Chemical Calculations of Phytoplanktonic Pigments for MALDI-MS Analysis,” *Orinoquia*, vol. 25, no. 1, pp. 13–23, Jun. 2021.

[36] D. Vavilin, D. Brune, and W. Vermaas, “15N-labeling to determine chlorophyll synthesis and degradation in Synechocystis sp. PCC 6803 strains lacking one or both photosystems,” *Biochim Biophys Acta Bioenerg*, vol. 1708, no. 1, pp. 91–101, Jun. 2005.

[37] A. Larkum, *The Evolution of Chlorophylls and Photosynthesis*, Segunda. University of Sydney, Australia: Springer, 2006. [Online]. Available: http://link.springer.com/10.1007/1-4020-4516-6_18

[38] S. Persson, C. Sönksen, N. Frigaard, R. Cox, P. Roepstorff, and M. Miller, “Pigments and proteins in green bacterial chlorosomes studied by matrix-assisted laser desorption ionization mass spectrometry,” *Eur J Biochem*, vol. 267, no. 2, pp. 450–456, 2000.

[39] D. I. Arnon, “Copper enzymes in isolated chloroplasts: Polyphenoloxidase in Beta vulgaris,” *Plant Physiol*, vol. 24, pp. 1–15, 1949.

[40] L. Vernon and G. Seely, *The Chlorophylls: Physical, Chemical and Biological Properties*, 1st ed. Academic Press, 2014.

[41] J. Wei, H. Li, M. P. Barrow, and P. B. O’Connor, “Structural characterization of chlorophyll-a by high resolution tandem mass spectrometry,” *J Am Soc Mass Spectrom*, vol. 24, no. 5, pp. 753–760, May 2013.

[42] R. van Breemen, F. Canjura, and S. Schwartz, “Identification of Chlorophyll Derivatives by Mass Spectrometry,” *J Agric Food Chem*, vol. 39, no. 8, pp. 1452–1456, 1991.

[43] “US EPA. 2023. Estimation Programs Interface Suite™ for Microsoft® Windows, v 4.11. United States Environmental Protection Agency, Washington, DC, USA.”

[44] M. Burford, D. Alongi, A. McKinnon, and L. Trott, “Primary production and nutrients in a tropical macrotidal estuary, Darwin Harbour, Australia,” *Estuar Coast Shelf Sci*, vol. 79, no. 3, pp. 440–448, 2008.

[45] M. Schagerl, C. Pichler, and K. Donabaum, “Patterns of major photosynthetic pigments in freshwater algae Dinophyta , Euglenophyta , Chlorophyceae and Charales,” *Ann. Limnol.*, vol. 39, pp. 49–62, 2000.

[46] H. A. Pantami *et al.*, “Comprehensive GCMS and LC-MS/MS metabolite profiling of chlorella vulgaris,” *Mar Drugs*, vol. 18, no. 7, Jul. 2020.

[47] L. Gouveia, V. Veloso, A. Reis, H. Fernandes, J. Novais, and J. Empis, “Evolution of pigment composition in Chlorella vulgaris,” *Bioresour Technol*, vol. 57, pp. 157–163, 1996.

[48] J. Gross, *Mass Spectrometry*, Third Edition. Heidelberg, Germany: Springer, 2017.

[49] J. Baldas, Q. Porter, L. Cholnoky, J. Szabolcs, and B. Weedon, “Mass Spectrometry of Carotenoid Epoxides and Furanoid Oxides,” *Chemistry Communications*, no. 23, pp. 852–854, 1966.

[50] R. Brown and C. Wilkins, “Laser Desorption Fourier Transform Mass Spectrometry of Chlorophyll a and Chlorophyll b,” *J. Am. Chem. Soc.*, vol. 108, pp. 2447–2448, 1986.

[51] C. Versluis, A. van der Staaij, E. Stokvis, and A. J. R. Heck, “Metastable Ion Formation and Disparate Charge Separation in the Gas-Phase Dissection of Protein Assemblies Studied by Orthogonal Time-of-Flight Mass Spectrometry,” 2001.

[52] Y. Wang, E. Nakajima, Y. Okamura, D. Wang, N. Okumura, and T. Takao, “Metastable decomposition at the peptide C-terminus: Possible use in protein identification,” *Rapid Communications in Mass Spectrometry*, vol. 34, no. 9, May 2020.

[53] J. Tabet, M. Jablonski, and R. Cotter, “Time-resolved laser desorption decomposition of chlorophyll a III. The metastable and some derivates,” *Int J Mass Spectrom Ion Process*, vol. 65, pp. 105–117, 1985.

[54] F. Hillenkamp and M. Karas, “Matrix-assisted laser desorption/ionisation, an experience,” *Int J Mass Spectrom*, vol. 200, no. 1–3, pp. 71–77, 2000.

[55] M. Karas and R. Krüger, “Ion formation in MALDI: The cluster ionization mechanism,” *Chem Rev*, vol. 103, no. 2, pp. 427–439, 2003.

[56] M. Karas, M. Glückmann, and J. Schäfer, “Ionization in matrix-assisted laser desorption/ionization: Singly charged molecular ions are the lucky survivors,” *Journal of Mass Spectrometry*, vol. 35, no. 1, pp. 1–12, 2000.

Chapter 2

Comparative Profiling of *Chlorella vulgaris* Cells, Extracts, and Intact Chloroplasts Using Electron Transfer Matrix-Assisted Laser Desorption/Ionization Mass Spectrometry (ET MALDI-MS)

Edited from: Luz A. Calderón-Vergara*, Luis M. Díaz-Sánchez*, Cristian Blanco-Tirado, Marianny Y. Combariza, Analytical Methods, 2024, 16, 5652-5664.
* These authors contributed equally. DOI https://doi.org/10.1039/D4AY00846D

Keywords
Electron transfer ionization; Profiling, Microalgae; Intact Chloroplasts; Chlorophylls; Carotenoids; Matrix Assisted Laser Desorption Ionization; MALDI; Mass Spectrometry.

Abstract
The intricate composition of microalgal pigments plays a crucial role in various biological processes, from photosynthesis to biomarker identification. Traditional pigment analysis methods involve complex extraction techniques, posing challenges in maintaining analyte integrity. In this study, we employ Electron Transfer Matrix-Assisted Laser Desorption/Ionization Mass Spectrometry (ET MALDI-MS) to compare the pigmentary profiles of *Chlorella vulgaris* intact cells, chloroplasts, and solvent extracts. Utilizing ultrasound-assisted and supercritical fluid extraction methods, we aim to obtain comprehensive extracts rich in polar and non-polar compounds. Additionally, intact chloroplasts are isolated using a lysis buffer and sucrose density gradient centrifugation. Our ET MALDI-MS analysis reveals distinct compositional differences, highlighting the impact of extraction protocols on microalgal pigment identification. We observe prominent signals corresponding to radical cations of key pigments, including chlorophylls and carotenoids, crucial for *C. vulgaris* identification. Furthermore, ET-MALDI facilitates the identification of specific lipids within chloroplast membranes and other organelles. This study underscores the rapid and precise nature of MALDI MS in microalgal biomarker analysis, providing valuable insights into phytoplankton dynamics, trophic levels, and environmental processes. *C. vulgaris* emerges as a promising model for studying pigment composition and membrane lipid diversity, enhancing our understanding of microalgal ecosystems.

Introduction

In aquifer ecosystems, microalgae communities play crucial roles as the foundation and primary food source. They are also fundamental in the carbon cycle, fixing a large portion of atmospheric CO_2 and producing a significant amount of molecular oxygen.[1] As autotrophs, microalgae possess a wide range of pigments that are crucial for photosynthesis and are also used as biomarkers to indicate the state of the ecosystem. For instance, by measuring chlorophyll pigment levels, researchers estimate the biomass and PPN (Net Primary Production) of aquatic ecosystems over time. Consequently, the search for pigments that serve as molecular biomarkers and are highly sensitive to changes in the aquatic environments remains a key area of research.

C. vulgaris is one of the most studied photosynthetic microorganisms and was the first genus of planktonic unicellular green algae to be isolated in culture and grown commercially to extract bioactive compounds.[2] *C. vulgaris* belongs to the phylum Chlorophyta and can grow autotrophically, heterotrophically, and mixotrophically under specific conditions of light/dark cycles, temperature, and pH. The biomass of *C. vulgaris* is rich in valuable compounds such as proteins (up to 60% of dry weight), lipids (12–15%), carbohydrates (10–15%), pigments (1-4%), vitamins, and minerals.[3,4] Currently, more than 70 companies worldwide produce over 2000 tons of *C. vulgaris* biomass annually.

The cells of *C. vulgaris* are spherical, with diameters ranging from 2-10 µm. They contain a cup-shaped chloroplast that stores pigments like chlorophylls (chl) and carotenoids. These pigments serve both photoprotective and photosynthetic functions and are embedded in stacked vesicles called thylakoids. Carotenoids can also be found attached to proteins or membranes within the chloroplasts.[5]

Chlorophyll *a* is the main photosynthetic pigment acting as a primary electron donor in the electron transport chain that occurs in the photosystems (reaction centres) where photons are converted into chemical energy. Chlorophyll *b* is considered an ancillary pigment whose main role is expanding the absorption spectrum of the chloroplast. Both chlorophyll *a* and *b* are magnesium coordination complexes of conjugated cyclic tetrapyrroles (or chlorin rings) with a hydrocarbon side chain known as phytol.[6] It is possible for chlorophylls to experience different changes, such as losing the Mg^{2+} ion resulting in pheophytins, losing the phytol chain resulting in chlorophyllides, or losing both the Mg^{2+} ion and phytol resulting in pheophorbides. They may also lose the C-13 carbomethoxy group to form pyro-derivatives or undergo spontaneous rearrangements to form epimers or oxidation to produce allomers.[7] Chlorophyll derivatives can be found naturally or as by-products of harsh extraction methods;[4] some even find uses as photosensitizers in photodynamic therapy.[8]

Methods for analyzing intracellular pigments in photosynthetic microorganisms typically involve chemical, physical, and/or mechanical treatments to induce cellular lysis and release pigments. The composition of the cell and thylakoid membranes, where lipids serve as protective layers, plays a pivotal role in pigment extraction. Therefore, the choice of extraction technique and conditions is fundamental in preventing light- and heat-sensitive pigment degradation and increasing extraction efficiencies.[9–12] The most commonly used method for pigment recovery from microalgae is solvent extraction. For instance, traditional Soxhlet extraction involves recirculating a heated solvent continuously to break down the cell membrane and release pigments. In Soxhlet extraction using supercritical fluids (SFE), parameters such as temperature, pressure, or the addition of a co-solvent can be adjusted to fine-tune the fluid's affinity towards specific compounds of interest. High-frequency ultrasonic waves are used during sonication to cause cell membrane lysis, facilitating the release of intracellular components, including pigments.[13–17] On the other hand, analysing whole intact cells may offer advantages for applications ranging from cell type identification to quality control assessment of cell culture and diagnostic applications. For example, Grassino et al. introduced a fast and non-destructive whole-cell pigment analysis of purple phototrophic bacteria using spectrophotometric methods

combined with principal component analysis (PCA).[9] Furthermore, Lee et al. conducted a direct transfer method for protein profiling of whole microalgae cells by MALDI-TOF MS without protein extraction and inactivation steps.[10] Similar studies of whole intact cells by mass spectrometry have been reported in the literature.[11,12] Other alternatives commonly used to analyze pigment-protein clusters from whole cells involve partial cell integrity disruption to isolate intact chloroplasts or thylakoids.[18,19] For instance, Mascia et al. analyzed pigments in *Haematococcus pluvialis* cells and thylakoid membranes using a lysis buffer, mechanical treatment, and ultracentrifugation in a sucrose gradient for purification.[18] Additionally, the pigment composition of thylakoid membranes from two strains of marine photosynthetic prokaryote *Prochlorococcus* was analyzed via reverse-phase HPLC by Garczarek et al. after using a sucrose gradient centrifugation and detergent pretreatment.[20] In parallel, Panintingjati et al. reported an analysis of pigment-protein complexes in chloroplasts using spectrophotometric methods.[21]

After the isolation of pigment extracts, separation, and identification is carried out using high-performance liquid chromatography-mass spectrometry (HPLC-MS), considered the analytical gold standard.[22] Despite being widely adopted, traditional extraction and identification techniques still pose analytical challenges in pigment characterization due to the broad polarity range of the target analytes. Challenges include strict storage requirements, multiple extraction steps, lengthy analysis times, and the use of organic solvents, which can introduce artifacts hindering molecular identification.[23,24] The potential for incorrect molecular misidentification of microalgae pigments at the molecular level has been reported when employing traditional analytical approaches.[24]

Previous studies, including our own work, suggest that employing soft analytical techniques, such as matrix-assisted laser desorption/ionization mass spectrometry (MALDI-MS), can yield rapid and reliable molecular information comparable to conventional methods.[25–33] For instance, MALDI-MS biotyping has become a fast, simple, and widely applicable tool for microorganism identification in clinical labs, relying on protein[11,34–38], lipid[39–41], and pigment[42–44] mass spectral profile analysis.[45,46] Traditional analysis of chlorophyll and carotenoid pigments using MALDI-MS involves proton-/cation-transfer matrices like 2,5-dihydroxybenzoic acid (DHB) or α-cyano-4-hydroxycinnamic acid (CHCA), which can lead to issues such as multiple adduct formation, central metal loss, and phytol-ester cleavage in chlorine derivatives. Notably, pigments exhibit a fascinating convergence in their photoactive and photoprotective functions, despite originating from diverse metabolic pathways in plants and microorganisms and featuring distinct chemical structures. This convergence results from their conjugated electronic structures, uniformly characterized by ionization energies consistently falling below the threshold of 7.5 eV, regardless of whether they belong to the chlorine or isoprenoid derivatives category. Thus, using MALDI matrices with ionization energies surpassing 8.0 eV should ensure efficient electron transfer (ET) processes and enable selective pigment analysis in MALDI-MS.[25,29–32]

This study uses Electron Transfer Matrix-Assisted Laser Desorption/Ionization Mass Spectrometry (ET MALDI-MS) to compare the pigmentary profiles of *C. vulgaris* intact cells, chloroplasts, and complementary polarity solvent extracts. Intact chloroplasts from *C. vulgaris* were isolated using a lysis buffer followed by sucrose density gradient centrifugation (see Figure 1). Additionally, solvent extraction from *C vulgaris* was aimed at obtaining extracts rich in polar and non-polar compounds using, respectively, ultrasound-assisted solvent extraction (acetone, e_r: 20.6)[47] and SFE extraction ($CO_{2(sc)}$ e_r:1.35)[48] from whole cells. The ET MALDI-MS analysis of *C. vulgaris* whole cells, pigment extracts, and intact chloroplasts revealed notable compositional differences. Comparisons between intact chloroplasts and whole cell ET MALDI-MS profiles exposed interferences associated with the solvent extraction protocol. ET MALDI analysis primarily detected signals from radical cations of pigments such as chlorophyll *a*, chlorophyll *b*,

and their derivatives, as well as carotenoids including loroxanthin, lutein, and carotene. These compounds are considered key markers for *C. vulgaris* identification. Furthermore, ET-MALDI facilitated the identification of specific lipids within the chloroplast membrane and other organelles.

By analyzing pigment profiles, MALDI MS demonstrated itself as a rapid and precise method for microalgae biomarker analysis. Understanding the dynamic composition of microalgae pigments through MALDI MS could provide valuable insights into the fate of phytoplankton, trophic levels in natural ecosystems, and the study of degradation rates and blooms, among other factors.[49] For these reasons*, C. vulgaris* can be used as a model microorganism for studying pigment composition and structural diversity of membrane lipids using them as chemotaxonomic biomarkers.

Experimental

Algal culture conditions

An inoculum of *C. vulgaris* ($1.4x10^6$ cells/mL, Carolina Biological Supply Company, Burlington, NC, USA) was cultured using Bold's basic medium (BBM) comprising 250 mg $NaNO_3$, 75 mg KH_2PO_4, 25 mg $CaCl_2 \bullet 2H_2O$, 75 mg $MgSO_4 \bullet 7H_2O$, 75 mg $K_2HPO_4 \bullet 3H_2O$, 25 mg NaCl, 11.42 mg H_3BO_3, 8.82 mg $ZnSO_4 \bullet 7H_2O$, 1.20 mg $MnSO_4 \bullet 2H_2O$, 8.70 mg $(NH_4)_2MoO_4$, 1.57 mg $CuSO_4 \bullet 5H_2O$, 0.41 mg $CoCl_2$, 4.98 mg $FeSO_4$, 1 µL H_2SO_4 (99.9%), 5 mg Na_2EDTA, and 3 mg KOH. A stock suspension culture of *C. vulgaris* (1 mL of *C. vulgaris* cells in 100 mL of BBM) was maintained under controlled conditions, including light intensity (150 µmol $m^{-2}s^{-1}$), light/dark cycles (12:12 h), temperature (25 °C), and air flow (1.6 L/min, 420 ppmv CO_2), for 15 days. New stock cultures were initiated every three days to ensure a continuous supply of cells of approximately the same physiological age and activity. For this, 10 mL of the stock suspension culture was added to 100 mL of BBM and placed in 250 mL glass reactors under the same culture conditions. Cultures were grown until reaching 100 mg of algal biomass per flask (wet weight). *C. vulgaris* cells harvested during the exponential growth phase (day 15) were selected for direct analysis, chloroplast isolation, and the evaluation of pigment extraction techniques using ET MALDI MS. This growth stage was chosen due to the abundance of fully developed and viable cells containing functioning chloroplasts.[19]

Chloroplast isolation and purification from *C. vulgaris* whole cells

Ascorbic acid and 2-[4-(2-hydroxyethyl)piperazin-1-yl]ethane sulfonic acid (HEPES) were obtained from Sigma Aldrich (Saint Louis, MO, USA), and sorbitol, magnesium chloride ($MgCl_2 \bullet 6H_2O$), and bovine serum albumin (BSA) were purchased from Merck (Darmstadt, Germany). Dithiothreitol (DTT) was sourced from PanReac AppliChem (Barcelona, Spain). All chemical reagents were used as received without further purification, and aqueous solutions and suspensions were prepared using ultrapure water (18 MΩ·cm at 25 ºC).

A total of 20 mg of algal cells were collected by centrifuging a culture sample at 9000 rpm for 15 minutes at 4 °C (Universal 320R, Hettich, Tuttlingen, Germany) using a 50 mL Falcon tube. The resulting pellet was dispersed and kept in 3 mL of ice-cold lysis buffer (LB) containing 5 mM dithiothreitol (DTT) and 5 mM ascorbic acid for 4 days. Subsequently, the mixture was centrifuged, and the *C. vulgaris* pellet was dispersed and maintained at 4 °C in 1 mL of resuspension buffer (RB) containing 10 mM HEPES, 600 mM sorbitol, 50 mM $MgCl_2$, and 0.1% bovine serum albumin (BSA) at pH 7.5–7.8. After

confirming chloroplast release through optical microscopy, the mixture was centrifuged in a 60 to 70% sucrose in RB gradient at 9000 rpm for 5 minutes at 10°C. The sample was then left for several hours to reach equilibrium, forming three distinct phases: intact cells, isolated chloroplasts, and lysed cells. The intact chloroplast fraction appeared as a single dark-green band between the layers of intact and lysed cells in the middle of the tube, visible under room light. The chloroplast-enriched fraction was collected using a Pasteur pipette and stored on ice and in darkness until ET-MALDI MS analysis.

Chloroplast Characterization

Optical microscopy confirmed the release of intact chloroplasts from *C. vulgaris* cells. Two microliters of each sample were deposited on a slide previously cleaned with isopropyl alcohol. Then, 1 µL of methylene blue solution (0.05 g L^{-1}) was added to the sample, which was then analyzed with a 10x magnification eyepiece and 10x, 50x, and 100x magnification objectives using an OLYMPUS BX53F optical microscope. Chloroplast surface morphology was further studied by field emission scanning electron microscopy (FESEM) using an FEI QUANTA FEG 650 (Oregon, USA) instrument operated at 20 kV and equipped with a large field detector. Samples were coated with gold using a Quorum 150T ES system (Oregon, USA).

***C. vulgaris* Pigment Extraction**

Supercritical fluid, and ultrasound-assisted solvent extractions were employed to obtain pigment-enriched extracts from the *C. vulgaris* culture. These extraction methods facilitated the isolation of fractions with varying polarities dictated by the solvents used, $CO_{2(sc)}$, and acetone.

In all cases, the extraction process was initiated with a pellet obtained from the *C. vulgaris* microalgae culture through centrifugation at 7000 rpm for 15 minutes at 4 °C (Universal 320R, Hettich, Tuttlingen, Germany), utilizing a 50 mL Falcon tube. The sample was filtered using black ribbon Whatman® quantitative filter paper, ashless, Grade 589/1. The recovered pellet was lyophilized. Isolating pigment-rich fractions through solvent extraction is recommended over crude extract analysis to prevent coelution and misidentification in HPLC analysis.[6,50] Two techniques were employed based on the differences in pigment polarities in the microalgae. In both cases, after the extraction process, the obtained extracts were concentrated to dryness using argon flow at room temperature for approximately 5 minutes.

Ultrasound-Assisted Extraction

Samples of untreated and dried *C. vulgaris* were subjected to ultrasound-assisted extraction using a Branson Ultrasonics CPX 1800 bath (Fisher Scientific, Hampton, New Hampshire, USA) operating at 35 W, 40 kHz, and room temperature (22–25 ºC) for 25 minutes. The samples were placed in a vial with a solid-to-solvent ratio of 5:1 mg dry weight per mL solvent (analytical grade acetone). The extraction process was performed in triplicate, and the specific solvent was selected according to Standard Methods N° 10200-H[51], and based on the bioactive content of *C. vulgaris*, as reported previously by us[52] and other authors.[53,54]

Supercritical Fluid Extraction

Supercritical fluid extraction (SFE) experiments were conducted using an Apeks Supercritical 1500-1L system (Johnstown, Ohio, USA). The operational procedure involved loading the extraction cartridge with approximately 3 g of lyophilized microalgae samples, previously homogenized with glass beads at a 1:10 wt/w ratio to maintain consistent apparent density in all experiments. The loaded cartridge was placed into the extractor and equilibrated for 15 minutes to reach the operating temperature of 40 °C.

Carbon dioxide was then introduced into the CO_2 pump until the operating pressure reached 10 MPa. Subsequently, the extractor was pressurized with CO_2, and a 15-minute static extraction period was observed. Upon reaching equilibrium, the micrometric valve was gradually opened until a constant CO_2 flow rate of 2.5 mL/min was achieved. The extraction was carried out for 2 hours and conducted in triplicate for reproducibility. After isolation, the resulting extracts were collected in glass vials and stored at 4 °C, shielded from light, until subsequent analysis.

Pigment extracts UV-vis characterization.
Absorption spectra of *C. vulgaris* pigment extracts were obtained by preparing 1.0 mg/mL solutions of each of the dry extracts in acetone. This process utilized a 1 cm quartz cell in a GENESYS 10S UV-Vis spectrophotometer (Thermo Scientific, Billerica, MA, USA) equipped with a Xenon lamp, covering a UV-Vis range of 300 to 800 nm.

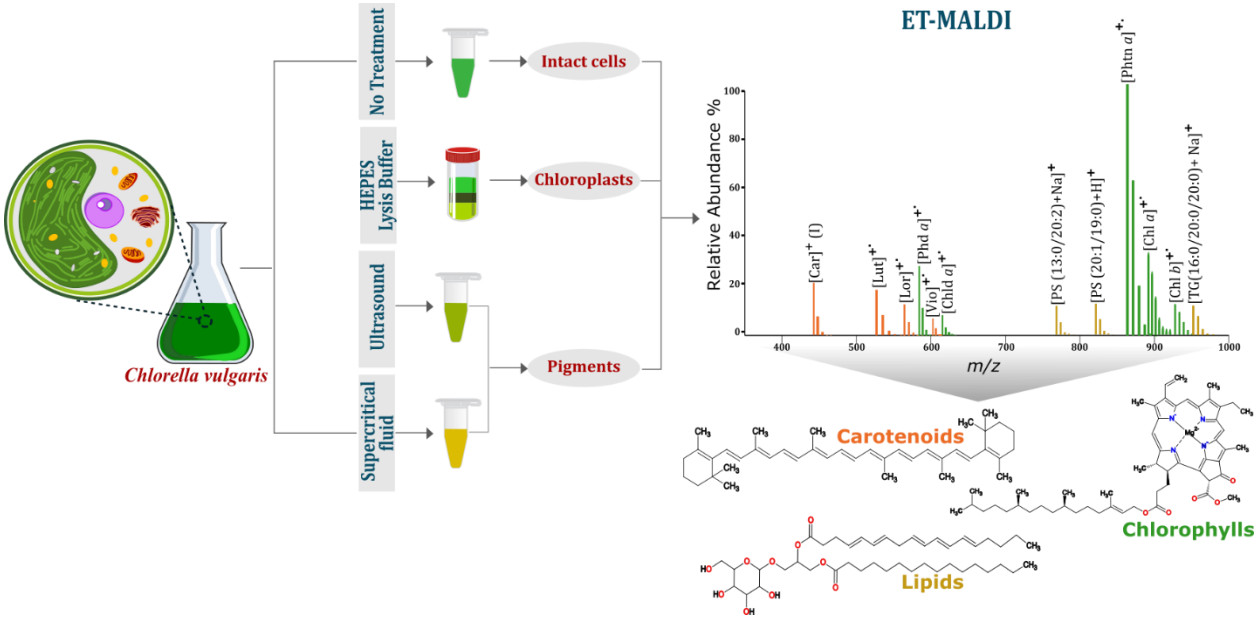

Fig. 1 General scheme for *C. vulgaris* pigment analysis using ET MALDI-MS.

Sample Preparation for Pigment Identification by Electron Transfer MALDI Mass Spectrometry
The seed-layer method was chosen for whole cells and intact chloroplast analysis to prevent solvent-induced lysis. A 1 µL solution of a 5 mM DCTB matrix in ACN was applied to a polished steel target. After solvent evaporation, 1 µL of intact cells and isolated intact chloroplast suspension (2 mg of cells in 500 µL of ultrapure water) was added to the matrix to achieve an analyte-to-matrix ratio of approximately 1:100. The concentration of chlorophyll *a* on day 15 of growth was used for the calculation, determined from the optical density at 665 and 649 nm using the mathematical equation applied by Griffiths. [55] In our case, the chlorophyll concentration in *C. vulgaris* on day 15 was approximately 0.99 wt%.

In the analysis of pigment extracts, DCTB was dissolved in acetonitrile (ACN) under ultrasonic waves (at a frequency of 40 kHz) for 2 min, reaching a concentration of 5 mM. Simultaneously, extracts from *C. vulgaris* were solubilized in ACN, using approximately 2

mg of the sample (approximately 0.05 mM), and subjected to 2 minutes of sonication. Equal volumes of the stock solutions for both matrix and analytes were combined and vigorously agitated using a vortex, operating at 1000 rpm for 5 min, resulting in an analyte-to-matrix ratio of 1:100. Each resultant mixture was then dispensed in a 1 µL volume onto a polished steel target using the dried droplet method for MALDI MS analysis.[25]

MALDI Mass Spectrometry:
Electron Transfer MALDI mass spectra of intact cells, isolated chloroplasts, and pigment extracts were acquired on a Bruker MALDI-TOF/TOF, UltraFleXtreme (Billerica, MA, USA) instrument equipped with an Nd: YAG solid-state laser (355nm) operating at a frequency of 1 kHz, pulse duration of 6 ns. Positive ion mass spectra were acquired from *m/z* 100 to 1000, with pulsed ion extraction (PIE) of 100 ns and an accelerating potential of 20 kV. ET MALDI experiments were conducted in reflectron mode (25 kV) using 2.0 µJ/laser pulse. External calibration utilized a mixture of standard peptides (leu-enkephalin, bradykinin, bombesin, and renin substrate purchased from Sigma Aldrich, St. Louis, MO) and α-CHCA as a matrix. Each reported analysis corresponds to the accumulation of 2000 individual spectra.

Results and discussion

***C. vulgaris* cells and chloroplast direct ET MALDI-MS analysis.**
Typical morphological characteristics of the algae are visible in the optical microscope images of *C. vulgaris* cells before and after chloroplast isolation. Fig. 2a shows whole cells with a well-defined cell wall, nucleus, and chloroplast. Each cell's cytoplasm, stained with methylene blue, appears as a light green-blue section in the optical images (Fig 2a). SEM images, Fig. 2b-d, reveal *C. vulgaris* individual cells ranging in size from 3 to 5 µm. The spherical and smooth shape of each *C. vulgaris* cell is evident, with some ruptured due to the high-vacuum conditions of the FESEM experiment. The chloroplast-nucleus complex, appearing as a dark-green structure, typically occupies 50-80% of a cell's volume, as observed in the optical images. However, environmental conditions, such as light, nutrients, and growth phase, can affect algae size, shape, and chloroplast activity.[56,57]
Fig. 3a provides compelling evidence of successful chloroplast isolation using the HEPES lysis buffer and the sucrose density gradient centrifugation protocol. The image clearly shows only dark-green structures consistent with chloroplasts, while the light green-blue cytoplasm of the cells appears to be completely absent. The HEPES lysis buffer effectively weakens the rigid cell wall structure in *C. vulgaris* without requiring additional mechanical treatment. We tested various incubation times 1, 2, 3, and 4 days with the HEPES lysis buffer and identified a four-day period as the optimal time required to effectively disrupt the *C. vulgaris* cell wall with minimal chloroplast damage. It should be noted that applying the HEPES lysis buffer to disrupt cell walls and extract chloroplasts from other microorganisms or phytoplankton species may require further experimentation. The inherent density differences between intact and lysed cells and chloroplasts were the basis for fractionation after cell treatment with HEPES. After a 60 and 70% sucrose gradient centrifugation step, three enriched fractions were formed. The top layer, with approximately 60% sucrose, contained intact cells. A thick, deep green layer, collected at approximately the middle of the gradient (i.e., 63-66%), contained most of the intact chloroplasts and only a limited number of intact cells (as shown in Figure 3a). The bottom layer contained cellular debris.

Fig. 3b-d present *C. vulgaris* chloroplasts ranging in size from 2 to 5 µm. Compared to the whole cell, the enlarged size of the chloroplasts results from the hypotonicity of the HEPES buffer that

causes water migration into the chloroplast, increasing their size. However, this effect does not interfere with the isolation of intact chloroplasts[58] or the ET MALDI MS analysis of the pigments. Interestingly, the spherical chloroplasts collapsed under SEM conditions due to the phospholipid wall's low mechanical strength and the experiment's high-vacuum conditions.
In Fig. 2e, the ET MALDI mass spectrum of intact *C. vulgaris* cells exhibits mainly molecular ions (radical cations) and fragments of chlorine-, isoprenoid-, and fatty acid- derivatives. The pigmentary complexity of photosynthetic microorganisms is defined by pigments or combinations of pigments with other compounds that are specific to certain taxonomic groups. In the case of *C. vulgaris*, neoxanthin, violaxanthin, astaxanthin, lutein, zeaxanthin, carotene, and chlorophyll *a* and *b* are the most prominent pigments. These pigments can be utilized for chemo-taxonomic identification of species belonging to the *Chlorophyta* division.[4,59] The electron transfer process in MALDI typically leads to detecting radical cations. This is because, once formed, the primary ions of the matrix ($M^{+\bullet}$)[60,61] can abstract an electron from the neutral analyte (A) to produce an analyte secondary ion ($A^{+\bullet}$). For this reaction to occur, the analyte ionization energy $E_{i(A)}$ should be lower than the matrix $E_{i(M)}$[61,62], according to:

$$\boldsymbol{M + nhv \rightarrow M^{+\bullet}}$$
$$\boldsymbol{M^{+\bullet} + A \rightarrow M + A^{+\bullet}}$$
$$\mathbf{E_{i\ (Analyte)} < E_{i\ (Matrix)}\ \Delta E_i > 0.5\ eV}$$

We used the commercial matrix *trans*-2-[3-(4-tert-butylphenyl)-2-methyl-2-propenylidene] malononitrile (DCTB) (E_i: 8.54 eV) as ET matrix because its low vapor pressure favors desorption of labile chlorine derivatives.[63] The ET MALDI-MS profile is dominated by radical cation (molecular ions) signals and few close shell fragments (cations). We observed 11 chlorophyll *a* and *b* – -related species, 1 carotenoid, and 3 lipid species in the ET MALDI-MS analysis of whole *C. vulgaris* cells. Chlorophyll *a* ($C_{55}H_{72}MgN_4O_5$) at *m/z* 892.534 and its derivatives; pheophytin *a* ($C_{55}H_{74}N_4O_5$) at *m/z* 870.568, chlorophyllide *a* ($C_{35}H_{34}MgN_4O_5$) at *m/z* 614.239,pheophorbide *a* ($C_{35}H_{36}N_4O_5$) at *m/z* 592.267 and the odd-mass fragment (I) from $M^{+\bullet}$ of chlorophyllide *a,* at *m/z* 555.229 $[M - 59]^+$, which correspond to the loss of the $-CH_3COO^{\bullet}$ radical, and the odd-mass fragment (II) at *m/z* 481.150 $[M - 133]^+$,which correspond to the loss of the $-CH_3COO^{\bullet}$ radical and the CH_3CH_2COOH neutral molecule, were identified with a high signal noise ratios > 7 as shown in **Table 1**.[64,65] Similarly, chlorophyll *b* ($C_{55}H_{70}MgN_4O_6$) at *m/z* 906.512, chlorophyllide *b* ($C_{35}H_{32}MgN_4O_6$) at *m/z* 628.218 were also observed.

The observed compositional pattern suggests the occurrence of transformations in chlorophylls *a* and *b*, resulting in the generation of pheophytins (loss of Mg^{2+} ion), chlorophyllides (loss of phytol chain), and pheophorbides (loss of both Mg^{2+} ion and phytol). These entities may either exist naturally within intact cells of *C. vulgaris* or manifest as artifacts during MALDI MS analysis due to chlorophyll decomposition. For instance, in the context of chlorophyll biosynthesis, a complex pathway involving multiple enzymatic reactions and stereo-specific reductions, chlorophyllides serve as intermediates formed from protochlorophyllides through the enzymatic action of protochlorophyllide reductase.[66] This intricate interplay of biochemical processes underscores the dynamic nature of chlorophyll metabolism within the microalga *C. vulgaris*, shedding light on the potential factors influencing the observed molecular profiles in MALDI MS analysis. Pheophytins and pheophorbides, on the other hand, represent breakdown products of chlorophyll metabolism, occurring through dephytylation and demetallation reactions mediated by chlorophyllase and Mg-dechelatase enzymes.[67,68] Furthermore, it has been reported in the literature that the biosynthesis of chlorophylls is susceptible to oxidative metabolism, driven by the presence of reactive oxygen species that lead to the formation of hydroxychlorophylls.[54,69] All these compounds have been previously identified and documented in scientific literature.[59,70] The theoretically calculated isotopic distribution of chlorophyll *a* (1.5 ppm, S/N 90.1) and chlorophyll *b* (2.9 ppm, S/N 15.6) is zoomed in Fig. 2. Additionally, we

observed the formation of adducts of pheophytin *a* with copper $[M + 63]^{+\bullet}$ (present in the microalgae culture medium) at *m/z* 931.485 and chlorophyll *b* with NH_4 $[M + 18]^+$ at *m/z* 924.539. The radical cation 7-hydroxymethyl-chlorophyll *a* at *m/z* 908.530 was also identified. Hydroxychlorophylls are prevalent in phytoplankton species in their natural habitats, and their presence is associated with responses to oxidative stress, defense mechanisms, grazing activities, and even senescence.[71,72] Lutein ($C_{40}H_{56}O_2$), a carotenoid recognized as a biomarker for *Chlorella* species, was identified at *m/z* 568.431, consistent with prior reports.[73]
The ionization energy of chlorophylls and their derivatives varies between 6.32 and 7.07 eV as previously reported by our research group.[74] Chlorophyll *a* has an $\boldsymbol{E_i}$ of 6.32 eV and its derivatives chlorophyllide *a* and pheophorbide *a* have an $\boldsymbol{E_i}$ of 6.40 and 6.80 eV, respectively. Similarly, chlorophyll *b* has an $\boldsymbol{E_i}$ of 6.74 and its derivative pheophorbide *b* has an $\boldsymbol{E_i}$ of 7.07 eV. On the other hand, an $\boldsymbol{E_i}$ of 6.67 eV was determined for lutein. These IP values were calculated using Koopman's Theorem, via Geometry Optimization and Single Point Energy within the Restricted Closed-Shell Hartree-Fock (RHF) technique with an absolute error rate of around 3.7%. All the $\boldsymbol{E_i}$ values of the detected molecules are below the $\boldsymbol{E_i}$ of the DCTB matrix ($\boldsymbol{E_i}$=8.5 eV, $\Delta\boldsymbol{E_i}$ >0.5 eV), showing how suitable it is to analyze this type of chemical species. Based on the ionization energy values of these species, the formation of radical cations was expected as a result of the abstraction of an electron from the neutral pigment and lipid molecules by the primary ions of the DCTB matrix.[74] The same results were previously reported by our research group where radical cations of chlorophyll *a* and *b* and their derivatives were detected using DCTB as a matrix.[25]

On the other hand, two lipid types in the *m/z* range of 750 to 790 were detected, including 1 class of glycerophospholipids and 1 class of sphingolipids. The glycerophospholipid phosphatidylcholine PC (14:0/18:1) at *m/z* 756.536 was identified with a high signal to noise ratio (6.7 ppm, S/N 16) as $[M + K]^+$ adduct. This glycerophospholipid has several structural isomers; PC (16:0/16:1), PC (18:0/14:1), PC (16:0/16:0), PC (18:0/14:0) and PC (20:0/12:0), so any of these structures could correspond to the observed signal. Previous studies have classified phosphatidylcholines as molecular biomarkers of the *Chlorella* species, constituting the highest percentage of the total phospholipids of this microalga.[75] Similarly, the sphingolipid glycosylceramide GlcCer (15:2/22:0) at *m/z* 778.559 was identified as $[M + K]^+$ adduct. Glycosylceramides play an important role in signal transduction, membrane formation, and intercellular reorganization, and most of their functions are related to their varied chemical structures.[76,77]

During the expanding process of the gas cloud made up of vaporized matrix and intact analyte molecules, ions (e.g., H^+, Na^+ or K^+) are exchanged between them generating adducts. Therefore, the identification of these cations is an expected result since lipids have a significant affinity for alkali metals and may desorb from the matrix as Na^+ or K^+ adducts due to the high intracellular concentration of these species in the sample.[78,79] Pei and co-workers also identified lipids, phospholipids and triacylglycerides (TAGS), in corn through MALDI–MS in positive ion mode with DCTB as a matrix, suggesting that these species, like the pigments, have a lower ionization energy than the DCTB matrix, favoring the formation of cations.[80] Similar results were reported by other authors, where lipids like PCs were detected in the form of $[M + H]^+$, $[M + Na]^+$ and $[M + K]^+$.[78,81,82]

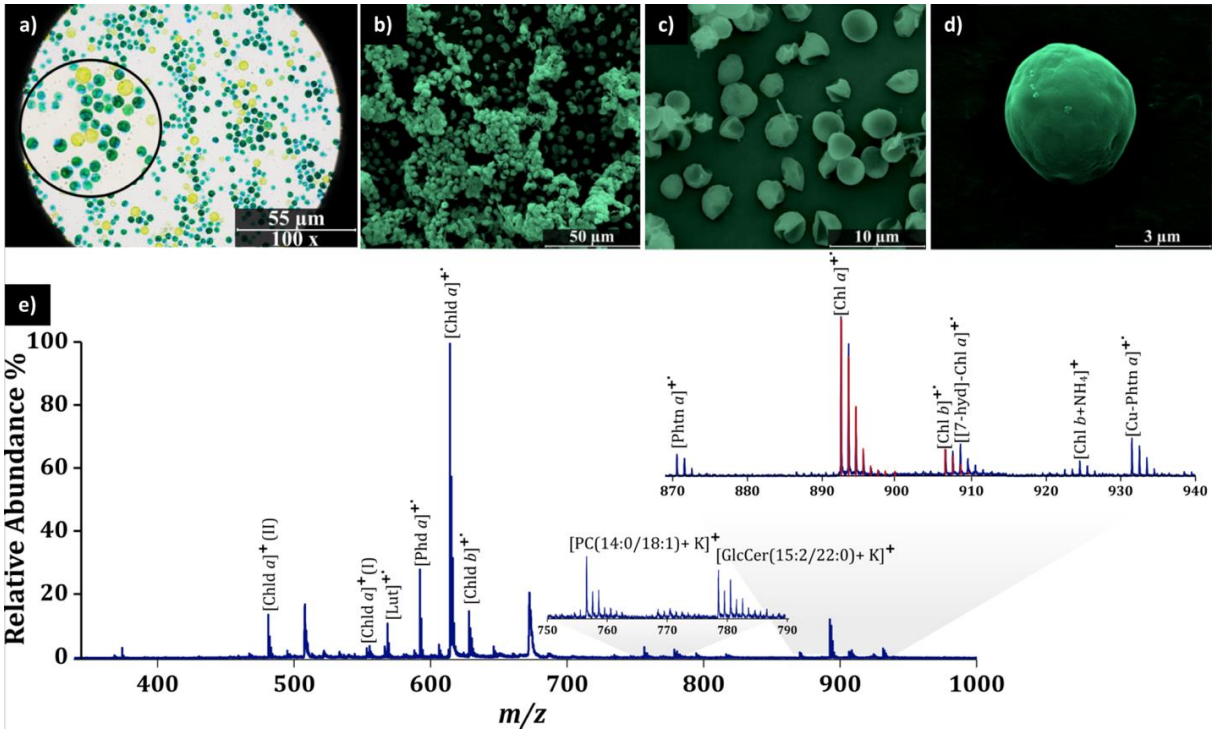

Fig. 2 a) Optical microscopy images of intact *C. vulgaris* cells stained with methylene blue. SEM images of intact cells at increasing resolution **b)** 50 µm, **c)** 10 µm **d)** 3 µm. **e)** MALDI mass spectrum (DCTB, 1:100 A:M, 2 µJ pulse) showing zoom-ins for the chlorophyll (*m/z* 870 - 940) and lipid (*m/z* 750 - 790) regions. SEM images were colored using Adobe Photoshop. Compound abbreviations are found in **Table 1**.

Table 1 Compounds detected in *C. vulgaris* intact cells by ET MALDI-MS.

Compound	**Abbreviation**	**Proposed Formula**	***m/z Theo***	**MALDI MS**		
				m/z Exp	**Mass Accuracy (ppm)**	**S/N**
Chlorophyll derivatives						
Chlorophyll *b*	Chld *b*	$[C_{35}H_{32}MgN_4O_6]^{+\bullet}$	628.217	628.218	1.3	38.1
	Chl *b*	$[C_{55}H_{70}MgN_4O_6]^{+\bullet}$	906.515	906.512	2.9	15.6
	Chl *b*-NH_4	$[C_{55}H_{70}MgN_4O_6 + NH_4]^+$	924.549	924.539	10.8	8.7
Pheophorbide *a*	Phd *a*	$[C_{35}H_{36}N_4O_5]^{+\bullet}$	592.269	592.267	3.4	100.3
Chlorophyllide *a*	Chld *a* (II)	$[C_{30}H_{25}MgN_4O]^+$	481.152	481.150	3.1	59.7
	Chld *a* (I)	$[C_{33}H_{31}MgN_4O_3]^+$	555.225	555.229	7.7	7.2
	Chld *a*	$[C_{35}H_{34}MgN_4O_5]^{+\bullet}$	614.238	614.239	1.6	245.0
Pheophytin *a*	Phtn *a*	$[C_{55}H_{74}N_4O_5]^{+\bullet}$	870.566	870.568	2.2	16.6
	Phtn *a*-Cu	$[C_{55}H_{72}N_4O_5Cu]^{+\bullet}$	931.480	931.485	5.6	25.1
Chlorophyll *a*	Chl *a*	$[C_{55}H_{72}MgN_4O_5]^{+\bullet}$	892.535	892.534	1.5	90.1
[7-hydroxymethyl]-Chl *a*	[7-hyd]-Chl *a*	$[C_{55}H_{72}MgN_4O_6]^{+\bullet}$	908.530	908.530	0.2	16.3
Carotenoids						
Lutein	Lut	$[C_{40}H_{56}O_2]^{+\bullet}$	568.428	568.431	5.3	33.3
Lipids						
Phosphatidylcholine	PC(14:0/18:1)	$[C_{40}H_{80}NO_7P + K]^+$	756.531	756.536	6.7	16.0
Glycosylceramide	GlcCer(15:2/22:0)	$[C_{43}H_{81}NO_8 + K]^+$	778.560	778.559	0.6	12.7

Figure 3e displays isolated chloroplasts' positive ion MS spectrum utilizing DCTB as an electron-transfer matrix. The ET MALDI-MS profile is dominated by radical cation (molecular ions) signals and few close shell fragments (cations). Notably, two molecular ions at *m/z* 892.533 and *m/z* 906.512, corresponding to chlorophyll *a* and *b* along with their derivatives (pheophytin *a* at *m/z* 870.562, chlorophyllide *a* at *m/z* 614.233, chlorophyllide *b* at *m/z* 628.221, and pheophorbide *a*), were identified with high signal-to-noise ratios. Additionally, lutein at *m/z* 568.427 and a novel carotenoid, loroxatin ($C_{40}H_{56}O_3$), at *m/z* 584.420 were detected, albeit with lower signal noise ratios (refer to Table 2). These carotenoids have been detected in *C. vulgaris* and other photosynthetic microorganisms such as Euglenophytas, blue-green, red and brown algae, among other species.[72–75] While Chlorophyta species typically harbour carotene, its non-identification in isolated chloroplasts may be attributed to the low bioavailability of the pigment on thylakoids or an ionization suppression effect caused by the membrane architecture. Li and colleagues reported a peak concentration of carotene within the first five days of *C. vulgaris* culture, diminishing significantly by day 13.[59] The samples analyzed in this study pertain to chloroplasts from 15- day-old cell cultures. Similarly, the microalgae growth phase might influence the absence of characteristic carotenoids such as astaxanthin, zeaxanthin, violaxanthin, and neoxanthin in the ET mass spectrum of intact chloroplasts.[59] In parallel with intact cell analysis, undetected sphingolipid (Cer(18:0/16:0) at *m/z* 556.536) were identified in intact chloroplasts. Identifying sphingolipid ceramides is noteworthy, as they constitute fundamental structural lipids in eukaryotic cell membranes, alongside sterols and glycerolipids, influencing membrane formation, stability, and fluidity, and playing a pivotal role in signalling pathways[83]

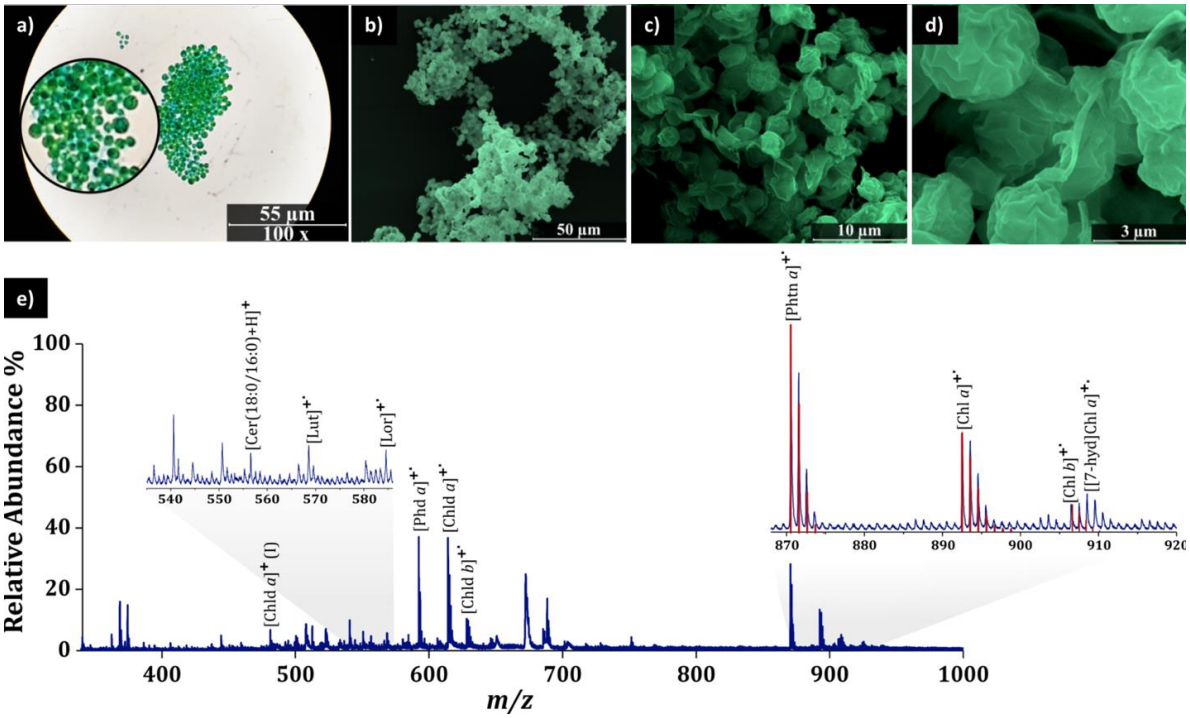

Fig. 3 a) Optical microscopy images of intact *C. vulgaris* chloroplasts stained with methylene blue. SEM images of collapsed chloroplasts at increasing resolution **b)** 50 µm, **c)** 10 µm **d)** 3 µm. **e)** MALDI mass spectrum (DCTB, 1:100 A:M, 2 µJ pulse) of chloroplasts showing zoom-ins for the chlorophyll (*m/z* 870 - 920), carotenoid and lipid (*m/z* 530 - 590) regions. See Table 2 for compound identification.

Table 2 Compounds detected in *C. vulgaris* intact chloroplasts by ET MALDI-MS.

Compound	Abbreviation	Proposed Formula	*m/z Theo*	MALDI MS		
				m/z Exp	Mass accuracy (ppm)	S/N
Chlorophyll derivatives						
Chlorophyllide *b*	Chld *b*	$[C_{35}H_{32}MgN_4O_6]^{+\bullet}$	628.217	628.221	6.1	10.3
Chlorophyll *b*	Chl *b*	$[C_{55}H_{70}MgN_4O_6]^{+\bullet}$	906.515	906.512	2.9	6.9
Pheophorbide *a*	Phd *a*	$[C_{35}H_{36}N_4O_5]^{+\bullet}$	592.269	592.273	7.4	44.8
Chlorophyllide *a*	Chld *a* (I)	$[C_{30}H_{25}MgN_4O]^{+}$	481.152	481.155	7.3	10.1
	Chld *a*	$[C_{35}H_{34}MgN_4O_5]^{+\bullet}$	614.238	614.233	8.1	41.0
Pheophytin *a*	Phtn *a*	$[C_{55}H_{74}N_4O_5]^{+\bullet}$	870.566	870.562	4.5	65.3
Chlorophyll *a*	Chl *a*	$[C_{55}H_{72}MgN_4O_5]^{+\bullet}$	892.535	892.533	2.6	27.4
[7-hydroxymethyl]-Chl *a*	[7-hyd]Chl *a*	$[C_{55}H_{72}MgN_4O_6]^{+\bullet}$	908.530	908.526	4.6	9.7
Carotenoids						
Lutein	Lut	$[C_{40}H_{56}O_2]^{+\bullet}$	568.428	568.427	1.8	4.7
Loroxanthin	Lor	$[C_{40}H_{56}O_3]^{+\bullet}$	584.423	584.420	5.0	3.3
Lipids						
Ceramide	Cer(18:0/16:0)	$[C_{34}H_{69}NO_4 + H]^{+}$	556.531	556.536	9.9	4.5

***C. vulgaris* whole cells extract ET MALDI-MS analysis.**

Ultrasound radiation-assisted extraction (UAE)

Through cavitation, UAE disrupts the cell wall of *C. vulgaris* microalgae, facilitating solvent interaction and enhancing access to pigments. In an ultrasonic procedure, the dynamic interplay between cavitation bubbles generates shockwaves, exerting powerful mechanical forces to breach cell walls and membranes, which is crucial for pigment extraction from microalgal species with resistant cell walls.[84,85] Notably, UAE is more efficient and convenient than other mechanical methods like pestle and mortar.[86] The UAE acetone pigment extract of *C. vulgaris* was analyzed using UV-Vis spectroscopy and ET MALDI mass spectrometry (see **Fig. 4** and **Table 3**). The method yielded a recovery of 56 ± 7% of *C. vulgaris* dry biomass (**Fig. 4a**). The high recovery rate achieved with acetone in UAE can be attributed to the solvent chemical structure, suitable for interactions with polar and non-polar compounds. Previous studies have reported extraction yields for *C. vulgaris* cells using UAE with acetone in the range of 20-52%.[87]

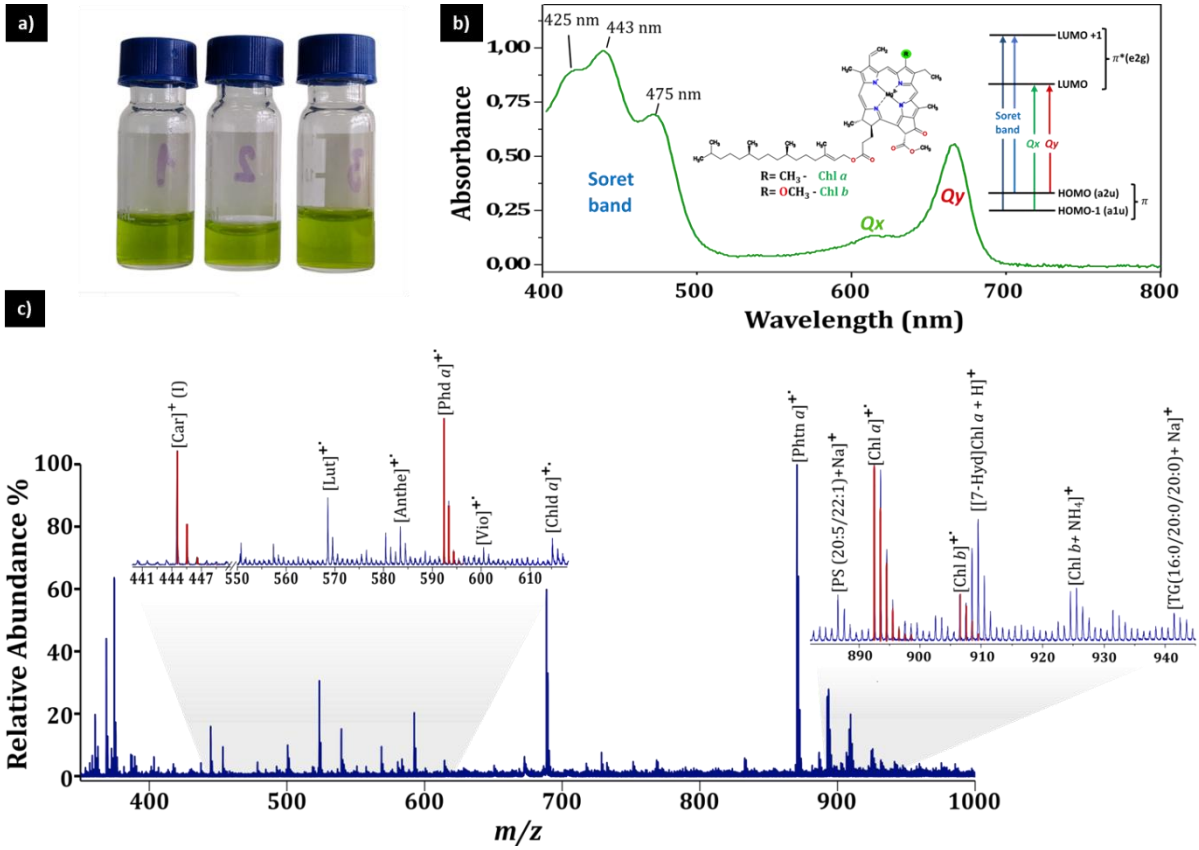

Fig 4 a) Ultrasound-assisted extracts (UAE) from biomass of *C. vulgaris* using acetone as a solvent, b) Absorption spectrum of the UAE extract, measured in acetone, and c) MALDI mass spectrum (DCTB, 1:100 A:M, 2 µJ pulse) of the extract showing zoom-ins for the chlorophyll (*m/z* 880 - 950) and carotenoids (*m/z* 441 - 620) regions. See Table 3 for compound identification.

Table 3 Compounds detected in *C. vulgaris* UAE extract by MALDI MS.

Compound	**Abbreviation**	**Proposed formula**	***m/z Theo***	**MALDI MS**		
				m/z Exp	**Mass accuracy(ppm)**	**S/N**
Chlorophyll pigments						
Pheophorbide *a*	Phd *a*	$[C_{35}H_{36}N_4O_5]^{+\bullet}$	592.268	592.266	3.4	54.7
Chlorophyllide *a*	Chld *a*	$[C_{35}H_{34}N_4O_5Mg]^{+\bullet}$	614.237	614.232	8.1	7.7
Pheophytin *a*	Phtn *a*	$[C_{55}H_{74}N_4O_5]^{+\bullet}$	870.565	870.566	1.1	169.9
[7-hydroxymethyl]-Chl *a*	[7-Hyd]Chl *a*	$[C_{55}H_{72}N_4O_6Mg]^{+\bullet}$	908.530	908.525	5.5	19.2
		$[C_{55}H_{72}N_4O_6Mg + H]^+$	909.538	909.528	11.0	19.4
Chlorophyll *b*	Chl *b*	$[C_{55}H_{70}N_4O_6Mg]^{+\bullet}$	906.514	906.499	16.5	12.7
		$[C_{55}H_{70}N_4O_6Mg + NH_4]^+$	924.548	924,533	16.2	10.6
Chlorophyll *a*	Chl *a*	$[C_{55}H_{72}N_4O_5Mg]^{+\bullet}$	892.535	892.535	0.1	42.0
		$[C_{55}H_{72}N_4O_5Mg + K]^+$	931.499	931.497	2.1	7.0
Carotenoids						
Carotene	Car	$[C_{40}H_{56} - C_7H_8]^+$	444.438	444.431	15.8	52.7
Lutein	Lut	$[C_{40}H_{56}O_2]^{+\bullet}$	568.428	568.432	7.0	23.3
Loroxanthin	Lor	$[C_{40}H_{56}O_3]^{+\bullet}$	584.422	584.427	8.6	10.0
Violaxanthin	Vio (I)	$[C_{40}H_{53}]^+$	583.617	583.621	6.9	12.6
	Vio	$[C_{40}H_{56}O_4]^{+\bullet}$	600.417	600.421	6.7	5.0
Lipids						
Ceramides	Cer(44:1;O4)	$[C_{44}H_{87}NO_5 + Na]^+$	732.648	732.629	25.9	7.2
Diacylglycerols	DG(22:2/22:2/0:0)	$[C_{47}H_{84}O_5 + Na]^+$	751.621	751.632	14.6	6.9

Phosphatidylserines	PS(13:0/20:2)	$[C_{39}H_{72}NO_{10}P + Na]^+$	768.479	768.491	15.6	9.5
	PS(19:0/20:1)	$[C_{45}H_{86}NO_{10}P + H]^+$	832.606	832.618	14.4	10.3
	PS(20:5/22:1)	$[C_{48}H_{82}NO_{10}P + Na]^+$	886.557	886.552	5.6	11.8
Triacylglycerols	TG(18:3/18:3/20:2)	$[C_{59}H_{98}O_6 + Na]^+$	925.726	925.719	7.6	7.1
	TG(16:0/20:0/20:0)	$[C_{59}H_{114}O_6 + Na]^+$	941.851	941.864	13.8	7.0

Fig. 4b depicts the UV-vis absorption regions characteristic of a chlorophyll and carotenoid mixture. Chlorophylls, derived from porphyrin, exhibit two absorption regions known as the Q and Soret bands. The Q band, weaker in strength, involves Qx and Qy transitions to the first excited state (LUMO), falling within the 550-700 nm range. Meanwhile, the Soret band, stronger in intensity, represents the transition to the second excited state (LUMO + 1), typically occurring within the 400-450 nm range.[88,89] Previous research extensively examined the frontier orbitals (HOMO and LUMO) of porphyrin macrocycles using computational and spectroscopic methods.[90–92] These studies revealed that metal-free porphyrins (e.g., pheophytin) and metal-containing porphyrins (e.g., chlorophyll) typically exhibit two a1u and a2u orbitals as HOMO and HOMO-1, along with two nearly degenerate e2g(π*) orbitals, mainly located on the porphyrin macrocycle, as depicted in **Fig. 4b**.

The presence of a1u(π) and a2u(π) orbitals is pivotal for the biochemical functions of chlorophylls in photo-oxidation processes. Chemical modifications of the macrocycle can alter the positions and strengths of the Q-bands, contingent on the specific structure of the chlorophyll derivative. For instance, chlorophyll *a* exhibits Q-bands and a Soret-band at wavelengths of 662 and 430 nm, respectively, while chlorophyll *b*'s are at 645 and 470 nm. In the case of pheophytin, the absorption maxima of the Q and Soret bands are located at 665 and 415 nm, respectively. [88,89] However, it's crucial to note that the maximum absorption values of extracted pigments may vary based on the solvent used. Previous studies have reported mixtures of chlorophylls and carotenoids in extracts obtained by UAE from *C. vulgaris* cells using UV-Vis spectroscopy. [93,94]

In MALDI MS experiments on the UAE extract of *C. vulgaris*, we identified 17 compounds, including 6 chlorophyll pigments, 4 carotenoids, and 7 lipids (see **Fig. 4c** and **Table 3**). The ET MALDI MS profile exhibits radical cation (molecular ions) signals and few close shell fragments (cations) for the chlorophylls and carotenoids. In addition, we observe lipids exclusively as sodium and potassium adducts. Chlorophyll *a* (*m/z* 892.535, $C_{55}H_{72}N_4O_5Mg$) and chlorophyll *b* (*m/z* 906.499, $C_{55}H_{70}N_4O_6Mg$) were identified as radical cations $M^{+\bullet}$, and as potassium $[M + K]^+$ and ammonium $[M + NH_4]^+$ adducts, respectively. Potassium and ammonium ions were present in the Bold Basal Medium (BMM) used to grow the microalgae. Pheophytin *a* (*m/z* 870.566, $C_{55}H_{74}N_4O_5$), chlorophyllide *a* (*m/z* 614.232, $C_{35}H_{34}N_4O_5Mg$), and pheophorbide a (*m/z* 592.266, $C_{35}H_{36}N_4O_5$) signals were detected, indicating Mg^{2+} and the phytyl chain loss.[95,96] The chlorophyll pigments were identified with relative mass accuracy values below 16.5 and high S/N values, with pheophytin *a* having the highest signal-to-noise ratio of 169.9 (**see Table 3**). Previously identified chlorophyll-derivatives in UAE extracts from *C. vulgaris* via HPLC were confirmed by ET-MALDI in this study.[22] Interestingly, the radical cation of hydroxychlorophyll *a* was detected at *m/z* 908.525 ($C_{55}H_{72}N_4O_6Mg$) with an accuracy of 5.5 ppm and a signal-to-noise ratio of 19.2. It has been previously reported that hydroxychlorophyll is a functional reaction center pigment that acts as the primary electron acceptor.[54]

Carotenoids, including carotene, lutein, antheraxanthin, and violaxanthin, considered biomarkers for *Chlorella* species, were identified through ET MALDI in the UAE extracts MS. A carotene fragment was detected at *m/z* 444.431 $[M - C_7H_8]^+$, and its isotopic distribution was compared, assigning signals with 15.8 ppm accuracy and an S/N of 52.7.[22,97] Although there are numerous potential isomers with the molecular formula $C_{40}H_{56}$, the literature indicates that β-carotene ($C_{40}H_{56}$) is the specific isomer present in

the cells of *C. vulgaris*.[98–100] Violaxanthin was identified as a cation radical at *m/z* 600.421, plus a characteristic fragment at *m/z* 583.621 $[M - 17]^+$.[22] However, fucoxanthin, commonly found in haptophytes, chrysophytes, raphidophytes, bolidophytes, and some dinoflagellates groups, [6] which was previously identified in *C. vulgaris* intact cells, was not detected in the UAE extracts. The signal at *m/z* 584.427 was assigned as antheraxanthin ($C_{40}H_{56}O_3$) or loroxanthin ($C_{40}H_{56}O_3$), structural isomers with an accuracy value of 8.6 ppm and S/N of 10 (see **Table 3**). Loroxanthin is recognized as a unique xanthophyll for identifying *Scenedesmus obliquus* and *C. vulgaris*. Research on the pigment composition of prasinophytes shows co-elution of loroxanthin ($C_{40}H_{56}O_3$) and neoxanthin ($C_{40}H_{56}O_4$) in HPLC.[101] Thus, by providing distinguishable signals for loroxanthin and neoxanthin, as radical cations, ET-MALDI offers a solution to challenges in HPLC.[52] ET MALDI MS identified various lipid species, as $[M + Na]^+$ adducts, in the UAE extracts, encompassing ceramides, diacylglycerols (DGs), phosphatidylserines (PSs), and triacylglycerols (TAGs). Some of the lipids detected in UAE extracts were not previously identified in either intact cells or chloroplasts, possibly due to differences in sample preparation. Changes in matrix disposition can impact the crystallization process, potentially leading to ion suppression. Furthermore, the abundance of a specific analyte is influenced by varying extraction and ionization efficiencies within a particular region, reflecting the outcome of changing chemical environments on the surface. This involves distinct chemical interferences and ionization suppression phenomena. Such phenomena have been previously reported in the literature.[102–104] Ceramide, Cer (44:1;O4) ($C_{44}H_{87}NO_5$) detected at *m/z* 732.629, has been previously reported in the microalgae's cell wall. [105] Diacylglycerols, such as DG (22:2/22:2/0:0) ($C_{47}H_{84}O_5$) detected at *m/z* 751.632, represent essential lipid components in microalgae chloroplasts with roles in structural membranes and cellular signaling. DGs constitute about 30% of total neutral lipids in *Chlorella*,[106,107] yet were not identified in direct analysis of *C. vulgaris* cells. Phosphatidylserines (PSs), reported in Chlorella by other authors, were detected via ET MALDI, likely facilitated by acetone extraction. PSs, found on the cytosolic side of cellular membranes, indicate apoptotic bodies. [108] Interestingly, PSs were also identified in the direct analysis of intact chloroplasts. Triacylglycerols (TAGs), widely reported in Chlorella,[106] were also detected. TAGs serve as energy reserves and are synthesized under stress conditions by microalgae. [109] TAG contents and types exhibit substantial variations in microalgae and are highly dependent on strains and growth conditions. [109] TAGs were not identified previously in either intact cells or chloroplasts.

Supercritical fluid extraction

Supercritical fluid extraction (SFE) with CO_2 as a solvent is a well-established method for obtaining extracts rich in non-polar lipid compounds from microalgae, including *C. vulgaris*.[72] Carbon dioxide, the most widely used supercritical solvent, offers benefits such as low temperature and pressure, low reactivity with many chemical compounds, low flammability, and cost-effectiveness.[110] In our study, SFE with CO_2 was applied to extract lipids from lyophilized biomass of *C. vulgaris*, with subsequent analysis using UV-Vis spectroscopy and MALDI mass spectrometry (see Fig. 5 and Table 4). The SFE method yielded an extract corresponding to 11 ± 4 wt % of the initial *C. vulgaris* dry biomass (Fig. 5a). Literature reports indicate lipid content in *C. vulgaris* cells ranging from 30-35 wt %. [111] However, the lipid yield and composition vary with growth conditions, stage, and extraction methodology; for SFE, typical recovery values of 15 to 24 are reported.[14,112] This recovery percentage depends on the physicochemical properties of supercritical CO_2, such as viscosity, diffusion, and solubility power, which are determined by density, pressure, temperature, polarity, acid-base properties, and hydrogen bond formation.[13] Some studies suggest improved extraction yields by adding co-solvents (acetone, ethanol) or

mechanical grinding of the microalgae biomass.[113] In this study, we added glass beads to prevent aggregate formation and enhance extraction efficiency.

Fig. 5 displays the UV-Vis spectrum of the SFE extract, revealing low absorbance bands related to carotenoids (400-450 nm) and chlorophyll derivatives (665 nm). Despite CO_2 selectivity towards non-polar compounds, the presence of chlorophyll derivatives is related to the phytol chain, an essential moiety for anchoring these molecules to the thylakoid membrane. The UV-Vis spectrum also shows characteristic bands of lutein at λ_{max} 421, 445, and 473 nm.[114] However, precise molecular differentiation of carotenoids via UV-Vis analysis is challenging due to broad absorption signals in the visible region due to their extended conjugated electron systems[115]

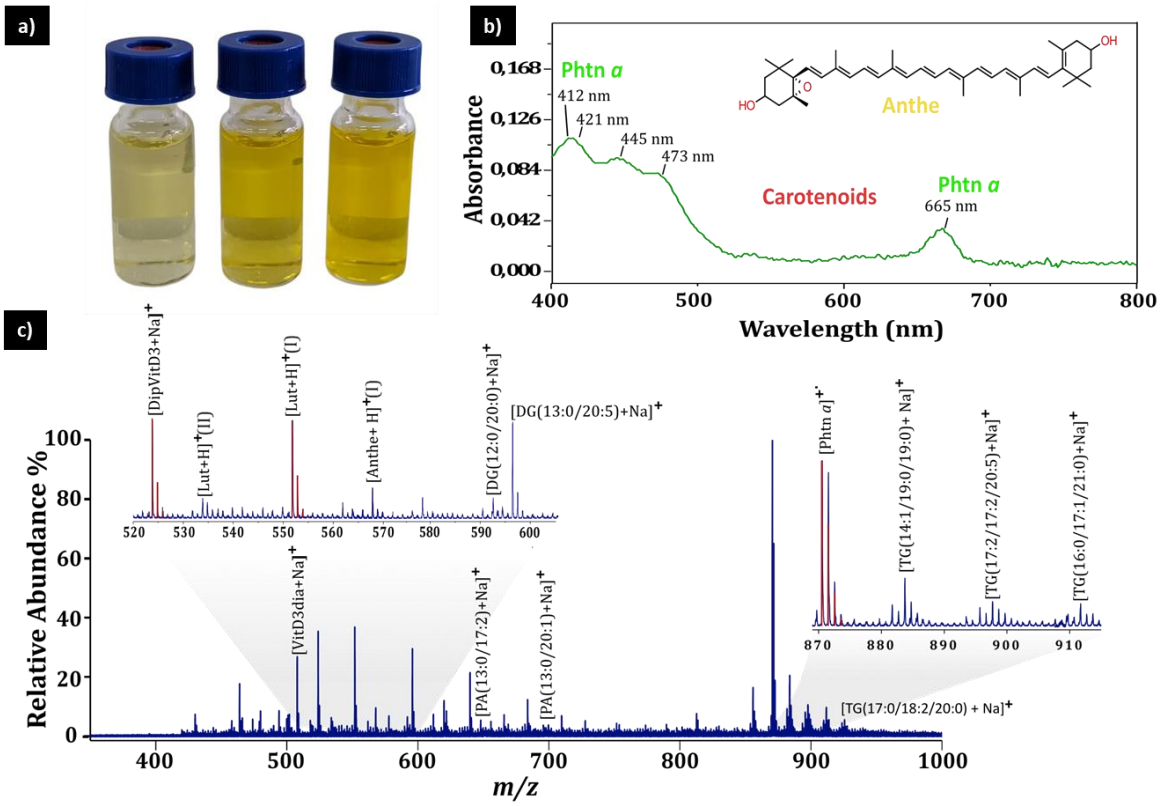

Fig. 5 a) Supercritical Fluid Extraction (SFE) from biomass of *C. vulgaris* using supercritical CO_2 as a solvent, b) Absorption spectrum of the SFE extract, measured in acetone, and c) MALDI mass spectrum (DCTB, 1:100 A:M, 2 µJ pulse) of the extract showing zoom-ins for chlorophyll pigments (*m/z* 870-915) and carotenoids (*m/z* 520-610) regions. See Table 4 for compound identification.

Table 4 Compounds detected in *C. vulgaris* SFE extract by MALDI MS.

Compound	Abbreviation	Proposed formula	*m/z Theo*	MALDI MS		
				m/z Exp	Mass accuracy (ppm)	S/N
Chlorophyll pigments						
Pheophytin *a*	Phtn *a*	$[C_{55}H_{74}N_4O_5]^{+\bullet}$	870.565	870.565	0.1	129.6
Carotenoids						
Lutein	Lut (II)	$[C_{40}H_{53}]^+$	533.428	533.431	5.6	7.8
	Lut(I)	$[C_{40}H_{55}O]^+$	551.428	551.440	21.8	55.5
Antheraxanthin	Ante	$[C_{40}H_{55}O_2]^+$	567.422	567.431	15.9	12.2
Lipids						
Vitamin D3 and derivatives	Vitamin D3 derivate	$[C_{29}H_{44}O_3 + Na]^+$	463.318	463.311	16.8	39.6

	Vitamin D3 diacetate	$[C_{31}H_{48}O_4 + Na]^+$	507.345	507.339	11.8	49.3
	DipropylVitamin D3	$[C_{33}H_{56}O_3 + Na]^+$	523.412	523.417	8.2	57.7
Diacylglycerophosphoglycerols	PG(10:0/10:0)	$[C_{26}H_{51}O_{10}P + Na]^+$	577.311	577.316	7.4	7.3
Diacylglycerols	DG(12:0/20:0)	$[C_{35}H_{68}O_5 + Na]^+$	591.496	591.500	6.8	8.2
	DG(13:0/20:5)	$[C_{36}H_{60}O_5 + Na]^+$	595.433	595.431	3.4	42.8
	DG(dO-36:4)	$[C_{39}H_{72}O_3 + Na]^+$	611.537	611.530	11.4	9.0
	DG(15:0/19:0)	$[C_{37}H_{72}O_5 + Na]^+$	619.527	619.535	12.9	16.7
	DG(13:0/22:6)	$[C_{38}H_{62}O_5 + Na]^+$	621.449	621.442	11.3	107.0
Diacylglycerophosphates	PA(13:0/17:2)	$[C_{33}H_{61}O_8P + Na]^+$	639.400	639.400	0.2	29.7
	PA(14:0/18:3)	$[C_{35}H_{63}O_8P + Na]^+$	665.415	665.411	6.0	8.1
	PA(13:0/20:1)	$[C_{36}H_{69}O_8P + Na]^+$	683.462	683.450	17.6	14.2
Phosphatidylserines	PS(20:1/22:6)	$[C_{48}H_{80}NO_{10}P + Na]^+$	812.541	812.550	11.1	8.9
Triacylglycerols	TG(16:0/16:0/18:1)	$[C_{53}H_{100}O_6 + Na]^+$	855.741	855.744	3.5	23.9
	TG(15:0/15:0/22:2)	$[C_{55}H_{102}O_6 + Na]^+$	881.757	881.748	10.2	12.3
	TG(14:1/19:0/19:0)	$[C_{55}H_{104}O_6 + Na]^+$	883.773	883.766	7.9	27.4
	TG(17:2/17:2/20:5)	$[C_{57}H_{92}O_6 + Na]^+$	895.679	895.683	4.5	10.5
	TG(17:2/17:2/20:4)	$[C_{57}H_{94}O_6 + Na]^+$	897.694	897.705	12.3	15.3
	TG(16:1/16:1/22:0)	$[C_{57}H_{106}O_6 + Na]^+$	909.788	909.783	5.5	7.3
	TG(16:0/17:1/21:0)	$[C_{57}H_{108}O_6 + Na]^+$	911.804	911.799	5.5	10.9
	TG(17:0/18:2/20:0)	$[C_{58}H_{108}O_6 + Na]^+$	923.804	923.794	10.8	6.0
	TG(18:3/18:3/20:2)	$[C_{59}H_{98}O_6 + Na]^+$	925.761	925.763	2.2	6.2

Using MALDI MS experiments, we identified 25 compounds in the SFE extract of *C. vulgaris*, comprising 1 chlorophyll pigment, 2 carotenoids, and 22 lipids (see **Fig. 5c** and **Table 4**). ET MALDI MS profile reveals radical cation signals and a few close-shell fragments for chlorophylls and carotenoids. Notably, unlike intact cells and chloroplasts ET-MALDI profiles, lipids are observed only as sodium and potassium adducts. Ions may possibly form through direct interactions between oxygen atoms in lipids and Na cations. Additionally, the electron-transfer matrix used (DCTB, 8.54 eV, vapor pressure $9.09x10^{-7}$ mm Hg at 25 °C)[116] could facilitate the desorption of preformed ions during the MALDI process. The MS profile of the SFE extract differs significantly from that of ultrasound-assisted extraction (UAE). Pheophytin was detected in the SFE extract at *m/z* 870.565 ($C_{55}H_{74}N_4O_5$) with S/N 129.6, isolation of this chlorophyll derivative is associated with the presence of the phytol moiety, as discussed previously. Additionally, lutein ($C_{40}H_{56}O_2$) and antheraxanthin ($C_{40}H_{56}O_3$) were identified in the SFE extract. The decomposition of the radical cation $M^{+\bullet}$ of lutein results in two fragments: one at *m/z* 551.440 attributed to the loss one $OH^{\bullet}$, and another at *m/z* 533.431 resulting from the loss of an $OH^{\bullet}$, and a water molecule.[22] Antheraxanthin, radical cation $M^{+\bullet}$ exhibited a distinctive loss of $OH^{\bullet}$ $[M - 17]^+$, with a signal-to-noise ratio of 12.2. Several studies have identified carotenoids with commercial potential in SFE extracts from *Chlorella*. For instance, Kitada K. et al. found that CO_2 has high selectivity for extracting lutein ($C_{40}H_{56}O_2$), a carotenoid with multiple health benefits.[113] Also, adding ethanol or acetone as a co-solvent extracts chlorophyll *a* and *b* and lutein. Fan et al. used ultrasound-assisted subcritical CO_2 extraction (USCCE) to extract lutein from *Chlorella pyrenoidosa* achieving high extraction yields under milder conditions compared to supercritical CO_2 extraction.[117]

As previously mentioned, the Supercritical Fluid Extraction (SFE) of *C. vulgaris* resulted in an extract enriched with lipid compounds. Interestingly, the analysis of this extract through MALDI revealed a profile of lipids, including vitamin D3 and some of its derivatives, diacylglycerophosphoglycerols, diacylglycerols, diacylglycerophosphates, diacylglycerophosphoserines, and triacylglycerols. $ScCO_2$, being non-polar, has high selectivity towards neutral lipids, especially acylglycerols (TAG, DAG) and sterols. This, together with its low capacity for solubilizing phospholipids, makes the process highly

specific towards TAGs and sterols.[118] As a result, SFE allowed for the isolation and detection of a higher number of TAGs and DAGs compared to ultrasound-assisted extraction (UAE) through MALDI. You can see the details in **Fig. 5c** and **Table 4.**

In this study, we identified a variety of phospholipids, including one diacylglycerophosphoglycerols (PG), PG (10:0/10:0) $C_{26}H_{51}O_{10}P$ (11.1 ppm and S/N 8.9); three PA, PA (13:0/17:2) $C_{33}H_{61}O_8P$ (0.2 ppm and S/N 29.7), PA (14:0/18:3) $C_{35}H_{63}O_8P$ (6.0 ppm and S/N 8.1), PA (13:0/20:1) $C_{36}H_{69}O_8P$ (17.6 ppm and S/N 14.2); and one PS, PS (20:1/22:6) $C_{48}H_{80}NO_{10}P$ (11.1 ppm and S/N 8.9). These glycerophospholipids are abundant in the molecular composition of microalgae membranes, and their amphiphilic nature makes them extractable using $ScCO_2$. However, we found that the number of PSs detected in the SFE extract using ScCO2 was lower than that in the UAE extract. We also observed that ceramides were not identified in the SFE extract, possibly due to their polar nature. We also conducted MALDI assays on the SFE extract and identified vitamin D3 derivatives. Vitamin D3 is a sterol derivative that has been previously reported in microalgae such as *Chlorella*. It is important to note that vitamin D3 is a crucial nutrient in the human diet, and fish is the main source of this vitamin due to its bioaccumulation from the microalgae they consume.[119,120] Interestingly, microalgae synthesize vitamin D3 by converting 7-dehydrocholesterol under exposure to ultraviolet B light.[121]

The number of chemical species that were identified based on criteria such as the previous literature, measurement accuracy, and comparison of isotopic patterns was relatively low compared to the total number of signals detected. This could be attributed to the fact that the database of pigments previously reported in *C. vulgaris* cells may not be comprehensive, and therefore, other ionizable and extracted chemical species that are not pigments may be present. High-resolution mass spectrometry (HR MS) analysis can help address this issue by providing greater accuracy in mass measurement and reducing the number of possible molecular formulas. Additionally, analyzing the fine isotopic pattern can help correlate these unidentified species with their molecular formulas.

Conclusions

The direct MALDI-ET analysis of intact cells and isolated chloroplasts from *C. vulgaris* allowed the identification of chlorophylls, carotenoids and lipids present in the different cell membranes (cell wall, thylakoids and chloroplasts envelope) classified as chemotaxonomic markers of this species. The DCTB matrix demonstrated to possess favorable thermochemical properties to undergo electron-transfer reactions with pigments from intact cells and isolated chloroplast, promoting their radical ion formation. The low ionization energy of chlorophyll *a*, *b*, their derivatives, carotenoids such as loroxanthin and lutein and lipids with respect to the ionization energy of the DCTB matrix (E_i: 8.54 eV) favored the ionization process generating radical cations and potassium adducts in the case of lipids.

Acknowledgements

We thank Guatiguará Technology Park and the Central Research Laboratory Facility (Microscopy laboratories) at Universidad Industrial de Santander for infrastructural support. We also acknowledge funding from MINCIENCIAS (Grant 2019000100020), and a graduate fellowship from COLCIENCIAS Program No. 812/2018.

References

1 Y. Sekerci and S. Petrovskii, *Bull Math Biol*, 2015, **77**, 2325–2353.

2 M. A. Borowitzka, in *Microalgae in Health and Disease Prevention*, 2018, pp. 23–72.

3 S. Marimuthu, Master thesis, University of Malaya, Malaysia, 2011.

4 C. Safi, B. Zebib, O. Merah, P.-Y. Pontalier and C. Vaca-Garcia, *Renewable and Sustainable Energy Reviews*, 2014, **35**, 265–278.

5 C. Safi, B. Zebib, O. Merah, P. Y. Pontalier and C. Vaca-Garcia, *Renewable and Sustainable Energy Reviews*, 2014, **35**, 265–278.

6 S. Roy, C. Llewellyn, E. Egeland and G. Johnsen, *Phytoplankton Pigments. Characterization, Chemotaxonomy and Applications in Oceanography*, 2013.

7 S. Jeffrey, *Phytoplankton pigments in oceanography: guidelines to modern methods*, 1997.

8 A. V. Kustov, D. V. Belykh, N. L. Smirnova, E. A. Venediktov, T. V. Kudayarova, S. O. Kruchin, I. S. Khudyaeva and D. B. Berezin, *Dyes and Pigments*, 2018, **149**, 553–559.

9 M. Grassino, D. J. Batstone, K. W. L. Yong, G. Capson-Tojo and T. Hülsen, *Talanta*, 2022, **246**.

10 H. W. Lee, S. W. Roh, K. Cho, K. N. Kim, I. T. Cha, K. J. Yim, H. S. Song, Y. Do Nam, T. Oda, Y. H. Chung, S. J. Kim, J. S. Choi and D. Kim, *Talanta*, 2015, **132**, 630–634.

11 T. U. H. Baumeister, M. Vallet, F. Kaftan, A. Svatoš and G. Pohnert, 2019, **10**, 1–9.

12 R. Ouedraogo, A. Daumas, C. Capo, J. L. Mege and J. Textoris, *J Vis Exp*, 2013, **82**, 50926.

13 S. Tzima, I. Georgiopoulou, V. Louli and K. Magoulas, *Molecules*, 2009, **84**, 657-661.

14 B. Kiwa Kitada, a Siti Machmudah, b, c Mitsuru Sasaki, a Motonobu Goto and d S. K. and T. H. Yuya Nakashima, *J Chem Technol Biotechnol*, 2009, **84**, 657–661.

15 M. Amin, P. Chetpattananondh, M. N. Khan, F. Mushtaq and S. K. Sami, in *IOP Conference Series: Materials Science and Engineering*, Institute of Physics Publishing, 2018, vol. 414.

16 F. Pagels, R. N. Pereira, A. A. Vicente and A. C. Guedes, *Applied Sciences (Switzerland)*, 2021, **11**.

17 R. Martins, C. Mouro, R. Pontes, J. Nunes and I. Gouveia, *Bioresour Bioprocess*, 2023, **10**, DOI:10.1186/s40643-023-00692-x.

18 F. Mascia, L. Girolomoni, M. J. P. Alcocer, I. Bargigia, F. Perozeni, S. Cazzaniga, G. Cerullo, C. D'Andrea and M. Ballottari, *Sci Rep*, 2017, **7**.

19 A. Angelova, S. H. Park, J. Kyndt, K. Fitzsimmons and J. K. Brown, *J Appl Phycol*, 2014, **26**, 209–218.

20 L. Garczarek, G. W. M. Van Der Staay, J. C. Thomas and F. Partensky, *Isolation and characterization of Photosystem I from two strains of the marine oxychlorobacterium Prochlorococcus*, 1998, vol. 56.

21 T. Hardo Panintingjati Brotosudarmo, L. Limantara, R. Dwi Chandra and Heriyanto, in *Plant Growth and Regulation - Alterations to Sustain Unfavorable Conditions*, IntechOpen, 2018.

22 H. A. Pantami, M. S. A. Bustamam, S. Y. Lee, I. S. Ismail, S. M. M. Faudzi, M. Nakakuni and K. Shaari, *Mar Drugs*, 2020, **18**.

23 T. Alam, L. Najam and A. Al Harrasi, *Journal of Agricultural and Marine Sciences*, 2019, **23**, 81–91.

24 X. Hu and R. Tanaka, *Plant Methods*, 2014, **9**, 1–19.

25 L. M. Díaz-sánchez, C. Blanco-tirado and M. Y. Combariza, 2023, **10**.

26 T. U. H. Baumeister, M. Vallet, F. Kaftan, L. Guillou, A. Svatoš and G. Pohnert, *Metabolomics*, 2020, **16**.

27 J. Wei, H. Li, M. P. Barrow and P. B. O'Connor, *J Am Soc Mass Spectrom*, 2013, **24**, 753–760.

28 D. Barbano, R. Diaz, L. Zhang, T. Sandrin and H. Gerken, 2015, 1–13.

29 L. J. Castellanos-García, B. C. Agudelo, H. F. Rosales, M. Cely, C. Ochoa-Puentes, C. Blanco-Tirado, C. A. Sierra and M. Y. Combariza, *J Am Soc Mass Spectrom*, 2017, **28**, 2548–2560.

30 D. Giraldo-Dávila, M. L. Chacón-Patiño, J. S. Ramirez-Pradilla, C. Blanco-Tirado and M. Y. Combariza, *Fuel*, 2018, **226**, 103–111.

31 J. S. Ramírez-Pradilla, C. Blanco-Tirado, M. Hubert-Roux, P. Giusti, C. Afonso and M. Y. Combariza, *Energy and Fuels*, 2019, **33**, 3899–3907.

32 J. S. Ramírez-Pradilla, C. Blanco-Tirado and M. Y. Combariza, *ACS Appl Mater Interfaces*, 2019, **11**, 10975–10987.

33 J. A. Oñate-Gutiérrez, L. M. Díaz-Sánchez, D. L. Urbina, J. R. Pinzón, C. Blanco-Tirado and M. Y. Combariza, *RSC Adv*, 2023, **13**, 12712–12722.

34 M. Von Bergen, A. Ihling, F. Schmidt and J. Murugaiyan, 2009, **3**, 774–784.

35 A. Nicolau, L. Sequeira, C. Santos and M. Mota, 2014, **20**, 139–144.

36 D. Barbano, R. Diaz, L. Zhang, T. Sandrin and H. Gerken, 2015, 1–13.

37 K. Emami, E. Hack, A. Nelson, C. M. Brain, F. M. Lyne, E. Mesbahi, J. G. Day and G. S. Caldwell, *Sci Rep*, 2015, **5**, 1–15.

38 L. M. De Andrade, M. A. Mendes, P. Kowalski, W. Corporation and C. A. O. Nascimento, 2017, **29**, 295–303.

39 A. Vieler, C. Wilhelm, R. Goss and S. Rosmarie, 2007, **150**, 143–155.

40 M. A. Danielewicz, L. A. Anderson, A. K. Franz and J. Lipid, 2011, **52**, 2101–2108.

41 P. L. Urban, T. Schmid, A. Amantonico and R. Zenobi, 2011, 1843–1849.

42 T. Suzuki, H. Midonoya and Y. Shioi, 2009, **390**, 57–62.

43 Y. Weesepoel, 2014, Thesis, Wageningen, NL.

44 T. U. H. Baumeister, M. Vallet, F. Kaftan, A. Svatoš and G. Pohnert, 2019, **10**, 1–9.

45 P. R. Hsueh, T. F. Lee, S. H. Du, S. H. Teng, C. H. Liao, W. H. Sheng and L. J. Teng, *J Clin Microbiol*, 2014, **52**, 2371–2379.

46 B. H. Schmitt, S. A. Cunningham, A. L. Dailey, D. R. Gustafson and R. Patel, *J Clin Microbiol*, 2013, **51**, 782–786.

47 A. P. Gregory and R. N. Clarke, *Meas Sci Technol*, 2005, **16**, 1506–1516.

48 Y. Zhang, J. Yang and Y. X. Yu, *Journal of Physical Chemistry B*, 2005, **109**, 13375–13382.

49 S. K. Saseendran, *J Algal Biomass Util*, 2017, **4**, 47–52.

50 M. M. Maroneze, L. Q. Zepka, E. J. Lopes, A. Pérez-Gálvez and M. Roca, *Antioxidants*, 2019, **8**.

51 America Public Health Association, Washington, DC, 20th edn.

52 L. M. Díaz-sánchez, C. Blanco-tirado and M. Y. Combariza, *MethodsX*, 2023, **10**.

53 E. Marisel Fernandez, *Dinámica de Nutrientes, Materia Orgánica y Clorofila a en planicies de marea cubiertas por matas microbianas*, 2017.

54 S. Roy, C. Llewellyn, E. Egeland and G. Johnsen, *Phytoplankton Pigments. Characterization, Chemotaxonomy and Applications in Oceanography*, 2013.

55 M. J. Griffiths, C. Garcin, R. P. van Hille and S. T. L. Harrison, *J Microbiol Methods*, 2011, **85**, 119–123.

56 S. Daliry, A. Hallajisani, J. Mohammadi Roshandeh, H. Nouri and A. Golzary, *Global Journal of Environmental Science and Management*, 2017, **3**, 217–230.

57 M. del P. Sánchez-Saavedra, D. Sauceda-Carvajal, F. Y. Castro-Ochoa and C. A. Molina-Cárdenas, *Bioenergy Res*, 2020, **13**, 487–498.

58 A. Angelova, S. H. Park, J. Kyndt, K. Fitzsimmons and J. K. Brown, *J Appl Phycol*, 2014, **26**, 209–218.

59 T. Li, J. Xu, B. Gao, W. Xiang, A. Li and C. Zhang, *Algal Res*, 2016, **16**, 481–491.

60 R. Knochenmuss and R. Zenobi, *Chem Rev*, 2003, **103**, 441–452.

61 R. Knochenmuss, *Analyst*, 2014, **139**, 147–156.

62 R. Knochenmuss, *Analyst*, 2006, **131**, 966–986.

63 C. A. Padilla Jaramillo, L. M. Díaz Sánchez, M. Y. Combariza Montañez, C. Blanco Tirado and A. F. Combariza Montañez, *Orinoquia*, 2021, **25**, 13–23.

64 C. D. Calvano, G. Ventura, T. R. I. Cataldi and F. Palmisano, *Anal Bioanal Chem*, 2016, **21**, 6369–6379.

65 J. Wei, H. Li, M. P. Barrow and P. B. O'Connor, *J Am Soc Mass Spectrom*, 2013, **24**, 753–760.

66 E. Jacob-Lopes, M. I. Queiroz and L. Q. Zepka, *Pigments from microalgae handbook*, 2020.

67 A. Saide, C. Lauritano and A. Ianora, *Mar Drugs*, 2020, 18.

68 N. W. Qiu, D. C. Jiang, X. S. Wang, B. S. Wang and F. Zhou, *Photosynthetica*, 2019, 57, 974–984.

69 S. Rose, University of Nebraska, 2015.

70 S. C. Silva, I. C. F. R. Ferreira, M. M. Dias and M. Filomena Barreiro, *Molecules*, 2020, **25**, 1–23.

71 L. Yao, J. A. Gerde, S. Lee, T. Wang and K. A. Harrata, *J. Agric. Food Chem*, 2015, **63**, 1773−1787.

72 M. Solana, C. S. Rizza and A. Bertucco, *Journal of Supercritical Fluids*, 2014, **92**, 311–318.

73 L. Gouveia, V. Veloso, A. Reis, H. Fernandes, J. Novais and J. Empis, *Bioresour Technol*, 1996, **57**, 157–159.

74 C. A. Padilla Jaramillo, L. M. Díaz Sánchez, M. Y. Combariza Montañez, C. Blanco Tirado and A. F. Combariza Montañez, *Orinoquia*, 2021, **25**, 13–23.

75 S. Lu, J. Wang, Q. Ma, J. Yang, X. Li and Y. J. Yuan, *PLoS One*, 2013.

76 A. Arakaki, D. Iwama, Y. Liang, N. Murakami, M. Ishikura, T. Tanaka and T. Matsunaga, *Phytochemistry*, 2013, **85**, 107–114.

77 A. Arakaki, D. Iwama, Y. Liang, N. Murakami, M. Ishikura, T. Tanaka and T. Matsunaga, *Phytochemistry*, 2014, 99, 135–136.

78 K. M. Engel, P. Prabutzki, J. Leopold, A. Nimptsch, K. Lemmnitzer, D. R. N. Vos, C. Hopf and J. Schiller, *Prog Lipid Res*, 2022, 86.

79 R. C. Murphy, J. A. Hankin and R. M. Barkley, *J Lipid Res*, 2009, 50.

80 X. L. Pei, X. N. Liu, J. L. Du, C. Gong and X. Xu, *Int J Mass Spectrom*, 2020, **455**.

81 P. Xie, H. Zhang, P. Wu, Y. Chen and Z. Cai, *Anal Chem*, 2022, **94**, 13667–13675.

82 Y. Zhang and H. Lu, *Chin J Chem*, 2012, **30**, 2091–2096.

83 S. Rose, University of Nebraska, 2015.

84 S. Sarkar, M. S. Manna, T. K. Bhowmick and K. Gayen, *Process Biochemistry*, 2020, **96**, 58–72.

85 M. Stramarkou, S. Papadaki, K. Kyriakopoulou and M. Krokida, *J Appl Phycol*, 2017, **29**, 2947–2960.

86 S. Weber, P. M. Grande, L. M. Blank and H. Klose, *PLoS One*, 2022, **17**, 1–14.

87 A. Carreira-Casais, P. Otero, P. Garcia-Perez, P. Garcia-Oliveira, A. G. Pereira, M. Carpena, A. Soria-Lopez, J. Simal-Gandara and M. A. Prieto, *Int J Environ Res Public Health*, 2021, **18**.

88 G. Calogero, A. Bartolotta, G. Di Marco, A. Di Carlo and F. Bonaccorso, *Chem Soc Rev*, 2015, **44**, 3244–3294.

89 C. Chen, N. Gong, Z. Li, C. Sun and Z. Men, *Molecules*, 2017, **22**.

90 V. Suendo and S. Viridi, *ITB Journal of Science*, 2012, **44 A**, 93–112.

91 Y. Kinoshita, Y. Kitagawa and H. Tamiaki, *Chemistry - A European Journal*, 2016, **22**, 9996–10001.

92 R. Giovannetti, *Macro To Nano Spectroscopy*, 2011, DOI:10.5772/38797.

93 P. Bhuvana, P. Sangeetha, V. Anuradha and M. S. Ali, *Biocatal Agric Biotechnol*, 2019, **19**, 101094.

94 H. K. Lichtenthaler and C. Buschmann, *Current Protocols in Food Analytical Chemistry*, 2001, **1**, F4.3.1-F4.3.8.

95 P. Matile, H. Stefan and H. Thomas, *Annu Rev Plant Physiol Plant Mol Biol*, 1999, **50**, 67–95.

96 S. H. Schanderl, C. O. Chichester and G. L. Marsh, *Journal of Organic Chemistry*, 1962, **27**, 3865–3868.

97 R. Kaufmann, T. Wingerath, D. Kirsch, W. Stahl and H. Sies, 1996, **128**, 1–12.

98 H. A. Pantami, M. S. A. Bustamam, S. Y. Lee, I. S. Ismail, S. M. M. Faudzi, M. Nakakuni and K. Shaari, *Mar Drugs*, 2020, **18**, DOI:10.3390/MD18070367.

99 R. Othman, N. H. Noh, F. A. M. Hatta and M. A. Jamaludin, *Journal of Pharmacy and Nutrition Sciences*, 2018, **8**, 1–5.

100 A. Gille, U. Neumann, S. Louis, S. C. Bischoff and K. Briviba, *J Funct Foods*, 2018, **49**, 285–294.

101 N. Sanz, A. García-Blanco, A. Gavalás-Olea, P. Loures and J. L. Garrido, *Methods Ecol Evol*, 2015, **6**, 1199–1209.

102 P. O. ¨ Nnerfjord, S. Ekström, J. Bergquist, J. Nilsson, T. Laurell and G. Marko-Varga, *Homogeneous Sample Preparation for Automated High Throughput Analysis with Matrix-assisted Laser Desorption/Ionisation Time-of-flight Mass Spectrometry*.

103 I. Rzagalinski and D. A. Volmer, *Biochim Biophys Acta Proteins Proteom*, 2017, 1865, 726–739.

104 K. Wiangnon and R. Cramer, *Anal Chem*, 2015, **87**, 1485–1488.

105 S. Yamashita, T. Miyazawa, O. Higuchi, H. Takekoshi, T. Miyazawa and M. Kinoshita, *J Nutr Sci Vitaminol (Tokyo)*, 2022, **68**, 353–357.

106 K. Y. Teh, S. H. Loh, A. Aziz, K. Takahashi, A. W. M. Effendy and T. S. Cha, *Sci Rep*, 2021, **11**, 1–12.

107 C. José de Andrade and L. Maria de Andrade, *Journal of Advanced Research in Biotechnology*, 2017, **2**, 1–9.

108 J. Schiller, R. Süß, J. Arnhold, B. Fuchs, J. Leßig, M. Müller, M. Petković, H. Spalteholz, O. Zschörnig and K. Arnold, *Prog Lipid Res*, 2004, **43**, 449–488.

109 L. Yao, J. A. Gerde, S. L. Lee, T. Wang and K. A. Harrata, *J Agric Food Chem*, 2015, **63**, 1773–1787.

110 L. Coco-Enríquez, J. Muñoz-Antón and J. M. Martínez-Val, *Int J Hydrogen Energy*, 2017, **42**, 17611–17631.

111 S. Tzima, I. Georgiopoulou, V. Louli and K. Magoulas, *Molecules*, 2023, **28**.

112 M. Solana, C. S. Rizza and A. Bertucco, *Journal of Supercritical Fluids*, 2014, **92**, 311–318.

113 B. Kiwa Kitada, a Siti Machmudah, b, c Mitsuru Sasaki, a Motonobu Goto and d S. K. and T. H. Yuya Nakashima, *J Chem Technol Biotechnol*, 2009, **84**, 657–661.

114 J. M. Kurniawan, M. M. Yusuf, S. S. Azmi, K. P. Salim, M. N. Utami Prihastyanti, R. Indrawati, Heriyanto, Y. Shioi, L. Limantara and T. H. P. Brotosudarmo, *IOP Conf Ser Mater Sci Eng*, 2019, **519**.

115 Y. Song and L. Lu, *J Lumin*, 2023, **257**, 119677.

116 United States Environmental Protection Agency, US EPA Estimation Programs Interface SuiteTM for Microsoft® Windows, v 4.11.

117 X. D. Fan, Y. Hou, X. X. Huang, T. Q. Qiu and J. G. Jiang, *J Agric Food Chem*, 2015, **63**, 4597–4605.

118 A. Patel, L. Matsakas, K. Sartaj and R. Chandra, *Extraction of lipids from algae using supercritical carbon dioxide*, Elsevier Inc., 2019.

119 F. Sandgruber, A. Gielsdorf, A. C. Baur, B. Schenz, S. M. Müller, T. Schwerdtle, G. I. Stangl, C. Griehl, S. Lorkowski and C. Dawczynski, *Mar Drugs*, 2021, **19**, 1–23.

120 T. Bito, E. Okumura, M. Fujishima and F. Watanabe, *Nutrients*, 2020, **12**, 1–21.

121 K. SS and D. SL, *J Pharmacogn Phytochem*, 2020, **9**, 69–71.

Chapter 3

Insights into the compositional space and molecular signatures of microalgae pigment extracts from MALDI 21T-FT-ICR mass spectrometry

Edited from: Luis M. Díaz-Sánchez, Martha L. Chacón-Patiño, Chad R. Weisbrod, Cristian Blanco-Tirado, Marianny Y. Combariza, Algal Research, Under review. 2024.

Keywords
Compositional space; Microalgae; Chlorophylls; Carotenoids; Matrix Assisted Laser Desorption Ionization; MALDI; Time-of-Flight (TOF); Fourier Transform Ion Cyclotron Resonance (FT-ICR); Mass Spectrometry.

Abstract
Microalgae are essential components of aquatic ecosystems, serving as primary producers and driving fundamental biogeochemical processes. Understanding the pigments and biomarkers present in these microorganisms is crucial to elucidating their ecological roles and physiological responses to environmental changes. Matrix-Assisted Laser Desorption/Ionization Mass spectrometry (MALDI MS) has been previously reported as a powerful tool for pigment profiling, enabling rapid and sensitive analysis of complex mixtures. In this study, we explore the influence of different mass analyzers, specifically Time-of-Flight (TOF) and 21-Tesla Fourier Transform Ion Cyclotron Resonance (FT-ICR), on MALDI pigment profiling of microalgae Chlorella vulgaris extracts. We investigate the impact of each analyzer on mass accuracy, isotopic patterns, and the number of detected signals. Additionally, we examine the elemental composition using Kendrick Mass Defect (KDM) Analysis, van Krevelen diagrams, and Double Bond Equivalent (DBE) calculations. Our results reveal that, while MALDI TOF enables accurate molecular assignments, FT-ICR provides a comprehensive characterization of all ionizable species, making it a promising approach for identifying new biomarkers in microalgae.

Introduction

Microalgae, considered one of the earliest life forms on Earth, make up a diverse group of photosynthetic prokaryotic and eukaryotic organisms playing a fundamental role in both marine and freshwater ecosystems. Microalgae's ability to absorb carbon dioxide through photosynthesis is a crucial component of the global carbon cycle, which helps to generate oxygen and support aquatic trophic webs.[1] These microorganisms are also highly valued for their capacity to produce bioactive compounds of great interest to industries such as energy, food, and cosmetics.[3,4] Among many microalgae species, *Chlorella* spp, is one of the most studied due to scientific and economic reasons.[5] *Chlorella vulgaris*, in particular, is a unicellular microalga with spherical or ellipsoidal morphology and diameters ranging from 2 to 10 μm. Its cell wall comprises a lipid bilayer with a cellulose wall that provides the organism with protection and rigidity.[6,7] *C. vulgaris* has found applications in many fields from biofuel and low/high molecular weight metabolites production to wastewater treatment, for heavy metals removal.[5, 8,9]

In nature, microalgae's secondary metabolites, such as pigments, can be species-specific or undergo chemical transformations due to changing environmental conditions.[2] For instance, the synthesis of photosynthetic and photoprotective pigments crucial for the photosynthesis process occurs within the single chloroplast present in the cell, specifically in the thylakoid membrane and the stroma. These pigments, primarily located in antenna complexes within both Photosystem I (PSI) and Photosystem II (PSII), capture energy from sunlight.[10,11] Chlorophylls, characterized by a tetrapyrrole ring coordinating nitrogen atoms within the ring and a divalent magnesium (Mg) ion, serve as the primary photosynthetic pigments. Additionally, chlorophyll possesses a side chain called phytol, anchoring it to the thylakoid membrane. Different chlorophyll types are distinguished by substituents on the tetrapyrrole ring, which acts as a chromophore, enabling light absorption.[12–14] Alongside chlorophylls, carotenoids, with their structural and functional diversity, play a crucial role in photoprotection and energy transfer. Most carotenoids consist of a tetraterpene chain and are further categorized as carotenes or xanthophylls.[14] Carotenoids function as both primary energy transfer agents and secondary antioxidants, mitigating oxidative damage. The chemical profiles of these pigments not only reflect the microalgae growth stage but also exhibit high taxonomic specificity, making them essential indicators for understanding the physiological responses of microalgae to environmental stressors such as temperature, light, oxygen content, pollutants presence, and nutrient availability fluctuations.[1,15]

Obtaining microalgae pigment profiles typically involves hyphenated chromatographic and spectroscopic techniques, which are considered gold standards for these compound analyses. However, these methods often require extensive sample preparation and have limitations regarding sensitivity and the simultaneous identification of a wide range of pigments.[16–18] Our previous work highlights matrix-assisted laser desorption/ionization mass spectrometry (MALDI MS) as a soft ionization technique offering significant advantages over conventional methods for characterizing pigments in microalgae.[19] MALDI-MS has gained traction due to its capacity to analyze various low molecular weight metabolites, including pigments, with minimal sample preparation and high sensitivity. This technique facilitates the direct ionization of intact compounds from complex mixtures, rendering it particularly suitable for pigment analysis in microalgae extracts.[20–25] Ionization in MALDI occurs through proton or cation transfer reactions between the analyte and the matrix, as well as secondary electron-transfer (ET) reactions from neutral analytes to the matrix's primary ions. These proton or cation transfer reactions result in the formation of ions such as $[A + M]^+$ or $[A - H]^-$, where M can represent various ions like H^+, Na^+, K^+, Ag^+, and others. On the other hand, charge-transfer reactions mainly produce radical species such as $[M]^{+\bullet}$ and $[M]^{-\bullet}$. These charge-transfer processes are closely related to the

physicochemical properties such as protonic/cationic affinities and ionization energies of both analytes and matrices.

MALDI proves particularly suitable for the compositional analysis of microalgae due to the molecular diversity present, ranging from non-polar compounds to polar compounds with diverse molecular structures. This diversity enables the generation of ions through different ionization channels. For instance, chlorophyll derivatives of chlorins with extended electronic conjugation ensure ionization energies below 7.5 eV, facilitating efficient electron transfer processes (ET). Furthermore, the choice of mass analyzer significantly influences the performance and analytical capabilities of the ET-MALDI MS technique. Although the properties of an ideal mass analyzer are well-described in the literature, no mass analyzer is without limitations.[30] However, the ability to resolve neighboring peaks, as measured by full width at half maximum (FWHM), is a crucial factor for complex mixture analysis.[31] High-resolution mass spectrometry enables exact mass measurements and the discernment of fine isotopic structures, facilitating the unequivocal identification of compounds. We have previously reported method development for microalgae pigment profile analysis using a MALDI-TOF-MS. Furthermore, recent advancements in analytical techniques, particularly Fourier transform ion cyclotron resonance mass spectrometry (FT-ICR MS), have significantly enhanced our understanding of complex sample composition. FT-ICR MS offers unparalleled resolution and mass accuracy, enabling the comprehensive analysis of biomarkers in natural organic matter (NOM), understanding their homologous series, and exploring compositional space. Its high resolving power allows for the discrimination of molecular species within highly intricate matrices, shedding light on the intricate chemical makeup of natural samples and providing invaluable insights into the molecular diversity and dynamics of complex systems.[34,35]

In this study, we explore the pigmentary complexity of *C. vulgaris* solvent extracts using Electron-Transfer MALDI 21T FT-ICR MS. We explore the capabilities of FT-ICR in identifying compound families of pigments through Kendrick Mass Defect (KMD) analysis and van Krevelen diagrams. Interestingly, we identified 58 distinct species of N_4O_5 and 38 species of N_4O_6 compounds, characterized by structural analogies to chlorophylls. Furthermore, the application of the van Krevelen diagram enabled the identification of lipid analogs, unsaturated hydrocarbons, and condensed aromatic compounds, thereby representing chlorophylls, lipids, and carotenoids. MALDI FT-ICR shows tremendous potential for rapidly profiling microalgae pigment biomarkers, including photosynthetic and photoprotective pigments.

Experimental

Microalgae sample preparation

The cultivation of *C. vulgaris* was conducted following previously described methods. A strain of *C. vulgaris* obtained from Carolina Biological Supply Company (Burlington, NC, USA) was utilized for this purpose. The strain was cultivated in 100 mL of Bold's basal media (BBM; PhytoTech Labs, USA). Subsequently, the culture was subjected to incubation at 25 ± 2 °C under a 12:12 h light:dark cycle, with a light intensity of 150 $\mu mol.m^{-2}.s^{-1}$, and received aeration. The cultivation process was carried out in an Excella E24 incubator shaker with stirring at 150 rpm for a duration of two weeks.

Pigment extract isolation

The pigments were extracted from the microalgae following established procedures.[19] A pellet was obtained from a 20 mL aliquot of the *C. vulgaris* culture by centrifuging at 7000 rpm for 15 minutes at 4 °C using a Hettich Universal 320 centrifuge (Tuttlingen, Germany). The culture medium was separated from the pellet via filtration using Whatman black band filters (grade 589/1). Subsequently, the pellet underwent lyophilization to remove residual water from the culture medium. For pigment extraction, 2.0 mg of the lyophilized material was combined with 1 mL of analytical-grade acetone in a 1.5 mL amber vial. The mixture was then sonicated at 40 kHz in a Branson UltrasonicsTM CPX bath (Danbury, CT, USA) operating at 35 W for 25 minutes at room temperature.

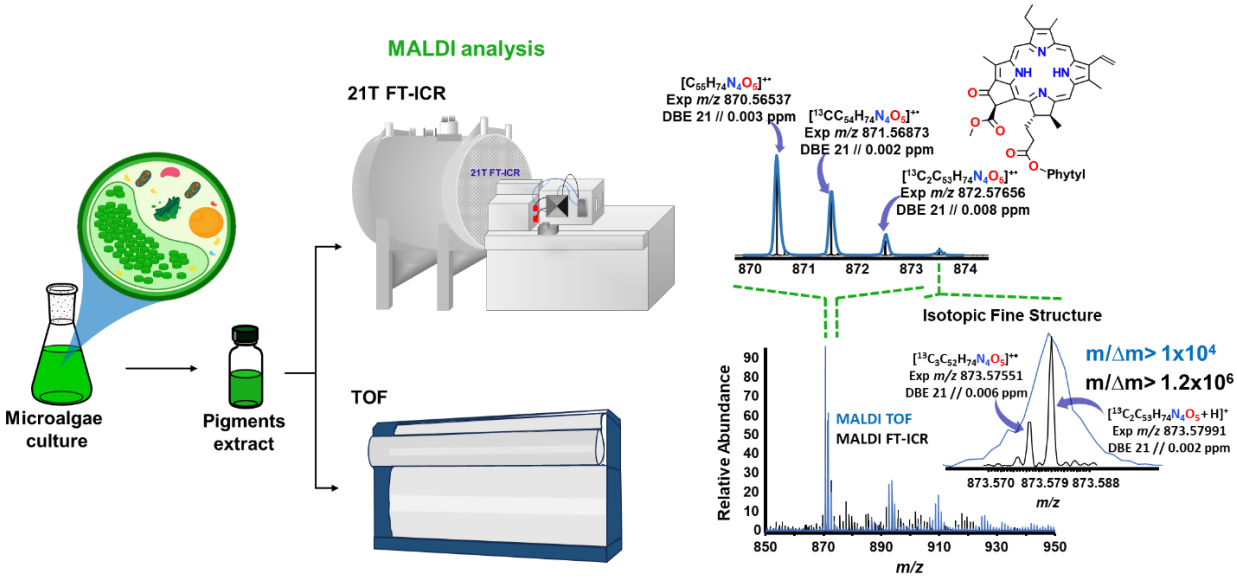

Figure. 1 General scheme for the characterization of pigments in *C. vulgaris* extracts using TOF and 21-T FT-ICR Mass analyzers in MALDI MS.

MALDI TOF mass spectrometry and data acquisition

A 5 mM matrix solution of *trans*-2-[3-(4-tert-butylphenyl)-2-methyl-2-propenylidene] malononitrile (DCTB) in acetonitrile (ACN) was prepared under sonication for 2 min at 40 kHz. This matrix solution was then combined with the pigment extract to achieve an analyte-to-matrix ratio of 1:100. The ratio was determined based on the approximate measurement of chlorophyll a in the extracts using UV-Vis spectroscopy.[38] The analyte-matrix mixture was deposited on a polished steel target using the dried droplet method, and the solvent was allowed to evaporate at room temperature following established protocols.

MALDI TOF mass spectra of the pigments extracted from the microalgae were acquired using a Bruker MALDI-TOF/TOF mass spectrometer, UltraFleXtreme (Bruker Daltonics, Billerica, MA, USA). The instrument was equipped with an Nd:YAG solid-state laser (λ= 355 nm) operating at a frequency of 1 kHz, with a pulse duration of 6 ns. Positive ion mass spectra were collected in the range of *m/z* 100 to 1000, employing pulsed ion extraction (PIE), a delay time of 100 ns, and an accelerating potential of 20 kV. MALDI experiments were conducted in reflectron mode at 25 kV using a laser pulse energy of 2.0 µJ per pulse. External calibration was achieved using a mixture of standard peptides: leu-enkephalin, bradykinin, bombesin, and renin substrate, all of which were purchased from Sigma Aldrich (St. Louis, MO), and α-cyano-4-hydroxycinnamic acid (α-CHCA) as a matrix. Each analysis reported represents the accumulation of individual 2000 spectra.

TOF data processing and analysis

Data analysis was carried out using the FlexAnalysis software provided by Bruker Daltonics (Billerica, MA, USA). The software automatically generated reports for ion abundances, signal-to-noise (S/N) ratios, signal mass resolution, peak area, and monoisotopic masses. Molecular formula assignment was conducted by constructing a database containing previously reported pigments in the microalga *C. vulgaris*, as described in previous studies.[19,39–41] Data visualization was performed using Origin Pro 9.0 64-bit. Experimental and theoretical isotope patterns, calculated with ChemCalc,[42] were compared to validate compound identification.

MALDI FT-ICR mass spectrometry and data acquisition

MALDI FT-ICR experiments were performed using a 21 T FT-ICR mass spectrometer at the National High Magnetic Field Laboratory (NHMFL), Florida State University. The instrument combined a Velos Pro linear ion trap (Thermo Scientific, San Jose, CA) with an NHMFL-designed ion trap and ion transfer optics. The dynamically harmonized ICR cell operated at a trapping potential of 7.5 V. The ion source was replaced with a high-pressure MALDI ion source incorporating a dual-ion funnel interface from Spectroglyph LLC (Kennewick, WA), as previously described.[43] Within the funnels, voltages were set at 625 kHz, 150 V peak-to-peak for the first high-pressure ion funnel, and 1.2 MHz, 90 V peak-to-peak for the second low-pressure ion funnel. An electric field gradient of approximately 10 V/cm was maintained within the dual-funnel system, with a gradient of 100 V/cm between the sample and funnel inlets. The diode-pumped, Q-Switched, Ultraviolet Laser System (Explorer One, Spectra Physics, Mountain View, CA) emitting at 349 nm was operated at 1 kHz repetition rate and 1.2 μJ of pulse energy. During mass spectrometry analysis, an ion injection time of 250 ms was utilized with the automatic gain control (AGC) deactivated. For ultrahigh mass resolving power analyses, a transient duration of 3.1 seconds was employed. All spectra were obtained in positive mode.

FT-ICR data processing and analysis

Time-domain transients of 3.1 seconds (21 T) were acquired using the Predator data station, with 100 time-domain acquisitions averaged for all experiments. Mass spectra were phase-corrected and internally calibrated using a high-abundance homologous series spanning the entire molecular weight distribution (∼100 calibrant peaks). This calibration was achieved through the "walking" calibration method. Peaks with signal magnitudes exceeding 6 times the baseline root-mean-square (rms) noise at *m/z* 400 were extracted into peak lists. Molecular formula assignments and data visualization were performed using PetroOrg© software[44] developed by the NHMFL Lab and Origin Pro 9.0 64-bit. Molecular formulas were assigned with specific parameters, including elemental composition of $C_{0-100}H_{0-100}N_{0-4}O_{0-15}Na_{0-1}$. Additionally, a maximum hydrogen-to-carbon ratio of 2 and a double bond equivalent value of 30 were considered.[45] Molecular formula assignments with a mass accuracy exceeding 0.25 parts-per-million (ppm) were excluded, and only chemical classes constituting a combined relative abundance of $\geq$ 0.2% of the total were retained.

Various graphical representations, such as KMD analysis, and van Krevelen diagrams (H/C ratio versus O/C ratio) were utilized for data analysis. These diagrams are vital to differentiation of biochemical classes such as lipids, lignin derivatives, carbohydrates, or unsaturated hydrocarbons. Accurate mass measurements of ions on the IUPAC scale were converted to Kendrick mass (KM), nominal Kendrick mass (NKM), and Kendrick mass defect KMD, employing the -CH_2- unit as reference mass. The Kendrick scale effectively standardized the mass of CH_2 from 14.01565 to precisely 14.00000.[46,47] Consequently, compounds with the same constitution of heteroatoms and number of Double Bond Equivalent (DBE) but varying numbers of CH_2 groups share identical KMD. The KM and KMD are calculated using the formula:

$$Kendrick\ mass = m/z\ x\ (14.00000/14.01565)$$

$$KDM = (Nominal\ Kendrick\ mass - Exact\ Kendrick\ mass)$$

Where *m/z* is the measured mass-to-charge ratio of the ions using the IUPAC scale. Moreover, DBE serves as a valuable tool for understanding the chemical composition in complex mixtures. DBE provides insights into the saturation of pigments isolated from *C. vulgaris* cells. The calculation of DBE is a well-established method in mass spectrometry, grounded in valence rules for distinguishing ions containing a different total number of double bonds and/or rings.[33] For organic molecules of the general type $C_cH_hN_nO_o$ DBE can be expressed as:

$$DBE = 1 + 0.5\ x\ (2c - h + n)$$

In molecules, DBE values increase with decreasing hydrogen atom count, but they are unaffected by the number of oxygen atoms. However, introducing oxygen can increase DBE values due to carbonyl unsaturation.

Results and discussion

We previously reported the pigment profiles of *C. vulgaris* extracts by UAE using MADI-TOF MS analysis. Through MALDI MS experiments we successfully identified ten compounds within the UAE-extracted sample. This included six chlorophyll pigments and four carotenoids, achieving a peak resolving power of $1x10^4$ at *m/z* 400. Among the primary chlorophylls identified, chlorophyll a ($C_{55}H_{72}N_4O_5Mg$, *m/z* 892.535) and chlorophyll b ($C_{55}H_{70}N_4O_6Mg$, *m/z* 906.499), were detected as radical cations $M^{+\bullet}$. Additionally, we detected signals corresponding to pheophytin a ($C_{55}H_{74}N_4O_5$, *m/z* 870.567), chlorophyllide a ($C_{35}H_{34}N_4O_5Mg$, *m/z* 614.231), and pheophorbide a ($C_{35}H_{36}N_4O_5$, *m/z* 592.263) as radical cations $M^{+\bullet}$. This indicated the detachment of Mg^{2+} and the phytol chain, or both, in these compounds, respectively. Interestingly, hydroxychlorophyll a, $M^{+\bullet}$, was detected at *m/z* 908.521 ($C_{55}H_{72}N_4O_6Mg$) with a mass accuracy of 9.8 ppm. The presence of hydroxychlorophylls in the sample suggests oxidative metabolic processes during chlorophyll biosynthesis, potentially induced by reactive oxygen species.[48,49] The identification of these chlorophylls aligns with previous findings employing High-Performance Liquid Chromatography (HPLC)[40,50,51] and reinforces the consistency of the chlorophyll profile detected using MALDI TOF. The mass accuracy values for these chlorophylls were less than 10 ppm, and signal-to-noise ratios ranged from 5.7 to 154.6, with pheophytin a exhibiting the highest signal-to-noise ratio (see **Table 1**).

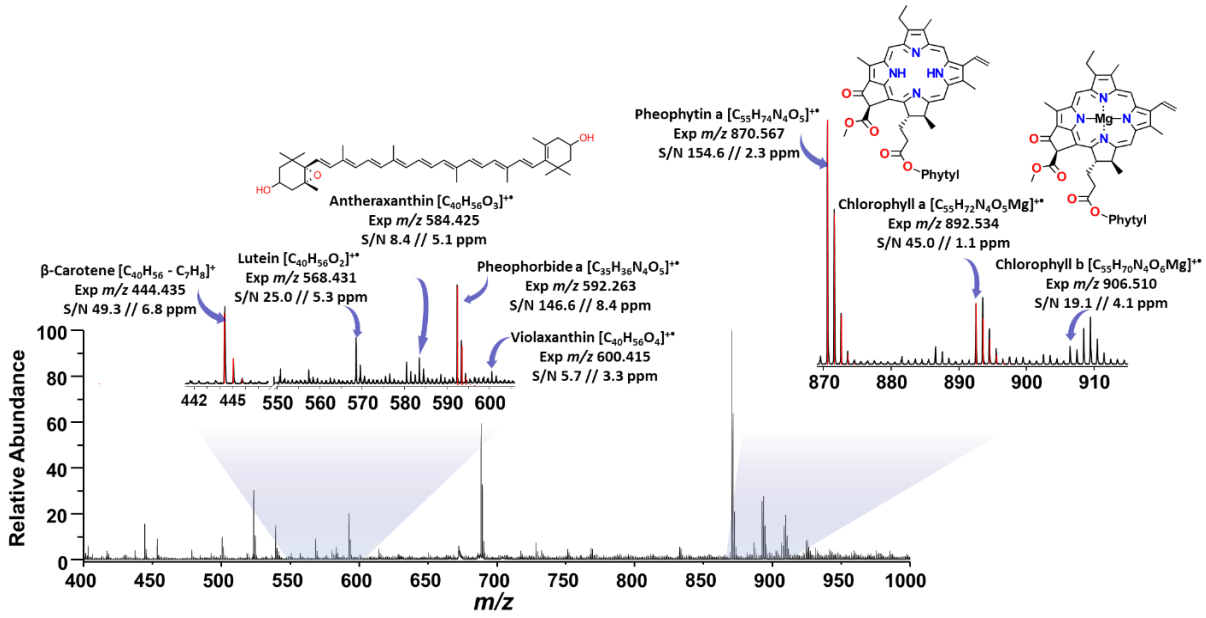

Figure 2. MALDI TOF MS spectrum showing zoom-ins on two distinct regions associated with carotenoids (*m/z* 441 - 610) and chlorophyll pigments (*m/z* 870 - 920) using DCTB as the electron transfer (ET) matrix, with an analyte-to-matrix ratio of 1:100 and a laser energy of 2 µJ per pulse. The insets provide information on the molecular formula, experimental mass, mass accuracy, signal-to-noise ratio, and the calculated/experimental isotopic pattern for the identified pigments. The resolving power at $m/\Delta m_{50\%}$ is $1x10^4$ (*m/z* 400).

Table 1. Pigment compounds of *C. vulgaris* detected by MALDI TOF MS.

Compound	Proposed Molecular formula	Isotopic pattern		*m/z*		Mass accuracy (ppm)	S/N
		Theoretical	Experimental	Theo.	Exp.		
Chlorophyll pigments							
Pheophorbide a	$[C_{35}H_{36}N_4O_5]^{+\bullet}$	100:39.92:8.79:1.39	100:40:9:2	592.268	592.263	8.4	146.6
Chlorophyllide a	$[C_{35}H_{34}N_4O_5Mg]^{+\bullet}$	100:52.56:27.77:8.06	100:53:30:8	614.237	614.231	9.8	9.2
Pheophytin a	$[C_{55}H_{74}N_4O_5]^{+\bullet}$	100:61.99:19.92	100:62:20	870.565	870.567	2.3	154.6
Hydroxychlorophyll a	$[C_{55}H_{72}N_4O_6Mg]^{+\bullet}$	100:74.66:41.92:15.73	100:75:42:16.5	908.530	908.521	9.8	21.0
Chlorophyll b	$[C_{55}H_{70}N_4O_6Mg]^{+\bullet}$	100:74.64:41.9:15.72	100:75:42:16	906.514	906.510	4.4	19.1
Chlorophyll a	$[C_{55}H_{72}N_4O_5Mg]^{+\bullet}$	100:74.63:41.69:15.56	100:74.8:42:16.2	892.535	892.534	1.1	45.0
Carotenoids							
Carotene	$[C_{40}H_{56} - C_7H_8]^+$	100:36.24:6.38	100:36:7	444.438	444.435	6.8	49.3
Lutein	$[C_{40}H_{56}O_2]^{+\bullet}$	100:43.98:9.85:1.50	100:44:11	568.428	568.431	5.3	25.0
Loroxanthin/Antheraxanthin	$[C_{40}H_{56}O_3]^{+\bullet}$	100:44.02:10.07:1.59	100:44:10	584.422	584.425	5.1	8.4
Violaxanthin	$[C_{40}H_{56}O_4 + H - H_2O]^+$	100:44.01:10.07:1.59	100:44:11	583.617	583.611	10.0	14.0
	$[C_{40}H_{56}O_4]^{+\bullet}$	100:44.06:10.29:1.69	100:44:12:2	600.417	600.415	3.3	5.7

Furthermore, MALDI TOF MS unveiled the presence of carotenoids, including carotene, lutein, antheraxanthin, loroxanthin, and violaxanthin, which are considered as biomarkers for *Chlorella* species.[39] Carotene ($[M - C_7H_8]^+$, *m/z* 444.435) was successfully identified, in accordance with previous records.[40,52]

The isotopic distribution was compared to assign the signals of carotene with a mass accuracy of 6.8 ppm and a signal-to-noise ratio of 49.3. Violaxanthin was detected as a radical cation at *m/z* 600.415, and its characteristic fragment at *m/z* 583.611 ($[M + H - 18]^+$), which indicated the removal of a water molecule from the protonated precursor ion, a feature previously reported in the literature.[40] It is important to note that fucoxanthin, a pigment identified in *C. vulgaris* cells in previous studies, was not detected in this investigation. This non-detection may be

attributed to variations in the carotenoid composition, dependent on the culture conditions and growth stage of the microalgae, as previously discussed. Additionally, it's worth highlighting that fucoxanthin ($C_{42}H_{58}O_6$) is not exclusive to *C. vulgaris* but is also found in other algal groups, including Haptophytes, Chrysophytes, Raphidophytes, Bolidophytes, and some Dinoflagellates.[49,53]

The signal detected at *m/z* 584.427 was assigned to either antheraxanthin ($C_{40}H_{56}O_3$) or loroxanthin ($C_{40}H_{56}O_3$), which are structural isomers. For this assignment, we achieved a mass accuracy value of 5.1 ppm and a signal-to-noise ratio of 8.4. Loroxanthin ($C_{40}H_{56}O_3$) has been reported in the scientific literature as a pigment characteristic of certain chlorophytes, rendering it a valuable biomarker for these algae. Importantly, loroxanthin has been recognized as a biomarker for identifying specific microalgal species such as *Scenedesmus obliquus* and *C. vulgaris*, with its biosynthetic pathway commencing from lutein ($C_{40}H_{56}O_2$).[54,55] The carotenoids identified in the *C. vulgaris* extract using TOF in MALDI MS in this study have also been corroborated with literature reports derived from standard techniques such as HPLC. TOF analyzer allows for efficient separation of molecular ions formed in the MALDI ionization source and enables the acquisition of detailed mass spectra of the chemical species present in the microalgae. Nevertheless, TOF may introduce energy dispersion, meaning ions with the same *m/z* ratio but with different initial energies can reach the detector at slightly different times, potentially affecting mass measurement accuracy.[33] Additionally, the resolution limitations of the TOF analyzer may pose challenges in distinguishing isobaric ions, which could lead to misidentification of potential biomarkers in the microalga extracts. Nonetheless, our results show the efficiency of MALDI TOF MS as a valuable tool in microalgae research, offering acceptable analytical descriptor values and expanding the scope of microalgal pigment analysis.

MALDI 21 T FT-ICR analysis for pigment identification in *C. vulgaris*

FT-ICR MS's remarkable mass resolution and sensitivity have positioned it as an invaluable tool across various scientific disciplines, including proteomics, metabolomics, metallomics, and petroleomics.[22,57–59] FT-ICR provides detailed molecular composition data for complex mixtures, a pivotal feature in our case for unraveling the compositional space of pigments in photosynthetic microorganisms. In the previous chapter and section, our group reported the ET-MALDI TOF profiles of *C. vulgaris* solvent extracts with an average number of 18 individual compounds identified. The high-field FT-ICR MS data of a similar extract, as shown in Figure 3 and Table 2, revealed 3837 cumulative peaks within the mass range of *m/z* 180-1000, with a peak resolving power upwards of 1.2×10^6 at *m/z* 400 and mass accuracy measurements within 1 to 250 ppb. After a data filtration protocol (see Materials and methods), 22% of the observed peaks in the *C. vulgaris* cell extract were classified as non-assigned peaks (no-hit). In other words, the chemical composition of these peaks does match with consistent Kendrick series.

The FT-ICR mass spectrum of the *C. vulgaris* pigment extract revealed two distinct mass regions corresponding to carotenoid- and chlorophyll- derivatives, a pattern that aligns with previous observations.[19] We identified nearly 80% of the observed peaks (2136 peaks) through our ET-MALDI FT-ICR MS experiments on the *C. vulgaris* cell extracts. Table 2 presents mass spectrometric figures of merit for representative pigments belonging to the chlorophyll and carotenoid families. The identified chemical species include radical cations, protonated molecules, and sodium adducts. The ionization channel employed for each molecular species depended on its molecular structure. Thus, chlorophyll derivatives were identified as radical cations and protonated molecules due to their base chlorin structure and lower ionization energy (E_i) values compared to the MALDI matrix DCTB (Ei: 8.54 eV), and the possibility of abstracting a proton in the gas phase, possibly due to the number of nitrogen/oxygen atoms in their structures, as discussed in our previous reports. Carotenoids also utilized different

ionization channels such as ET, detected as $[M]^{+\bullet}$, and the formation of sodium adducts $[M + Na]^+$, according to the molecular structure, Ei values, and cationic/protonic affinities in each case.

Interestingly, although the detection of molecular ions formed via electron transfer was expected due to the use of the ET matrix DCTB (E_i: 8.54 eV), protonated molecules $[M + H]^+$ and sodium adducts $[M + Na]^+$ were detected in higher proportions. Some authors, as well as our previous studies, have noted that DCTB has the capability to induce protonation of other molecules during MALDI ionization, attributed to the presence of an acidic hydrogen within its structure. For this protonation to take place, the analyte's proton affinity must surpass that of DCTB. Compounds detected as $[M + H]^+$ or $[M + Na]^+$ typically exhibit high nitrogen or oxygen content, thereby possessing elevated proton and cation affinities. Given the nature of the analyzed samples, cultivated in a medium with high salt concentrations and subjected to minimal pretreatment prior to analysis, the formation of pre-existing ions in solution requiring only MALDI matrix assistance for desorption in the MALDI ionization chamber, is possible. Nonetheless, we have MALDI 21T FT-ICR MS data measured on microalgae pigment extracts using entirely ET matrices, which allows for experiments with selective ionization, to be reported in the future.

Carotene ($M^{+\bullet}$, $C_{40}H_{56}$ *m/z* 536.43763), lutein ($M^{+\bullet}$, $C_{40}H_{56}O_2$ *m/z* 568.42744), loraxanthin, ($M^{+\bullet}$, $C_{40}H_{56}O_3$ *m/z* 584.4224), and violaxanthin ($M^{+\bullet}$, $C_{40}H_{56}O_4$ *m/z* 600.41734) were identified with mass accuracy values ranging from 3 to 240 ppb. We also detected intact chlorophyll b ($M^{+\bullet}$, $C_{55}H_{70}N_4O_6Mg$ *m/z* 906.51401), along with pheophytin b ($M^{+\bullet}$, $C_{55}H_{72}N_4O_6$ *m/z* 884.54464), pheophytin a ($M^{+\bullet}$, $C_{55}H_{74}N_4O_5$ *m/z* 870.56537, chlorophyllide b ($M^{+\bullet}$, $C_{35}H_{32}N_4O_6Mg$ *m/z* 628.21669), and chlorophyllide a ($M^{+\bullet}$, $C_{35}H_{34}N_4O_5Mg$ *m/z* 614.23745). Interestingly, we detected pirofeophorbide a ($M^{+\bullet}$, $C_{33}H_{34}N_4O_3$ *m/z* 534.24253), and pirofeophorbide b ($M^{+\bullet}$, $C_{33}H_{32}N_4O_4$ *m/z* 548.24179), which were not observed in TOF experiments. Pirofeophorbide a and b serve as crucial biomarkers for cellular senescence and are derived from chlorophyll through demethylation reactions. [48,60–62]

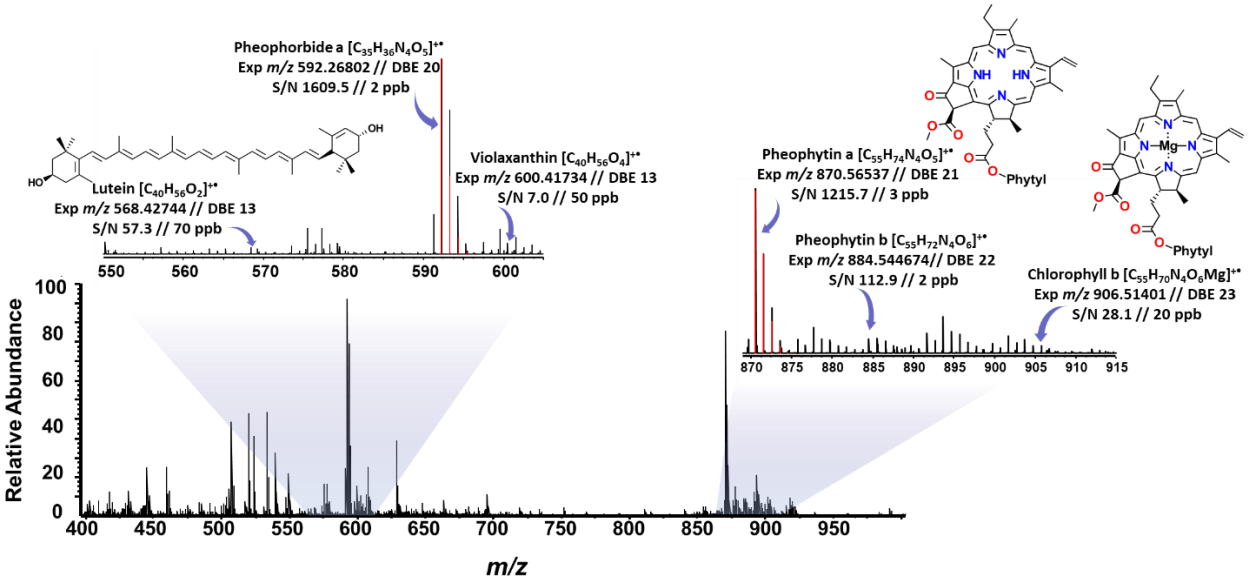

Figure 3. MALDI FT-ICR MS spectrum showing zoom-ins on two distinct regions *m/z* 550 – 610, and *m/z* 870 – 915, using DCTB as the electron transfer (ET) matrix, with an analyte-to-matrix ratio of 1:100. The insets provide information on the molecular formula, experimental mass, mass accuracy, signal-to-noise ratio, and the calculated/experimental isotopic pattern for the identified pigments. The resolving power at $m/\Delta m_{50\%}$ is 1.2×10^6 (*m/z* 400).

Table 2. Main pigment compounds of *C. vulgaris* detected by MALDI 21 T FT-ICR MS.

Compound	Proposed Molecular formula	Isotopic pattern		*m/z*		Mass accuracy (ppb)	S/N
		Theoretical	Experimental	Theo.	Exp.		
Chlorophyll pigments							
Pyropheophorbide a	$[C_{33}H_{34}N_4O_3]^{+\bullet}$	100:1:35:0.3:0.5:0.6:6:0.1:0.2:0.7	100:1:35:0.6:6:0.7	534.26254	534.26253	20	40.0
Pyropheophorbide b	$[C_{33}H_{32}N_4O_4]^{+\bullet}$	100:1:35:0.3:0.5:0.8:6:0.1:0.3:0.7	100:1:35:0.8:6:0.7	548.24180	548.24179	30	38.9
Pheophorbide a	$[C_{35}H_{36}N_4O_5]^{+\bullet}$	100:1:38:0.4:0.5:1:7:0.1:0.1:0.3:0.8	100:1:38:0.4:0.5:1:7:0.8	592.26802	592.26802	2	1609.5
Pheophorbide b	$[C_{35}H_{34}N_4O_5]^{+\bullet}$	100:1:38:0.3:0.5:1:7:0.1:0.1:0.4:0.8	100:1:38:1:7:0.8	606.24729	606.24728	10	159.3
Chlorophyllide a	$[C_{35}H_{34}N_4O_5Mg]^{+\bullet}$	100:1:12:38:0.3:14:0.5:5:7:0.1:0.2:5:1:0.8	100:12:38:14:5:7	614.23741	614.23745	60	11.9
Chlorophyllide b	$[C_{35}H_{32}N_4O_5Mg]^{+\bullet}$	100:1:12:38:0.3:14:0.5:6:7:0.1:5:0.1:1:0.8:1	100:1:12:38:14:0.5:6:7:5:1:0.8:1	628.21668	628.21669	20	555.1
Pheophytin a	$[C_{55}H_{74}N_4O_5]^{+\bullet}$	100:1:59:0.8:0.8:1:17:0.5:3:0.1	100:1:59:0.8:0.8:1:17:0.5:3	870.56537	870.56537	3	1215.7
Pheophytin b	$[C_{55}H_{72}N_4O_5]^{+\bullet}$	100:1:59:0.8:0.8:1:17:0.4:0.2:0.7:3	100:1:59:0.8:1:17:0.7:3	884.54463	884.54464	2	112.9
Chlorophyll b	$[C_{55}H_{70}N_4O_6Mg]^{+\bullet}$	100:1:12:59:0.8:14:0.8:8:17:0.4:0.2:8:0.3:2:3:0.1:0.1:2:0.6:0.5	100:1:12:59:14:8:17:8:2:3:2	906.51402	906.51401	20	28.1
Carotenoids							
β-Carotene	$[C_{40}H_{56}]^{+\bullet}$	100:43:0.6:9:0.2:1	100:43:9	536.43765	536.43762	37	5.4
Lutein	$[C_{40}H_{56}O_2]^{+\bullet}$	100:43:0.6:0.4:9:0.2:0.1:1	100:43:0.6:9:1	568.42748	568.42744	70	57.3
Loroxanthin/Antheraxanthin	$[C_{40}H_{56}O_3]^{+\bullet}$	100:43:0.6:0.6:9:0.2:0.2:1	100:43:9	584.42240	584.42243	50	5.0
Violaxanthin	$[C_{40}H_{56}O_4 + Na]^{+}$	100:43:0.6:0.8:9:0.2:0.3:1	100:43:9	623.40708	623.40723	240	9.3
	$[C_{40}H_{56}O_4]^{+\bullet}$	100:43:0.6:0.8:9:0.2:0.3:1	100:43:9	600.41731	600.41734	50	7.0

The ultra-high mass resolving power of FT-ICR facilitates analysis of isobaric compounds in microalgal pigments. For instance, narrow mass differences such as $^{13}C_2$ vs C_2H_2 mass splits (Δm = 0.009 u) in carotenoids, and lipids analogs can be resolved, while achieving mass accuracy values below 400 ppb, which are necessary for nearly unambiguous mass determination, as previously reported in the literature.[31,45] Here, as illustrated in Figure 4, we successfully resolved the very narrow mass difference among isotopologues that constitute the M+3 ion of pheophytin a ($C_{55}H_{74}N_4O_5$), including $^{12}C_{54}{}^{13}C^1H_{74}{}^{14}N_4{}^{16}O_4{}^{18}O$ and $^{12}C_{52}{}^{13}C_3{}^1H_{74}{}^{14}N_4{}^{16}O_5$, with mass splits (Δm = 0.00234 u). We achieved mass accuracy below 250 ppb, underscoring the precision of our molecular composition assignments. For instance, the pheophytin a radical cation at *m/z* 870.56537 corresponds to a unique elemental composition assignment as $C_{55}H_{74}N_4O_5$ (Figure. 4). Furthermore, when analyzing molecules with known composition, it is crucial that the calculated isotope distribution closely aligns with the observed isotope distribution obtained from a high-resolution mass spectrometer. Our findings emphasize the importance of both mass accuracy and ultra-high mass resolving power for precise compound identification.

Kendrick mass sorting and van Krevelen diagrams were utilized for molecular composition assignment, providing a comprehensive understanding of the compound class and DBE. The high-resolution measurements enabled isotope fine structure observation, which aligned with theoretical values calculated using the ChemCal molecular formula calculator algorithm at the same resolving power.[42]

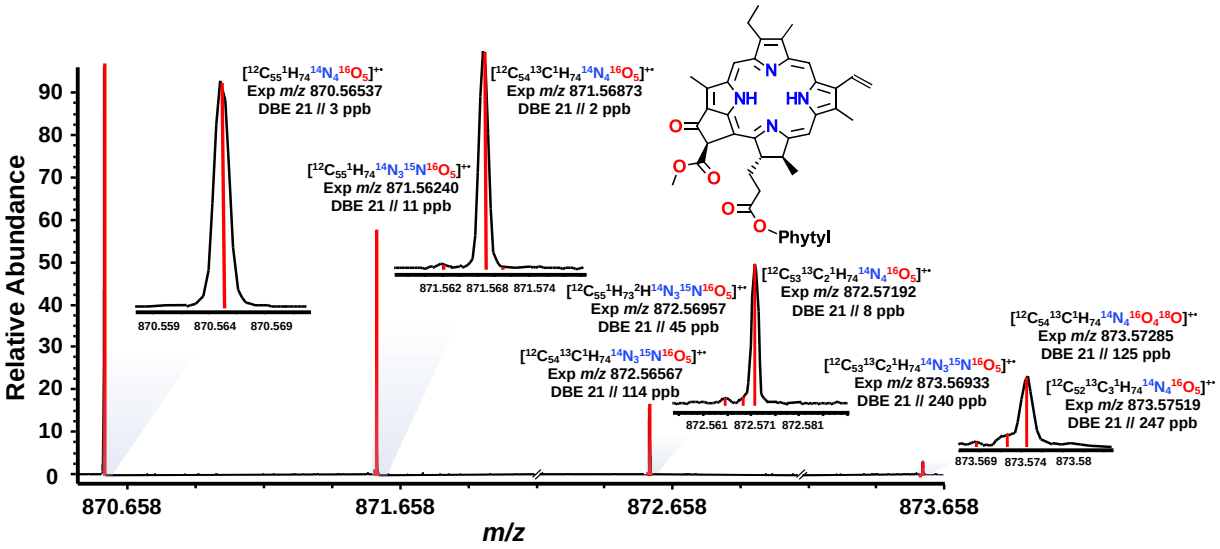

Figure 4. Zoom-in on a 3 u window displaying monoisotopic and isotopic signals for pheophytin a ($M^{+\bullet}$, $C_{55}H_{74}N_4O_5$) measured with a 21T FT-ICR mass spectrometer (black trace). Theoretical isotopic distribution calculated at $1.2x10^6$ (at *m/z* 400) resolving power using the ChemCal molecular formula calculator algorithm.

As depicted in Fig. 4, the ultra-high resolving power of FT-ICR MS enables the differentiation of the isotopic fine structure (IFS), allowing for the distinction of various isotopic compositions sharing identical nominal mass.[33] The IFS arises from naturally occurring isotopes within the analyzed molecule.[63] Thus, isobaric ions with distinct molecular formulas present in complex mixtures can be identified.[64,65] Ultra-high-resolution mass spectrometry measurements are not only beneficial but frequently essential for the analysis of biomarkers in complex samples.

Compound class distribution in *C. vulgaris* pigment extracts

Compound class analysis involved grouping elemental compositions sharing the same molecular formula as seen in the histogram of Fig. 5. We found twenty-seven individual compound classes corresponding to hydrocarbons (HC), oxygenated (O_o, o=2-7), and nitrogenated (N_nO_o, n=1-3, o=1-5), compound series with 1.4%, 17% and 23.4% relative abundances. Also, the porphyrin series (N_4O_o/N_4O_oMg, o=0-6) make up 58% of the species observed. These family classes were detected as protonated molecules, radical cations, and sodium adducts.

Protonated molecules make up most of the species detected. For instance, the N_1, N_2, and N_3 series exhibit predominantly $[M + H]^+$ ions suggesting the basic nature of these compounds. Mono-, di-, and tri-nitrogenated compounds in *C. vulgaris* cells are associated with betain lipid derivatives such as monoacylglyceryl-N,N,N-trimethyl-homoserine (MGTS), diacylglyceryl-N,N,N-trimethyl-homoserine (DGTS), diacylglyceryl-carboxyhydroxymethylcholine (DCC), and monoacylglyceryl-carboxyhydroxymethylcholine (MGCC).[68] Lipid accumulation in microalgae is known to vary among species and is influenced by harvest time and growth stage.[6,37] The chlorin series N_4O_o (o=0-6), structural analogues of porphyrins, is also observed as protonated molecules. However, family classes N_4O_5, N_4O_6, and N_4O_6Mg exhibit similar or higher relative abundances of radical cations compared to protonated molecules. This observation may be related to the molecular structures of these compounds, derived from highly unsaturated chlorins, which confer upon them lower values of ionization energy compared to the MALDI matrix DCTB (8.54 eV). We have previously reported the ionization energy values for chlorophyll-type pigments and carotenoids[66]. Overall, N_4O_o (o=0-6) species have DBE values ranging from 12 to 30 and carbon atom numbers between 12 and 57. N_4O_o species serve as indicators of autotrophic organisms because these structures are the foundational architectures of

chlorophylls, crucial photosynthetic pigments responsible for converting electromagnetic energy into chemical energy.[12,73] N_4O_5/N_4O_5Mg and N_4O_6/N_4O_6Mg species are linked to chlorophyll a and b analogues, respectively.[72] The reported chlorophyll a/chlorophyll b ratios for *C. vulgaris* cells ranges between 2.5 to 3.0 in literature, interestingly we observe a ratio of 2.8 between the relative abundance of both compound series.[74]

Sodium adducts are exclusive of oxygenated compound families of the type O_4 to O_7 with characteristic high cationic affinities.[66] In *C. vulgaris* extracts, these compounds are linked to xanthophylls and certain lipids.[69–71] In positive ion mode, the type of ions formed in MALDI mass spectrometry depends on various physicochemical properties of the analyte and matrix, such as ionization energy, proton affinity, electron affinity, and cation affinities. In our experiments, we employed DCTB as the matrix, a commercially available electron transfer matrix with an ionization energy (Ei) of 8.54 eV, which would ensure the ionization of compounds with ionization energies lower than 8.0 eV. Interestingly, in experiments using the TOF analyzer, predominantly radical cations were detected, contrary to the analysis using the FT-ICR analyzer. This observation can be attributed to the presence of acidic hydrogen in the structure of DCTB, facilitating the transfer of protons to analytes with higher proton affinities than DCTB in the gas phase, thus resulting in the detection of protonated species. Furthermore, the high proportion of protonated species detected in the sample may also be influenced by the ionization source conditions. For example, in MALDI TOF experiments, a Nd:YAG laser (355 nm) was used, while in MALDI FT-ICR experiments, a laser emitting at 349 nm was employed. This variation in laser wavelengths could potentially lead to differences in the ionization mechanisms. Some reports have shown that the choice of laser wavelength can indeed influence the ionization process in MALDI. Varying the laser wavelength on the ionization of peptides led to differences in the ionization efficiency and fragmentation patterns of analytes.

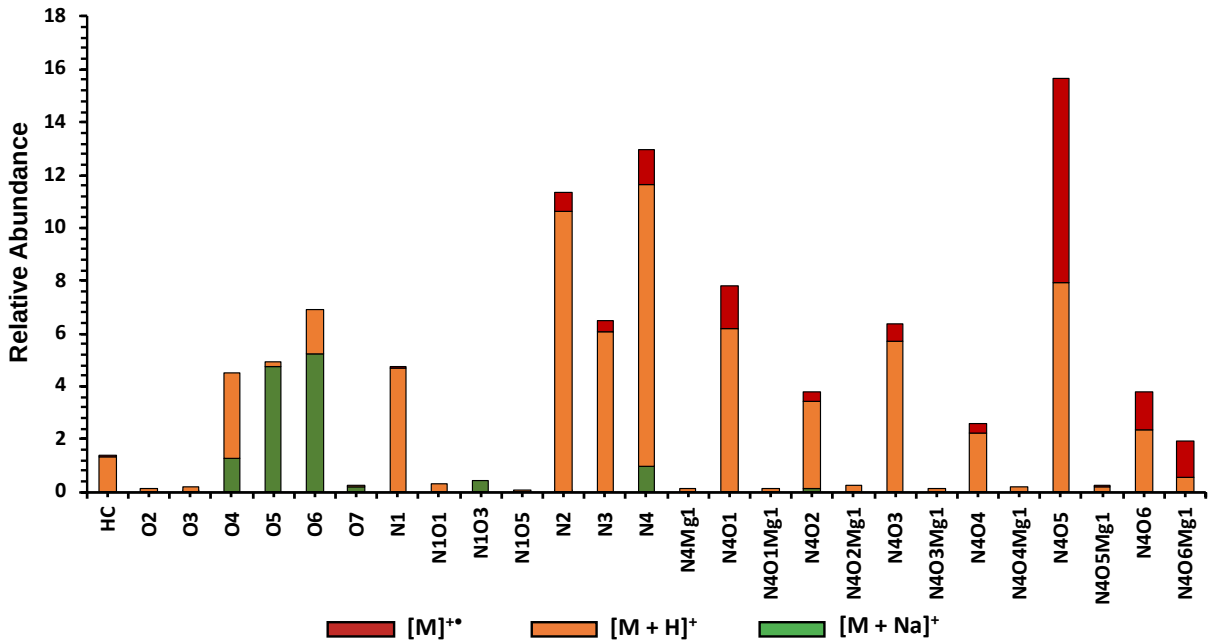

Figure 5. Compound class distribution for *C. vulgaris* pigment extracts derived from positive-ion MALDI 21 T FT-ICR MS.

Kendrick mass defect analysis for *C. vulgaris* pigment extracts

Ultra-high-resolution FT-ICR MS enables the differentiation and identification of thousands of distinct elemental compositions within a single mass spectrum. Each elemental composition possesses a unique mass defect, defined as the difference between the exact mass and the nominal mass.[33] The mass defect becomes an invaluable tool to accurately assign a single elemental composition to an ion in FT-ICR MS measurements.[75] Furthermore, periodic mass differences in the spectrum arise from repeating units within compound families. For example, mass differences of 2.0157 u within a compound series suggest changes in the number of rings plus double bonds (DBE), while differences of 14.01565 indicate repeating CH_2 units in a hydrocarbon family. Thus, converting the experimental IUPAC mass into the Kendrick mass (KM), followed by calculation of the Kendrick mass defect (KMD), facilitates data visualization, series identification and spectral interpretation for high-resolution mass spectrometric data. KMD analysis provides crucial molecular insights from samples, even without prior molecular formula assignments.[78] It can also reveal differences and similarities between diverse datasets, as extensively reviewed in the literature. [47,75,78] Some researchers have utilized Kendrick's analysis as a visualization tool for qualitative, non-targeted examinations of lipid classes.[78]

To the best of our knowledge, this is the first report analyzing pigment extracts from the microalgae *C. vulgaris* using FT-ICR MS. While previous studies have concentrated on lipid analysis of *C. vulgaris*, as mentioned earlier, none have delved into the analysis of photosynthetic and photoprotective pigments present in these cells by FT-ICR MS. Microalgae synthesize photoprotective and photosynthetic pigments through metabolic pathways, leading to the generation of metabolite families. [60,72,76] Consequently, KMD analysis can be utilized to identify metabolic compound families in *C. vulgaris* and other photosynthetic microorganisms' extracts. In KMD analysis, Kendrick mass defects are plotted against nominal Kendrick mass values across the experimentally measured mass range. The KMD plots in Figure 6 illustrate the complexity, compositional space, and extent of alkylation for the metabolite's series O_o, N_nO_o, and N_4O_o in *C. vulgaris* pigment extracts. Figures 6A, 6C, and 6D illustrate the KMD for the detected compounds as radical cations ($M^{+\bullet}$), protonated molecules ($[M + H]^+$), and sodium adducts ($[M + Na]^+$), respectively. Figure 6B portrays the chlorophyll cycle linking biosynthesis and degradation. Compounds with increasing number of CH_2 units share the same KMD value, aligning horizontally. In contrast, compounds within the same class but with increasing degrees of unsaturation (DBE) are shifted upwards by a KMD difference of 0.0134.

Chlorine derivatives (Figure 6) exhibit high KMD owing to the presence of heteroatoms (O, N) within their aromatic complex structure, crucial for their role in the photosynthesis process. [72,76] Furthermore, as shown in Fig 6B, the analogs of chlorophyllide a detected can convert into chlorophyllide b via enzymatic action by chlorophyllide a oxygenase, a phenomenon outlined in the chlorophyll cycle. This cycle acts not as a continuous biosynthesis pathway for chlorophyllide b from chlorophyllide a, but rather as a linkage between chlorophyll biosynthesis and degradation. This connection potentially regulates chlorophyll a/b ratios in response to varying light conditions. [72] Within this cycle, chlorophyll a and chlorophyll b undergo degradation via dephytylation to chlorophyllides, followed by Mg-dechelatase activity (not depicted), resulting in the formation of linear-tetrapyrrolic bilins. [72]

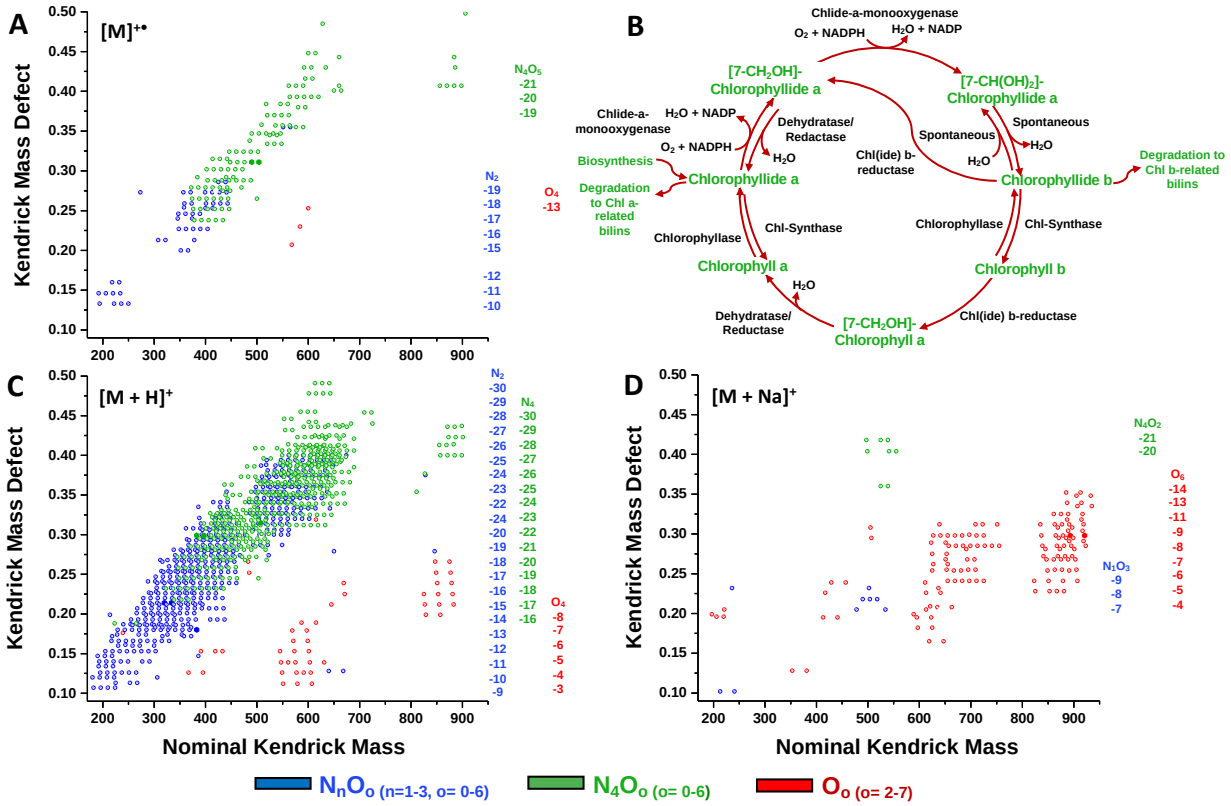

Figure 6. Kendrick Mass Defect plots for metabolite series detected as A) radical cations, C) protonated molecules, and D) sodium adducts in *C. vulgaris* pigment extracts from MALDI FT-ICR MS data. The inset (B) provides insight into the chlorophyll cycle, illustrating the connection between chlorophyll biosynthesis and degradation through a sequence of reactions.[72,76]

In this study, we identified N_4O_o species, among which N_4O_5 stands out with 17 and 42 different elemental compositions detected as radical cations and protonated molecules, respectively. The N_4O_5 species were not detected as sodium adducts. These species are distributed across two subregions, spanning nominal Kendrick mass (NKM) values of 300 to 642, and 871 to 900, respectively. Interestingly, within the first region, the section of NKM values from 578 to 674 corresponds to the chlorophyllide b series (with Mg but without the phytol chain), while the section of NKM values from 601 to 642 corresponds to the pheophytin b series (without Mg but with the phytol chain). [79] The region of NKM values between 871 and 900 corresponds to the pheophorbide b (without Mg and the phytol chain). Signals detected at lower NKM values correspond to less oxygenated species (e.g., N_4O_1, N_4O_2, N_4O_3), series that have also been previously reported by other authors in other species of microalgae and in marine sediments.

Elemental compositions within chlorophyllide b derivatives along horizontal lines correspond to homologous series of compounds with increasing CH_2 units. Likewise, some authors have reported possible molecular structures for series with different units of CH_2 in chlorins and porphyrins, indicate methylation of the chlorin core or increased alkylation on a side chain (in chlorophylls and pheophytins). The DBE values of these species correspond to the expected values for tetrapyrrole macrocycles (number of rings and double bonds) found in the most common phorbin and chlorin analogs detected in aquatic environments (e.g., pheophytins, pheophorbides, purpurins). Enzyme-mediated methylation reactions play a pivotal role in chlorophyll biosynthesis, as seen in the formation of Mg-protoporphyrin IX-monomethyl ester (Mg-protoMME) from (Mg-proto).[72]

Previous reports on the analysis of marine sediments via APPI FT-ICR-MS have indicated that within the N_4O_5 series, species with carbon atom numbers 33, 35, 44, and 53 most likely correspond to degradation products of tetrapyrrole chlorophyll. Among the assigned N_4O_5 species, $C_{35}H_{36}N_4O_5$ detected as $M^{+\bullet}$ with a DBE of 20, probably corresponds to a pheophorbide-a analog, produced by the hydrolytic cleavage of the phytyl chain from pheophytin-a, subsequent to the demetallation of chlorophyll-a, as previously described by other authors. Furthermore, various other N_4O_5/N_4O_6 species with carbon atom numbers between 31–55 exhibit DBE distributions corresponding to tetrapyrrole structures, strongly suggesting other intermediates in the chlorophyll degradation pathway. Reduction reactions, similar to methylation, are integral to chlorophyll biosynthesis, such as the conversion of protochlorophyllide a to chlorophyllide a by protochlorophyllide a oxidoreductases (POR) [72], and the reduction of chlorophyllide b to chlorophyllide a as shown in the chlorophyll cycle (Fig 6). Among these species, chlorophyll b ($C_{55}H_{70}N_4O_6$) plays a pivotal role in charge transfer processes during photosynthesis reactions in *C. vulgaris* cells, observed as $M^{+\bullet}$ at NKM 906 with KMD 0.49. Notably, this species does not conform to any CH_2 series (see Fig 6A).

Here, we identify demetallated and phytol-free porphyrinic core N_4O_o (o=0-6), which, could be considered the first step in the catagenic/anagenic process for the formation of petroporphyrins, biomarkers in petroleum. In 1934, Alfred Treibs proposed that the fossil fuels might have a biogenic origin after examining chlorophyll-like compounds found within asphaltenes. As expected, this study did not detect the N_4VOo, N_4VOS, and N_4Ni species. These porphyrins are outcomes of geochemical alterations to the primary chlorophyll core, influenced by the mineral matrix and the conditions of the organic matter during the initial stages of diagenesis and catagenesis processes. Interestingly, our results show a relationship between the series of N_4O_o porphyrins (o=0-6) present in microalgae and the series of porphyrins reported in petroleum samples by our group in previous reports, e.g., $C_cH_hN_4$, detected as $M^{+\bullet}$, c= 25-29 DBE 17, c= 25-30 DBE 18, c= 25-34 DBE 19, c= 25-32 DBE 20, and $C_cH_hN_4VO/C_cH_hN_4Ni$, detected as $M^{+\bullet}$, c= 25-29 DBE 17, c= 25-30 DBE 18, c= 25-34 DBE 19, c= 25-32 DBE 20, respectively. Additionally, and in accordance with the literature, generally, the homologous series in the microalgae are shorter compared to the homologous series in the petroleum sample.

N_4O_5 species exhibit lower KMD values compared to the N_4O_6 species. For example, pheophytin b ($C_{55}H_{72}N_4O_6$), NKM 884, exhibits a KMD of 0.44, while pheophytin a ($C_{55}H_{74}N_4O_5$), NKM 870, boasts a KMD of 0.40. Interestingly, the species $C_{34}H_{32}N_4O_5Mg$, $M^{+\bullet}$, was detected at NKM 600, KMD 0.448, of which there is no previous report. However, $C_{34}H_{34}N_4O_5$ (M - Mg + H_2), known as phellophyll a, a derivative of chlorophyll a, was reported by Wu et al.[80] The entire spectrum of N_4O_o species identified aligns based on their elemental composition in the KMD analysis plot, creating a standardized reference for these subgroups and simplifying the exploration of photosynthetic pigment derivatives within such samples using high-resolution mass spectrometry. Furthermore, it's worth noting that these N_4O_o derivatives are systematically arranged within the KMD analysis plot in ascending order, signifying the number of oxygen atoms present in their structures.
In addition, among the assigned N_4O_4 species, we find pyropheophorbide b ($M^{+\bullet}$, $C_{33}H_{32}N_4O_4$, NKM 548) and protoporphyrin IX ($M^{+\bullet}$, $C_{34}H_{34}N_4O_4$, NKM 562), which are part of the same Kendrick series with a KMD of 0.37. Protoporphyrin IX plays a fundamental role in the biosynthesis of chlorophylls and serves as a pivotal point for the formation of other tetrapyrrolic pigments, such as heme.[72] Additionally, we detected pyropheophorbide a ($M^{+\bullet}$, $C_{33}H_{34}N_4O_3$, NKM 534) with a KMD of 0.33. Both pyropheophorbide a and b are considered indicators of cellular senescence and have been employed as photosensitizers capable of inducing cellular apoptosis.[61] Furthermore, other researchers have reported the isolation and identification of new chlorophyll derivatives using advanced methods, including HPLC, nuclear magnetic

resonance (NMR), and MS.[72] As shown in this study, the chlorophyll derivatives reported by various authors typically vary due to methylation, oxidation, or dehydration reactions.

Carotenoids are highly conjugated compounds that exhibit significantly different KMD values compared to saturated aliphatic compounds within a similar *m/z* range (red data points in **Fig 6**). Detected O_2, O_3, and O_4 species can be associated with carotenoid analogs, while O_5, O_6, and O_7 have previously been linked to the presence of lipids in microalgae. Chu, F., et al.,[81] have reported the use of mass defect filtering for carotenoid analysis in complex algal samples using high-resolution mass spectrometry. The authors selected unique mass defect windows that allowed them to exclude all non-carotenoid compounds from a non-polar extract of algal cells, demonstrating a semi-targeted metabolomics approach to identify carotenoid compounds in algae. Additionally, other researchers have developed a tool based on mass defect filtering to screen natural products. This tool uses a known elemental formula as a filter template to identify structurally similar compounds.[82–84] Some researchers have applied Kendrick mass defect filtering to screen for glucosinolates in crude extracts of rhizome of leaf.[83] Moreover, the presence of compounds with higher degrees of oxidation, such as the $O_{5\text{-}7}$ species, may result from oxidative processes inherent to microalgal cells or the accumulation of oxygen-containing compounds (e.g., GDGTs in the O_6 class), which have been previously reported in other microalgal species.[85] IsoGDGTs have been identified as components of the cell membrane in *Archaea*, ubiquitous prokaryotic microorganisms found in diverse aquatic systems.[86] Additionally, the O_6 species may be related to the presence of triacylglycerides (TAGs) in *C. vulgaris* cells, which have been widely reported in the literature and can be isolated using the employed extraction methodology.[85]

Among the N_n (n =1-3) nitrogen-containing species detected within microalgae samples, their attribution to lipids in *C. vulgaris* microalgae membranes is well-founded.[51,67,77] Interestingly, we have identified a series of pyridoindole derivatives ($C_{11}H_8N_2$) with a DBE of 9, detected as $[M + H]^+$, differing by zero to six CH_2 units in their structure. These pyridoindole derivatives have demonstrated potent antioxidant properties in various experimental models, including those pertaining to central nervous system pathologies.[87] Such derivatives have been previously reported in microalgae samples using FT-ICR.[67,77] Additionally, a series featuring a DBE of 10 was detected and attributed to derivatives of 9-aminocridine ($C_{13}H_{10}N_2$), identified as $[M + H]^+$ and distinguished by variations in the number of CH_2 units within their structures. Wang et al.[88] showcased the anticancer potential of a novel compound, 6-chloro-2-methoxy-N-(phenylmethyl)-9-acridinamine, isolated from a marine sponge (species unspecified). This aminocridine derivative exhibited the ability to inhibit *in vitro* cell proliferation and hamper *in vivo* tumor growth in human liver carcinoma SMMC-7221 cells and SMMC-7221 subcutaneous xenografts. [88] Here, we've uncovered peaks likely representing previously unreported analogs that have undergone additional methylations or unsaturations.
Fig 6 provides a snapshot of the signals detected in *C. vulgaris* cells via high-resolution mass spectrometry. KMD analysis is a powerful tool for sieving through background signals and isolating minor yet crucial features within complex mixtures.

van Krevelen analysis for *C. vulgaris* cells
The van Krevelen diagram, named after the Dutch chemical engineer Dirk Willem van Krevelen (1914–2001), presents a powerful graphical method for the analysis of high-resolution mass spectrometry (HRMS) data. This diagram is particularly compelling because it goes beyond merely classifying elemental compositions based on saturation or aromaticity; it also shows trends and structural variations among the identified species, potentially shedding light on the origin of the analyzed samples.[89] To construct the van Krevelen diagram, elemental compositions are projected onto two or three axes: hydrogen-to-carbon (H/C) atomic ratio in relation to oxygen-to-carbon (O/C) and/or nitrogen-to-carbon (N/C) ratios. The H/C ratio

segregates compounds with differing degrees of unsaturation, while the O/C and N/C ratios distinguish compounds based on their oxygen and nitrogen content.[90] As mentioned earlier, shifts in elemental composition, as observed in the van Krevelen diagram, can be linked to metabolic pathways, such as hydroxylation and methylation. The utility of the van Krevelen diagram in metabolomics has been well-documented in previous studies.[91,92] **Fig 7** provides van Krevelen diagrams that visualize data derived from 21 T MALDI FT-ICR MS analyses.

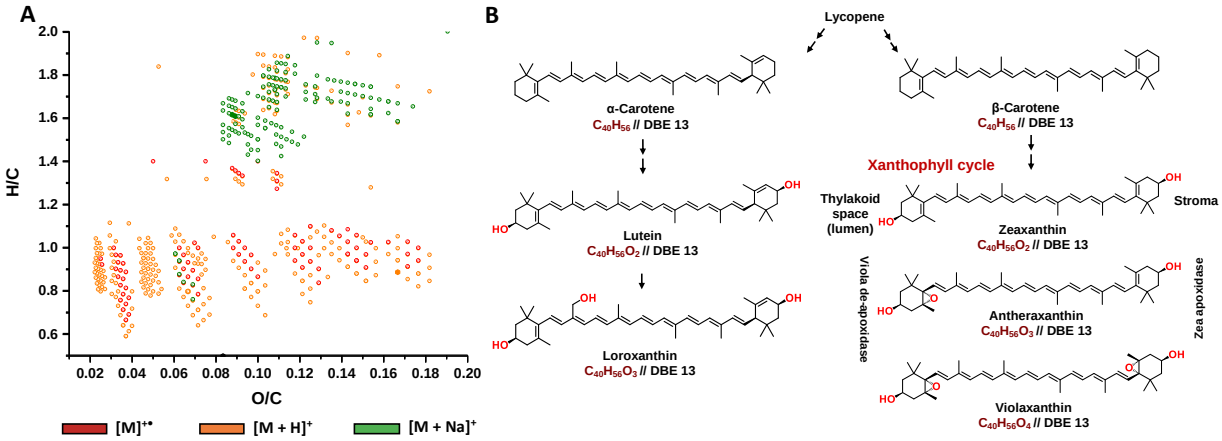

Figure 7. A van Krevelen diagram overlapped obtained from MALDI 21 Tesla FT-ICR mass spectrometry for all molecular information detected as radical cations, protonated molecules, and sodium adducts in *C. vulgaris* pigment extracts. **B** overview of the biosynthetic pathways for certain carotenoids and the xanthophyll cycles.[54,79]

These diagrams illustrate the variations in the elemental compositions of *C. vulgaris* cells concerning their O/C ratios. Biologically derived compounds, such as lipids, lignin, peptides, and condensed polyaromatic compounds, exhibit characteristic H/C and O/C ratios.[93,94] Therefore, different compound types can be identified based on the positions of points within the van Krevelen plot. Compounds of biological origin, e.g., lipids and condensed polyaromatic compounds, are characterized by specific H/C and O/C ratios, resulting from reactions (e.g., oxidation, condensation) that involve changes in the carbon, hydrogen, oxygen, or nitrogen content, which are reflected in their positioning on the van Krevelen plot. The entirety of the molecular compositions identified in this study clusters in a region where O/C ratios range from 0 to 0.2 and H/C ratios from 0.5 to 2. These regions are associated with structures resembling fatty acids (or lipids), isoprenes (carotenoids), and condensed aromatic compounds, as discussed earlier. Other groups with higher O/C ratios, such as proteins and carbohydrates/cellulose, known to be present in *C. vulgaris* cells,[5,95] were not detected due to the specific extraction methodology employed in this study.

Interestingly, regions with lower H/C ratios (ranging from 0.6 to 1.1) are predominantly occupied by nitrogenated species N_4O_o (o=0-5), which are grouped based on the number of oxygen atoms in their structures. The low H/C ratio suggests a notable hydrogen deficiency in these molecules, indicative of the presence of condensed ring structures with numerous double bonds. This is notably observed in chlorophyll derivatives within the sample, which can possess up to 30 double bond equivalents (DBE). Compositions found between O/C ratios of 0.08 and 0.10 and H/C ratios of 1.2 and 1.4 correspond to analogs of pheophytin a, $C_{55}H_{74}N_4O_5$, DBE 21. Interestingly, all analogs of pheophytin a were detected just as a radical cation or protonated molecules and share the same DBE value but differ in the number of CH_2 units within their structures. The DBE values of oxygenated species suggest highly conjugated compounds, linked to the alternating double bond structures of carotenoids, and were detected mostly as sodium adducts. Compounds in the C_{40} series, significant biomarkers in microalgal analysis, display low

variability in the number of DBEs, suggesting variations in oxygen units (**Fig. 7B**). This variability is pertinent to the search for biomarkers related to microalgal adaptation to changing environments, and growth stages.[96] Interestingly, some analogs of carotenoids share the same DBE value and the same number of carbons in their structures, such as carotene ($C_{40}H_{56}$, DBE 13), lutein ($C_{40}H_{56}O_2$, DBE 13), and loroxanthin ($C_{40}H_{56}O_3$, DBE 13). This similarity adds complexity to the analysis of these compounds, as they are challenging to differentiate based on commonly employed graphs like DBE vs. number of carbon atoms. However, the molecular assignments made are supported by the available scientific literature.[39–41,55,95]

In the van Krevelen diagram, data are organized in patterns with certain gaps (e.g., vertical lines that indicate an increase in DBE values). According to existing literature,[94] these patterns may be attributed to constraints on the numbers of carbon, oxygen, and hydrogen atoms in the observed peaks. From these lines, a series of compounds, possibly products of various chemical reactions, can be visually identified. For example, several lines converge at (O/C= 0, H/C= 2), indicating the presence of a series of hydrogen-rich molecules differing by integer numbers of CH_2 units, signifying methylation/demethylation reactions. The biosynthetic pathway of carotenoids in microalgae commences with an active isoprene, which, through a series of desaturation and isomerization reactions, elongates the conjugated double bond system and the absorption spectrum of the molecule into the visible light range, ultimately yielding lycopene. The linear ends of lycopene are cyclized to produce cyclic carotenes like α-carotene or β-carotene. Molecular oxygen is gradually introduced, leading to a wide array of xanthophylls. The literature also explores other crucial oxygenation reactions, including xanthophyll cycles, ketolation, and epoxidation of b-ionone rings.[54] These reactions result in xanthophylls present in photosynthetic pigment-protein complexes. Ketolation, in particular, is characteristic of secondary carotenoids that accumulate in algal resting stages under unfavorable environmental conditions.[54,97] The precise reactions governing the major light-harvesting xanthophylls in certain microorganisms, remain a subject of ongoing research. Therefore, the van Krevelen diagram could be a tool for tracking oxidation or reduction reactions in samples rich in carotenoids.

The analysis of ultra-high-resolution MALDI data using various techniques, such as KMD, DBE, and van Krevelen analysis, affords a comprehensive insight into the elemental composition and structure of chlorophylls, carotenoids, and lipids in *C. vulgaris* cells. While the results of the *C. vulgaris* sample analysis aligns with expected compositions based on other techniques, it is always possible that certain molecular information may be inadvertently overlooked.

Conclusions

This work shows the potential of MALDI 21 T FT-ICR MS in enabling a comprehensive analysis of photoprotective and photosynthetic pigments within microalgae. Interestingly, we identified ionized compounds through different pathways such as radical cations, protonated molecules, and sodium adducts, depending on the structure and properties of the molecules. Here, we report 113, 467, and 8, compounds analogous to chlorins (N_4O_o(o=0-6)) detected as cation radical, protonated molecules and sodium adducts, respectively. The molecular identification in *C. vulgaris* extracts matched with H/C, O/C, Kendrick mass defect (KMD), and Double Bond Equivalent (DBE) values, and with previous reports in the literature. We propose KMD analysis for the swift and precise filtration of pigmentary biomarkers in microalgae. Furthermore, van Krevelen diagram enabled the identification of lipid analogues, unsaturated hydrocarbons, and condensed aromatic compounds, each linked to specific H/C, and O/C elemental composition ratios,

thereby representing chlorophylls, lipids, and carotenoids. Additionally, this diagram provided a deeper understanding of the methylation and oxidation reaction pathways, closely intertwined with the biosynthetic and degradation routes of chlorophylls and carotenoids. The discovery of new biomarkers within molecular profiles is closely related to the resolution used in measurement, which is why MALDI 21 T FT-ICR MS plays an important role in metabolomic analysis. Nevertheless, MALDI TOF is an accessible tool that, due to its efficiency and acceptable analytical descriptors such as signal-to-noise ratio (S/N) and resolution, has proven to be a rapid and reliable method for the identification of microalgae based on their pigment biomarker profiles. This study highlights the synergy between high-resolution analysis and rapid profiling for a comprehensive understanding of the chemistry of these unique organisms.

Acknowledgements

The authors acknowledge the Guatiguará Technology Park and the Central Research Laboratory Facility at Universidad Industrial de Santander (UIS) for infrastructural support. The authors acknowledge funding from MINCIENCIAS (Grant 2019000100020). A portion of this work was performed at the National High Magnetic Field Laboratory, which is supported by the National Science Foundation Cooperative Agreement No. DMR-2128556 and the State of Florida.

References

1 B. Elisabeth, F. Rayen and T. Behnam, *Crit Rev Biotechnol*, 2021, **41**, 457–473.

2 M. Rizwan, G. Mujtaba, S. A. Memon, K. Lee and N. Rashid, *Renewable and Sustainable Energy Reviews*, 2018, **92**, 394–404.

3 B. Rodriguez, *Food Carotenoids: Chemistry, Biology and Technology*, 1st edn., 2015, vol. 3.

4 M. Roca, K. Chen and A. Pérez-Galvez, in *Handbook on Natural Pigments in Food and Beverages*, eds. R. Carle and R. M. Schweiggert, Sevilla,España, 2016, pp. 125–158.

5 C. Safi, B. Zebib, O. Merah, P. Y. Pontalier and C. Vaca-Garcia, *Renewable and Sustainable Energy Reviews*, 2014, **35**, 265–278.

6 S. Daliry, A. Hallajisani, J. Mohammadi Roshandeh, H. Nouri and A. Golzary, *Global Journal of Environmental Science and Management*, 2017, **3**, 217–230.

7 C. J. de Andrade and L. M. de Andrade, *Journal of Advanced Research in Biotechnology*, 2017, **2**, 1–9.

8 F. Manzoor, A. Karbassi and A. Golzary, *Current Environmental Management*, 2019, **6**, 174–187.

9 D. A. Silva, L. G. Cardoso, J. S. de Jesus Silva, C. O. de Souza, P. V. F. Lemos, P. F. de Almeida, E. de S. Ferreira, A. T. Lombardi and J. I. Druzian, *Environ Technol Innov*, 2022, **25**, 1–11.

10 S. L. Bender and B. A. Barry, *Biophys J*, 2008, **95**, 3927–3934.

11 J. Whitmarsh and Govindjee, *Biochem Soc Trans*, 2002, **6**, 901–913.

12 L. Vernon and G. Seely, *The Chlorophylls: Physical, Chemical and Biological Properties*, Academic Press, 1st edn., 2014.

13 A. Larkum, *The Evolution of Chlorophylls and Photosynthesis*, Springer, University of Sydney, Australia, Segunda edn., 2006.

14 H. Scheer, in *Encyclopedia of Biological Chemistry: Second Edition*, eds. W. J. Lennarz and M. D. Lane, Elsevier Inc., Munich, 2nd edn., 2013, pp. 498–505.

15 S. Mohammed Ali, H. Shafeek Nasr and W. Tawfok Abbs, *pakistan journal of Biological Sciences*, 2012, **16**, 775–782.

16 J. W. Louda, *J Liq Chromatogr Relat Technol*, 2007, **31**, 295–323.

17 V. Brotas and M. Plante-cuny, *Acta Oecologica*, 2003, **24**, 109–115.

18 M. Krajewska, M. Szymczak-Żyła and G. Kowalewska, *Current Chemistry Letters*, 2017, **6**, 91–104.

19 L. M. Díaz-Sánchez, C. Blanco-Tirado and M. Y. Combariza, *MethodsX*, 2023, **10**, 102140.

20 J. S. Ramírez-Pradilla, C. Blanco-Tirado and M. Y. Combariza, *ACS Appl Mater Interfaces*, 2019, **11**, 10975–10987.

21 J. S. Ramírez-Pradilla, C. Blanco-Tirado and M. Y. Combariza, *ACS Appl Mater Interfaces*, 2019, **11**, 10975–10987.

22 J. S. Ramírez-Pradilla, C. Blanco-Tirado, M. Hubert-Roux, P. Giusti, C. Afonso and M. Y. Combariza, *Energy and Fuels*, 2019, **33**, 3899–3907.

23 D. Giraldo-Dávila, M. L. Chacón-Patiño, J. S. Ramirez-Pradilla, C. Blanco-Tirado and M. Y. Combariza, *Fuel*, 2018, **226**, 103–111.

24 L. Castellanos-García, B. Agudelo, H. Rosales, M. Cely, C. Ochoa-Puentes, C. Blanco-Tirado, C. Sierra and M. Combariza, *J Am Soc Mass Spectrom*, 2017, **28**, 2548–2560.

25 J. A. Oñate-Gutiérrez, L. M. Díaz-Sánchez, D. L. Urbina, J. R. Pinzón, C. Blanco-Tirado and M. Y. Combariza, *RSC Adv*, 2023, **13**, 12712–12722.

26 R. Knochenmuss, *Analyst*, 2006, **131**, 966–986.

27 R. Knochenmuss, *Analyst*, 2014, **139**, 147–156.

28 R. Knochenmuss, *Journal of Mass Spectrometry*.

29 R. Zenobi and R. Knochenmuss, *Mass Spectrom Rev*, 1999, **17**, 337–366.

30 C. Brunnee, *International Journal of Mass Spectrometty and Ion Processes*, 1987, **76**, 125–237.

31 K. K. Murray, *J Am Soc Mass Spectrom*, 2022, **33**, 2342–2347.

32 M. M. Wolff and W. E. Stephens, *Review of Scientific Instruments*, 1953, **24**, 616–617.

33 J. Gross, *Mass Spectrometry*, Springer, Heidelberg, Germany, Third Edition., 2017.

34 M. B. Comisarow and A. G. Marshall, *The Early Development of Fourier Transform Ion Cyclotron Resonance (FT-ICR) Spectroscopy*, 1996, vol. 31.

35 E. O. Lawrence and S. M. Livingston, *Physical Review*, 1932, **40**, 19–37.

36 I. Tolosa, I. Vescovali, N. LeBlond, J. C. Marty, S. De Mora and L. Prieur, *Mar Chem*, 2004, **88**, 103–125.

37 Y. K. Wong, Y. H. Ho, K. Co, H. M. Leung and K. K. L. Tung, *Journal of Aquaculture & Marine Biology*, 2017, **6**, 6–12.

38 H. Lichtenthaler and A. Wellburn, *Biochem Soc Trans*, 1983, **11**, 591–592.

39 L. Gouveia, V. Veloso, A. Reis, H. Fernandes, J. Novais and J. Empis, *Bioresour Technol*, 1996, **57**, 157–163.

40 H. A. Pantami, M. S. A. Bustamam, S. Y. Lee, I. S. Ismail, S. M. M. Faudzi, M. Nakakuni and K. Shaari, *Mar Drugs*.

41 V. Hynstova, D. Sterbova, B. Klejdus, J. Hedbavny, D. Huska and V. Adam, *J Pharm Biomed Anal*, 2018, **148**, 108–118.

42 L. Patiny and A. Borel, *J Chem Inf Model*, 2013, **53**, 1223–1250.

43 C. L. Hendrickson, J. P. Quinn, N. K. Kaiser, D. F. Smith, G. T. Blakney, T. Chen, A. G. Marshall, C. R. Weisbrod and S. C. Beu, *J Am Soc Mass Spectrom*, 2015, **26**, 1626–1632.

44 Y. E. P. Software. (The F. S. U. T. F. U. 2014) Corilo, 2014.

45 T. Kind and O. Fiehn, *BMC Bioinformatics*, 2007, **8**, 1–12.

46 Edward Kendrick, *Anal Chem*, 1963, **35**, 2146–2154.

47 M. W. Alton, H. Stark, M. R. Canagaratna and E. C. Browne, *Atmos Meas Tech*, 2023, **16**, 3273–3282.

48 M. M. Maroneze, L. Q. Zepka, E. J. Lopes, A. Pérez-Gálvez and M. Roca, *Antioxidants*, 2019, **8**, 1–15.

49 S. Jeffrey, R. Mantoura and S. Wright, *Phytoplankton pigments in oceanography: guidelines to modern methods*, Paris, Primera., 1997, vol. 48.

50 Y. Silveira, L. Gómez and M. D. Kufundala, *Revista Cubana de Química*, 2018, **30**, 55–67.

51 T. Luangpipat and Y. Chisti, *J Biotechnol*, 2017, **257**, 47–57.

52 R. Kaufmann, T. Wingerath, D. Kirsch, W. Stahl and H. Sies, *Anal Biochem*, 1996, **128**, 117–128.

53 S. Wright and S. Jeffrey, *Hdb. Env. Chem.*, 2006, **2**, 71–104.

54 S. Roy, C. Llewellyn, E. Skarstad and G. Johnsen, *Phytoplankton Pigments: Characterization, Chemotaxonomy and Applications in Oceanography*, 2011.

55 K. Aitzetmuller, H. Strain, W. Svec, M. Grandolfo and J. Katz, *Phytochemistry*, 1969, **8**, 1761–1770.

56 F. Xian, C. L. Hendrickson and A. G. Marshall, *Anal Chem*, 2012, **84**, 708–719.

57 J. M. Jarvis, J. M. Billing, R. T. Hallen, A. J. Schmidt and T. M. Schaub, *Energy and Fuels*, 2017, **31**, 2896–2906.

58 W. Bahureksa, T. Borch, R. B. Young, C. R. Weisbrod, G. T. Blakney and A. M. McKenna, *Anal Chem*, 2022, **94**, 11382–11389.

59 D. F. Smith, D. C. Podgorski, R. P. Rodgers, G. T. Blakney and C. L. Hendrickson, *Anal Chem*, 2018, **90**, 2041–2047.

60 M. Roca and A. Pérez-Gálvez, *Antioxidants*, 2021, **10**, 1622–1645.

61 S. Hörtensteiner, *Annu Rev Plant Biol*, 2006, **57**, 55–77.

62 X. Zhu, J. Chen, K. Qiu and B. Kuai, *Front Plant Sci*, 2017, **8**, 1–8.

63 J. Claesen, A. Rockwood, M. Gorshkov and D. Valkenborg, *Mass Spectrom Rev*, 2023, 1–21.

64 C. J. Thompson, M. Witt, S. Forcisi, F. Moritz, N. Kessler, F. H. Laukien and P. Schmitt-Kopplin, *J Am Soc Mass Spectrom*, 2020, **31**, 2025–2034.

65 E. Rathahao-Paris, S. Alves, C. Junot and J. C. Tabet, *Metabolomics*, 2016, **12**, 1–15.

66 C. Padilla-Jaramillo, L. Díaz-Sánchez, M. Combariza, C. Blanco-Tirado and A. Combariza, *Orinoquia*, 2021, **25**, 13–23.

67 T. San Cha, J. Y. Chee, S. H. Loh and M. Jusoh, *Bioresour Technol Rep*, 2018, **3**, 218–223.

68 N. Sudasinghe, H. Reddy, N. Csakan, S. Deng, P. Lammers and T. Schaub, *Bioenergy Res*, 2015, **8**, 1962–1972.

69 J. M. Jarvis, K. O. Albrecht, J. M. Billing, A. J. Schmidt, R. T. Hallen and T. M. Schaub, *Energy and Fuels*, 2018, **32**, 8483–8493.

70 J. M. Jarvis, J. M. Billing, Y. E. Corilo, A. J. Schmidt, R. T. Hallen and T. M. Schaub, *Fuel*, 2018, **216**, 341–348.

71 C. Geantet, D. Laurenti, N. Guilhaume, C. Lorentz, I. Borghol, B. Bujoli, E. Chailleux, R. Checa, S. Schramm, V. Carré, F. Aubriet and C. Queffélec, *J Environ Chem Eng*, 2022, **10**, 107361.

72 Porra Robert, Oster Ulrike and Scheer Hugo, in *Phytoplankton Pigments: Characterization, Chemotaxonomy and Applications in Oceanography*, eds. S. Roy, C. Llewellyng, E. Skarstad and G. Jhonsen, Cambridge University Press, United Kingdom, First Edit., 2011, pp. 78–112.

73 N. Chen, T. Bianchi and J. M. Bland, *Mar Chem*, 2003, **81**, 37–55.

74 K. Kumari, S. Samantaray, D. Sahoo and B. C. Tripathy, *Photosynth Res*, 2021, **148**, 17–32.

75 C. A. Hughey, C. L. Hendrickson, R. P. Rodgers, A. G. Marshall and K. Qian, *Anal Chem*, 2001, **73**, 4676–4681.

76 M. O. Senge, A. A. Ryan, K. A. Letchford, S. A. MacGowan and T. Mielke, *Symmetry (Basel)*, 2014, **6**, 781–843.

77 J. M. Jarvis, J. M. Billing, R. T. Hallen, A. J. Schmidt and T. M. Schaub, *Energy and Fuels*, 2017, **31**, 2896–2906.

78 J. Hustin, C. Kune, J. Far, G. Eppe, D. Debois, L. Quinton and E. De Pauw, *J Am Soc Mass Spectrom*, 2022, **33**, 2273–2282.

79 E. Jacob-lopes, M. I. Queiroz and L. Queiroz Zepka, *Pigments from Microalgae Handbook*, Springer Nature, 2020.

80 M. O. Senge and S. A. MacGowan, in *Handbook of Porphyrin Science*, 2011, vol. 13, pp. 253–297.

81 F. L. Chu, L. Pirastru, R. Popovic and L. Sleno, *J Agric Food Chem*, 2011, **59**, 3004–3013.

82 L. Sleno, *Journal of Mass Spectrometry*, 2012, **47**, 226–236.

83 J. Geng, L. Xiao, C. Chen, Z. Wang, W. Xiao and Q. Wang, *J Chromatogr A*.

84 X. Wu, Y. Liu, Z. Zhang, Z. Ou, G. Wang, T. Zhang, H. Long, M. Lei, L. Liu, W. Huang, J. Hou, W. Wu and D. A. Guo, 2022, *Molecules*.

85 F. O. Holguin and T. Schaub, *Algal Res*, 2013, **2**, 43–50.

86 C. Lizama, J. Romero-Parra, D. Andrade, F. Riveros, J. Bórquez, S. Ahmed, L. Venegas-Salas, C. Cabalín and M. J. Simirgiotis, *Antioxidants*

87 N. Mrvová, M. Škandík, Š. Bezek, N. Sedláčková, M. MacH, Z. Gaspárová, D. Luptáková, I. Padej and L. Račková, *Interdiscip Toxicol*, 2017, **10**, 11–19.

88 E. Wang, M. A. Sorolla, P. D. G. Krishnan and A. Sorolla, *Biomolecules*, 2020, 10.

89 J. R. Laszakovits and A. A. MacKay, *J Am Soc Mass Spectrom*, 2022, **33**, 198–202.

90 Z. Wu, R. P. Rodgers and A. G. Marshall, *Anal Chem*, 2004, **76**, 2511–2516.

91 H. J. Smith, M. Tigges, J. D'Andrilli, A. Parker, B. Bothner and C. M. Foreman, *Limnol Oceanogr Lett*, 2018, **3**, 225–235.

92 Y. Liu, C. Ma and J. Sun, *iScience*.

93 V. Mangal, N. L. Stock and C. Guéguen, *Anal Bioanal Chem*, 2016, **408**, 1891–1900.

94 S. Kim, R. W. Kramer and P. G. Hatcher, *Anal Chem*, 2003, **75**, 5336–5344.

95 S. Weber, P. Grande, L. Blank and H. Klose, *PLoS One*, 2022, **17**, 1–14.

96 J. R. Radovic, R. C. Silva, R. W. Snowdon, M. Brown, S. Larter and T. B. P. Oldenburg, *Rapid Communications in Mass Spectrometry*, 2016, **30**, 1273–1282.

97 A. Sánchez, L. Flores, E. Langley, R. Martín, G. Maldonado and S. Sánchez, *Rev Latinoam Microbiol (1958)*, 1999, **41**, 175–191.

Chapter 4

Linking MALDI FT-ICR MS pigment profiles with phytoplankton community to study aquatic ecosystems

Edited from: Luis M. Díaz-Sánchez, Martha L. Chacón-Patiño, Chad R. Weisbrod, Lizbeth J. Vivas-Aguas, David Stranz, Scott Campbell, Cristian Blanco-Tirado, Marianny Y. Combariza, Algal Research, Under review. 2024.

Keywords

Aquatic ecosystems; Microalgae; Phytoplankton; Biomarkers; Matrix Assisted Laser Desorption Ionization; MALDI; Fourier Transform Ion Cyclotron Resonance (FT-ICR); Mass Spectrometry.

Abstract

The Ciénaga Grande de Santa Marta (CGSM), located in the Colombian Caribbean, is a biodiverse ecosystem of significant ecological importance. This study aims to analyze the pigmentary fingerprint of phytoplankton samples from CGSM using electron-transfer Matrix-Assisted Laser Desorption/Ionization Mass Spectrometry (MALDI MS) and Fourier Transform Ion Cyclotron Resonance Mass Spectrometry (FT-ICR MS). Through the analysis of phytoplankton pigments, we aim to understand the intricate web of interactions within CGSM and to shed light on the influence of anthropogenic activities and environmental factors on phytoplankton communities, which reflects the entire ecosystem. Phytoplankton samples were collected from various locations within the CGSM, representing different seasons, allowing for a comprehensive analysis of the molecular composition in both freshwater and Caribbean-connected environments. The study's findings provide valuable insights into the intricate chemistry of CGSM, with implications for its conservation and sustainable management.

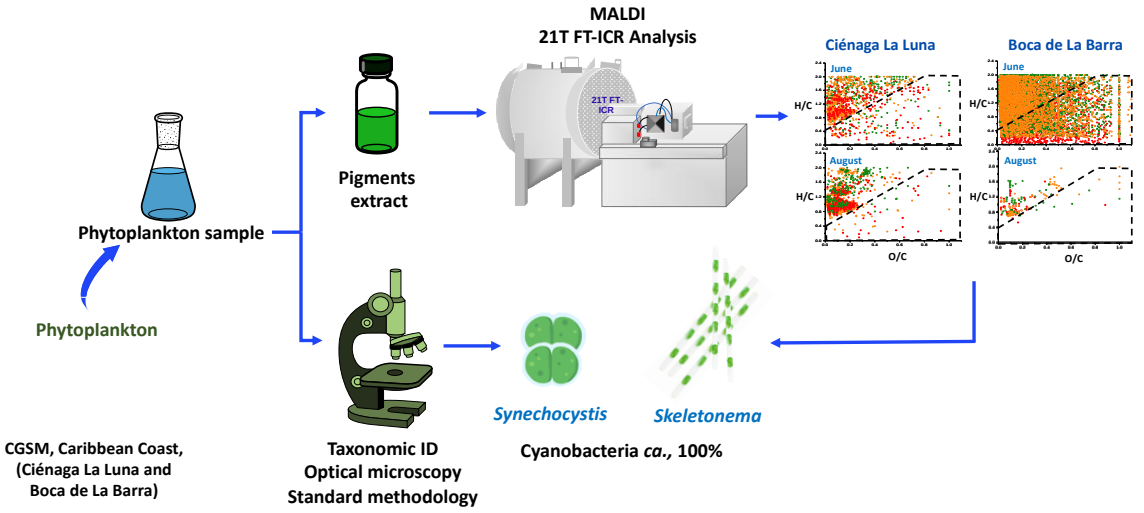

Introduction

The Ciénaga Grande de Santa Marta (CGSM), located in the Colombian Caribbean, is a remarkable and diverse ecosystem that has long captivated ecologists, biologists, and conservationists.[1] Encompassing an area of approximately 4,280 square kilometers, this expansive wetland is nestled between the Caribbean Sea and the Santa Marta Mountains, thus ranking among the most biodiverse ecosystems in the region.[2] Recognized as Colombia's largest and most significant coastal wetland, the CGSM is celebrated for its distinctive topography, featuring a complex system of lagoons, estuaries, marshes, and mangroves, which collectively foster a wide array of ecosystems within its boundaries[3]. The CGSM ecoregion has five conservation designations due to its immense natural richness and unique ecological conditions. These designations include the Vía Parque Isla de Salamanca National Natural Park (Est. 1964), the Ciénaga Grande de Santa Marta Flora and Fauna Sanctuary (Est. 1977), Ramsar Wetland (Est. 1998), Biosphere Reserve (Est. 2000), and an International Importance Area for Bird Conservation (IBA/AICA), under the auspices of Birdlife International and the International Union for Conservation of Nature (IUCN).[4]

Estuaries function a unique biogeochemical interfaces between terrestrial and marine environments[5]. River discharges introduce natural and anthropogenic organic matter from the mainland, altering salinity levels and other physical-chemical gradients along the land-sea continuum.[3] The varying ecosystem conditions within estuaries create a dynamic community structure of microorganisms, with these intricate processes and interactions ultimately reflected in the chemical composition of both water columns and bottom sediments. At the core of ecological complexity within the CGSM lies the phytoplankton community[6–8]. Comprising microalgae and cyanobacteria, phytoplankton are a diverse group of microscopic photosynthetic organisms that play a vital role in the aquatic food chain.[9] In addition to being a primary food source for many aquatic organisms, phytoplankton is at the core of the carbon and nutrient cycles of the ecosystem. They are also prolific producers of natural organic matter, essential for the overall health and functioning of aquatic ecosystems[10]. The ecological significance of phytoplankton extends beyond sustenance and organic matter production as contributors to oxygen production through photosynthesis and effective carbon dioxide sinks. Their photosynthetic activity plays a vital role in regulating global climate patterns and maintaining atmospheric oxygen-carbon dioxide balance[11,12]. Furthermore, phytoplankton contribute to various ecosystem services, including water quality regulation, nitrogen fixation, and support for higher trophic levels, making them an indispensable component of the CGSM ecosystem. Thus, understanding phytoplankton community dynamics in the CGSM is crucial for the conservation and sustainable management of this unique ecosystem. Phytoplankton biomarkers, specific molecular compounds found in these microorganisms, serve as valuable indicators of ecosystem health and status.[8,13] Classifying phytoplankton species into different functional groups based on the chemical composition of these biomarkers offers valuable insights into nutrient dynamics and ecological interactions within the wetland.

However, molecular-level characterization of phytoplankton biomarkers poses analytical challenges due to their chemical complexity and the presence of high molecular weight and/or heteroatom-bearing species, such as carbohydrates, lignocellulosic compounds, pigments, lipids, and many other yet-to-be-characterized compounds[14–16]. Pigment analyses in phytoplankton samples typically involve specific and laborious protocols, often including fractionation steps and the use of various complementary instruments, all aimed at enhancing sensitivity, resolution, and species identification. To unravel the complexities of phytoplankton biomarkers in the CGSM, advanced analytical techniques are required. Recently, we have reported an electron-transfer Matrix-Assisted Laser Desorption/Ionization Mass Spectrometry (MALDI MS) methodology for the characterization of microalgae pigments, yielding results comparable to, or even surpassing, those achieved with standard techniques such as High-Performance Liquid Chromatography (HPLC)[17]. MALDI MS offers several advantages for generating phytoplankton

pigment profiles, including ionization selectivity, molecular ion survival, high impurity tolerance, and low detection limits.[18] In positive ion mode, the ET mechanism involves electron transfer from an analyte (A) neutral molecule with ionization energy (E_i) below the matrix's E_i to a primary ion of the matrix (M). This process results in the formation of an analyte molecular ion ($A^{+\bullet}$)[19–24] according to the following reaction pathway:

$$M^{+\bullet} + A \longrightarrow A^{+\bullet} + M$$
$$E_{i(Matrix)} > E_{i(Analyte)} \therefore \Delta E_i > 0.5\ eV$$

MALDI Fourier Transform Ion Cyclotron Resonance (MALDI FT-ICR) stands out as a powerful technique for targeted analysis of biomarkers in complex mixtures. Recent advancements in single-run methods enable the simultaneous monitoring of multiple target biomarkers, utilizing the capability of FT-ICR MS to screen for thousands of compounds with high resolution over a broad analytical window of polarity and molecular weights[25–29]. Furthermore, MALDI FT-ICR MS approaches simplify sample preparation and have broad-range screening capabilities that can reveal new biomarkers. In addition, the detection of fine isotopic patterns enables unequivocal identification of molecular species. Analysis using high-resolution mass spectrometry provide valuable compositional information that can guide subsequent confirmatory studies using targeted approaches. The use of double bond equivalents versus carbon number atom plots and van Krevelen diagrams allows for a comprehensive understanding of the ecological role and potential sources of these biomarkers.

In this context, we employed our recently reported ET MALDI FT-ICR methodology[17,30] to evaluate the molecular composition of phytoplankton samples collected at two distinct points at the CGSM, during different seasons. The objective of this study was to investigate the molecular composition of phytoplankton samples in freshwater and Caribbean-connected environments, to gain fresh insights into the intricate chemistry of this estuarine system. This comprehensive analysis has the potential to elucidate the complex network of interactions within the CGSM, shedding light on the influence of anthropogenic activities and environmental factors on phytoplankton communities and the wider ecosystem.

Experimental

Study area

The CGSM encompasses a vast estuarine complex situated in the northern coastal region of Colombia (Department of Magdalena), between 10°44' and 11°00' N latitude and 74°16' to 74°31' W longitude. Isolated from the Caribbean Sea by Isla de Salamanca, the CGSM is bordered by the floodplain of the Magdalena River to the west and southwest and the Sierra Nevada de Santa Marta (SNSM) to the east and southeast (**Fig. 1**). The marsh covers an area of 4,280 km^2, with a depth ranging from 1.8 to 3 meters.[5] The CGSM's hydrological dynamics are governed by freshwater inflows from the Magdalena River and saltwater from the Caribbean Sea. The water exchange is facilitated through a narrow artificial opening in the northeastern corner of the marsh. The eastern and southeastern sectors are affected by tributaries from the SNSM that provide a consistent water flow. In contrast, the western and northwestern sectors are directly influenced by the Magdalena River watershed where water flow depends on rainfall.[4] Seasonal and regional fluctuations in salinity range from 0 to 40, while water temperatures maintain an average of 30 °C annually. Global climatic phenomena, such as El Niño and La Niña, have a partial impact on water resource inputs, leading to modifications in tributary discharge and salinity parameters, thereby altering the water quality of CGSM.[4] Despite these influences, the CGSM demonstrates high productivity, as evidenced by its notably elevated annual gross primary production rates.[4]

Water and phytoplankton sampling

The samples were collected at two stations: Boca de La Barra (located between 10°59´38.47" and 74°17´39.63") and Ciénaga La Luna (located between 10°55´7.31" and 74°34´45.56"). These stations, established by the Instituto de Investigaciones Marinas y Costeras José Benito Vives de Andréis (INVEMAR) are part of a network of 28 sampling stations situated across various zones within the CGSM complex, each exhibiting different hydrographic characteristics.[4] Water samples were collected in June and August of 2022, corresponding to dry and rainy seasons, respectively, between 07:00 h and 11:00 h (**Fig. 1**). Boca de La Barra is a key sampling place where the CGSM estuarine complex and the Caribbean Sea connect, while Ciénaga La Luna is where the CGSM is most influenced by the Magdalena River and the floodplain.

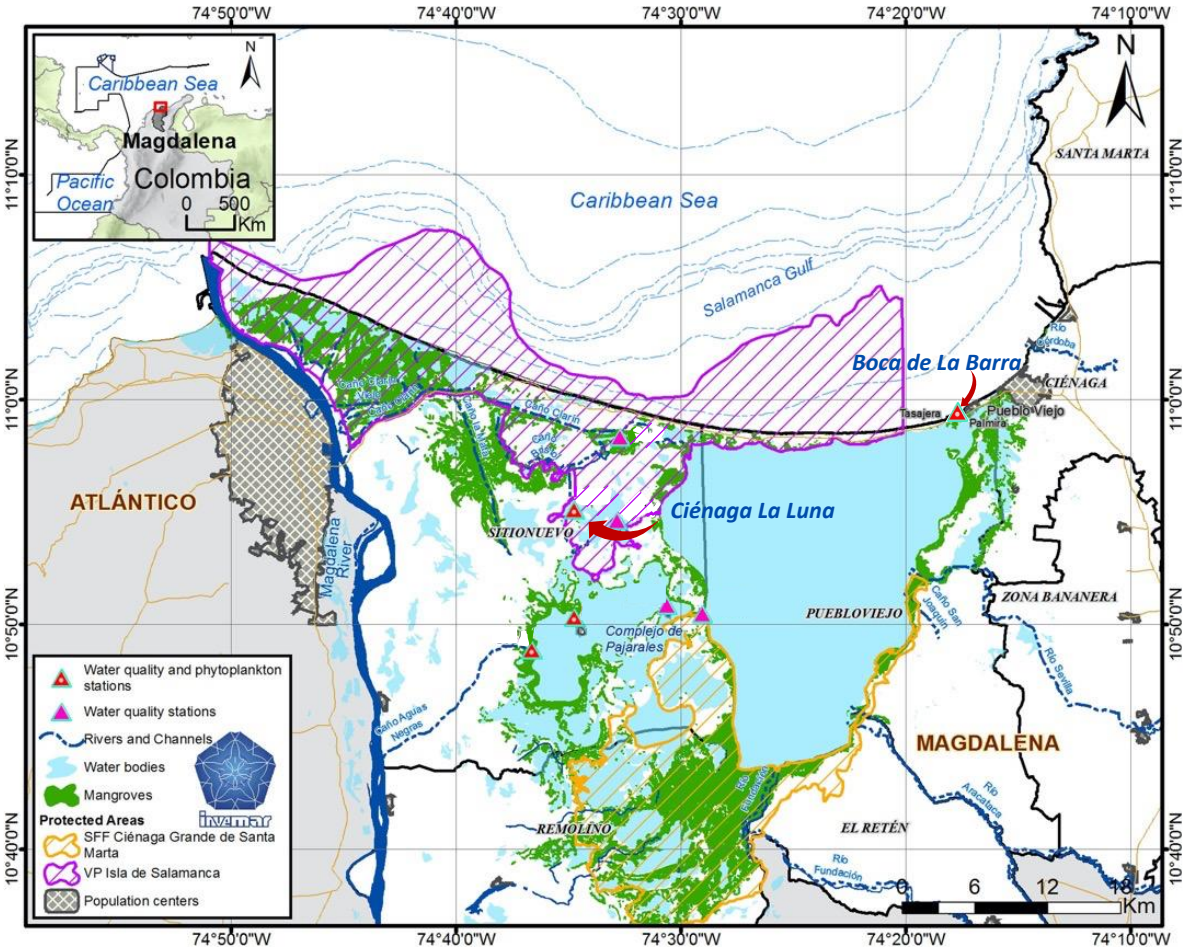

Figure 1. Map of the Ciénaga Grande de Santa Marta (CGSM) in the Colombian Caribbean Sea, indicating the locations where phytoplankton samples were gathered, as well as other sampling points designated by INVEMAR for water quality and phytoplankton stations. The map also illustrates the rivers, channels, bodies of water, mangroves, and protected areas that make up the CGMS. Image adapted from.[1]

Phytoplankton samples were provided by the INVEMAR technical team. The samples were collected using a standard conical phytoplankton net (30 cm diameter, 70 cm length) fitted with a metal bridle ring, a 23-micrometer polyester mesh net, a cod end PVC collection cup (250 mL) with two side windows covered with the same mesh as the net, and a rope (Biológika, Medellín, Colombia).[4] The net was deployed at the sampling point and continuously towed at low speed for 5 minutes, following a prior rinsing of both the

net and the cod end. The samples were transferred to amber-colored bottles and stored in an ice bath for approximately 2 h until reaching the laboratory. The samples were then filtered using 0.45 μm PTFE membrane filters and stored for pigment extraction and analysis. Additionally, for phytoplankton community taxonomy, water samples were collected following the manual and guides of the intergovernmental Oceanographic Commission, UNESCO.[31] The samples were deposited in 250 mL polyethylene bottles, preserved with Lugol's iodine solution at a ratio of 1:100,[32] and stored away from direct sunlight until transportation to the laboratory for analysis.

Water physicochemical parameters measurement

In situ water salinity, temperature, and pH measurements were performed by the INVEMAR technical team using multiparameter handheld meters following Standard Methods 2520-B (salinity, temperature) and Standard Methods No. 4500-H B (pH). *In situ* dissolved oxygen (DO) was measured with a membrane electrode according to Standard Methods 4500-O G. Transparency was evaluated using a Secchi disk[4]. Values for chemical environmental factors, such as orthophosphate ($P\text{-}PO_4$), which is related to excess nutrients from anthropogenic sources, were determined using the ascorbic acid colorimetric method as previously described[4].

Phytoplankton community structure analysis

The phytoplankton taxonomic analysis follows a series of standard processes. Initially, the Utermöhl sedimentation method was employed. Settled phytoplankton cells, previously placed into a settling chamber, were examined using an inverted microscope.[32] Genus-level identification was conducted based on morphological cell characteristics. This involves the use of taxonomic descriptions, such as cell shape, size, the presence of specific organelles, colony formation, and keys from the scientific literature.[33–36] Qualitative and quantitative information on phytoplankton was organized into matrices for calculating relative abundances per taxonomic group and for generating graphs to determine the overall behavior of the communities.

Phytoplankton chemical profiles

Pigment extraction

The extraction of pigments from the phytoplankton samples followed established procedures[17,30] One-quarter piece of the filter with the retained phytoplankton was placed in contact with 1 mL of analytical-grade acetone in a 1.5 mL amber vial. The mixture was then sonicated at 40 kHz in a Branson UltrasonicsTM CPX bath (Danbury, CT, USA), operating at 35 W for 25 min at room temperature. Following the extraction period, the sample was filtered using 0.45 mm Whatman GF/F filters and stored in amber vials at 4 °C until analysis. Chlorophyll a quantitation was carried out using UV-Vis spectroscopy according to the Lorenzen method as described in Standard Methods 10200-H.[4,37]

MALDI FT-ICR MS pigment analysis

A 5 mM solution of *trans*-2-[3-(4-tert-butylphenyl)-2-methyl-2-propenylidene] malononitrile (DCTB) in acetonitrile (ACN) was prepared by dissolving the solid with the aid of ultrasound energy (40 kHz) for 2 min. The concentration of the phytoplankton extracts was estimated to be approximately 0.03 mM, based on the concentration of chlorophyll a.[4,37,38] DCTB and phytoplankton solutions were mixed to reach an analyte-to-matrix ratio of 1:100. Samples (1 μL) were dispensed onto a stainless-steel sample holder using the dried droplet method. MALDI FT-ICR experiments were carried out using a 21 T FT-ICR mass spectrometer at the National High Magnetic Field Laboratory (NHMFL), Florida State University. The instrumental setup comprises a Velos Pro linear ion trap (Thermo Scientific, San Jose, CA) front end, along with a proprietary NHMFL ICR cell and ion transfer optics. The dynamically harmonized ICR cell operated

at a trapping potential of 7.5 V. Ionization was performed at an elevated-pressure MALDI source that included a dual-ion funnel interface (Spectroglyph LLC, Kennewick, WA). The funnels voltages were set at 625 kHz with a 150 V_{p-p} for the first high-pressure ion funnel, and 1.2 MHz with 90 V_{p-p} for the second low-pressure ion funnel. An electric field gradient of approximately 10 V/cm was maintained within the dual-funnel system, with a gradient of 100 V/cm between the source and the funnel inlet. The MALDI source was fitted with a Q-switched, frequency-tripled Nd:YLF laser emitting 349 nm photons (Explorer One, Spectra Physics, Mountain View, CA). The laser operated at a repetition rate of 1 kHz with a pulse energy of approximately 1.2 μJ. During the mass spectrometry analysis, an ion injection time of 250 ms was used with the automatic gain control (AGC) turned off. For ultrahigh mass resolving power analyses, a transient duration of 3.1 seconds was employed. All spectra were obtained in positive mode. The time-domain transients were acquired using the Predator data station, with an average of 100 time-domain acquisitions for all experiments. After data collection, data processing and visualization were conducted using the Investigator software (v. 1.3, Sierra Analytics, Modesto, CA) and Origin Pro 9.0 64-bit. The mass spectra were internally recalibrated using a series of highly abundant known ions and the recalibration equations provided by the Investigator software. Additionally, we considered a maximum hydrogen-to-carbon ratio of 2, and a double bond equivalent (DBE) value of 30. To validate molecular formula assignments, we compared theoretical (ChemCalc) isotopic patterns with experimental data.[39] Additionally, a resolving power at *m/z* 400 of approximately $1.6x10^6$ was achieved for all mass spectra, with errors below 0.25 ppm,[29] ensuring unambiguous molecular formula assignments for singly charged molecular ions ($M^{+\bullet}$), protonated molecules ($[M + H]^+$), and sodium adducts ($[M + Na]^+$) with relative abundances above 0.2%.[28] Carotenoids and cyanobacteria's secondary metabolites were identified by cross-referencing the list of molecular formulas assigned with the Investigator software with the Carotenoids Database[40] and CyanoMetDBm[41], respectively.

Results and discussion

Water quality at the sampling points

The water quality at the sampling points in the CGSM is greatly affected by various factors. These include continental inputs from rivers (Magdalena, Sevilla, Aracataca, and Fundación), atmospheric inputs, and saltwater inflow from the Caribbean Sea.[4] The mixing ratios of freshwater and seawater, circulation patterns, water residence time, environmental changes due to human activities and local and global climatic events all play a role in regulating the water quality in the CGSM.[35] Because of these factors, the water in the CGSM is sensitive to issues like deoxygenation, eutrophication, and algal blooms, which are commonly associated with estuaries and coastal systems[1]. Below are the environmental parameters reported by the INVEMAR at the sampling points Ciénaga La Luna and Boca de La Barra, in June and August of 2022 (**Table 1**).

Table 1. Average water quality parameters at the Ciénaga La Luna and Boca de La Barra sampling points in the CGSM.

Parameter	Ciénaga La Luna						Boca de La Barra					
	June			August			June			August		
Transparency (m)	0.4	±	0.1	0.7	±	0.1	1.0	±	0.1	0.3	±	0.1
Salinity (g/L)	3.0	±	0.1	1.0	±	0.1	9.0	±	0.2	3.0	±	0.1
Temperature (°C)	32.0	±	1.0	31.5	±	1.0	28.5	±	1.0	30.0	±	1.0
DO (mg O_2/L)	6.1	±	0.1	6.0	±	0.1	6.1	±	0.1	7.0	±	0.1
pH	8.0	±	0.1	7.8	±	0.1	8.5	±	0.1	8.0	±	0.1
Chlorophyll a (µg/L)	48.0	±	1.0	10.0	±	1.0	40.0	±	1.0	29.0	±	1.0
P-PO_4 (µg/L)	10.0	±	1.0	8.0	±	1.0	3.0	±	1.0	100.0	±	1.0

The surface water salinity measured in June and August of 2022 at Cienaga La Luna and Boca de La Barra ranged from 1.0 to 9.0 g/L. These lower salinity levels, in contrast to the typical values for estuarine water (10 g/L) and seawater from the Caribbean Ocean (29 g/L), may be attributable to the prevailing La Niña climate conditions during the study period. This led to increased precipitation in the CGSM area since early May, as indicated in the monthly climatological bulletin reported by the Institute of Hydrology, Meteorology, and Environmental Studies (IDEAM).[4] The low salinity conditions were especially noticeable at the Ciénaga La Luna station. This station receives its primary freshwater supply from sources such as the Magdalena River, in contrast to Boca de La Barra, which connects with the Caribbean Sea. The overall range of salinity was comparable to the values reported in previous years with similar precipitation conditions.[1,42–44]

The surface water temperature measurements show slight variations in Ciénaga La Luna and Boca de La Barra, ranging from 32.0 to 31.0 ºC and from 28.0 to 30.0 ºC, respectively. Ciénaga La Luna sustained higher temperatures likely the result of restricted water flow and intense solar radiation during the sampling period (09:00 h and 11:00 h). These values align with historical data reported by INVEMAR for the sampling points involved.[4] Water temperature significantly influences biological, chemical, and physical processes, as well as the distribution and health of aquatic life.[45] Elevated water temperature induces water hypoxia, pathogen presence, infectious disease outbreaks, and exacerbates the frequency, intensity, and duration of harmful algal blooms. Primary climatic drivers affecting water temperature include solar radiation, water temperature in river and ocean discharges, and wind intensity.[10] Furthermore, both sampling points exhibited dissolved oxygen (DO) values above the prescribed limit of 4.00 mg O_2/L for the preservation of flora and fauna in warm freshwater, estuarine, and marine waters as per the Regulatory Decree 1076 of 2015 of the Colombian Ministry of Environment and Sustainable Development.[46] The DO values displayed minimal variability between June and August at the two sampling points. Moreover, the pH at the sampling points in June and August 2022 (pH: 7.8 - 8.5) lie within the appropriate range for preserving flora and fauna in these ecosystems (pH: 6.5 – 8.5) in accordance with the Ministry of Environment and Sustainable Development.[4,46] However, the pH value of 8.5 in Boca de La Barra in June approaches the upper limit, potentially indicating heightened photosynthetic activity. Chlorophyll content in water is directly associated with the quantity of phytoplankton. This parameter also serves as an indicator of the trophic status or primary production of an ecosystem. In June, higher concentrations of chlorophyll a were detected compared to August at both sampling points. This correlates with increased precipitation in August. At the Ciénaga La Luna sampling point, there was a larger variation in chlorophyll concentration (from 48.0 to 10.0 µg/L) compared to the Boca de La Barra sampling point (from 40.0 to 29.0 µg/L). In August, the chlorophyll value at Ciénaga La Luna was 10.0 µg/L indicating mesotrophic conditions in the ecosystem, whereas the higher values in June at the same sampling point (48.0 µg/L) and in Boca de La Barra (40.0 µg/L) indicate eutrophic conditions.[4,47] According

to a previous report, there seems to be a relationship between chlorophyll a concentration and salinity.[48] High chlorophyl concentration in June at both sampling points is related to increased biomass of photosynthetic microorganisms. Chlorophyll a concentration can also be related to solar radiation, temperature, and nutrient availability in the water body.

The presence and composition of nutrients in the water, such as orthophosphates, nitrites, nitrates, and ammonia, also influence the condition of the ecosystems. Nitrogen and phosphorus availability is essential for photosynthetic microorganisms' growth.[49,50] However, excessive nutrients can lead to an increase in microalgae biomass, creating eutrophic and anoxic conditions that result in organism mortality. The Ciénaga La Luna and Boca de La Barra sampling points showed orthophosphate concentrations within the typical values reported previously for these ecosystems (3.0 to 100.0 µg $P\text{-}PO_4^{3-}/L$)[4]. The increase in orthophosphate concentration in June at Boca de La Barra is attributed to increased rainfall, which promotes the flow between freshwater and nutrient-laden seawater.

Phytoplankton communities in the CGSM

In aquatic ecosystems, the composition and density of phytoplankton communities are closely linked to water quality parameters. Microscopic analysis of phytoplankton samples collected at Ciénaga La Luna and Boca de La Barra identified five taxonomic groups (phyla), with Cyanophyta (commonly known as cyanobacteria) as the most prevalent (**Fig 2**). Among the cyanobacteria, there were nine potentially harmful genera (see **Fig 2**).

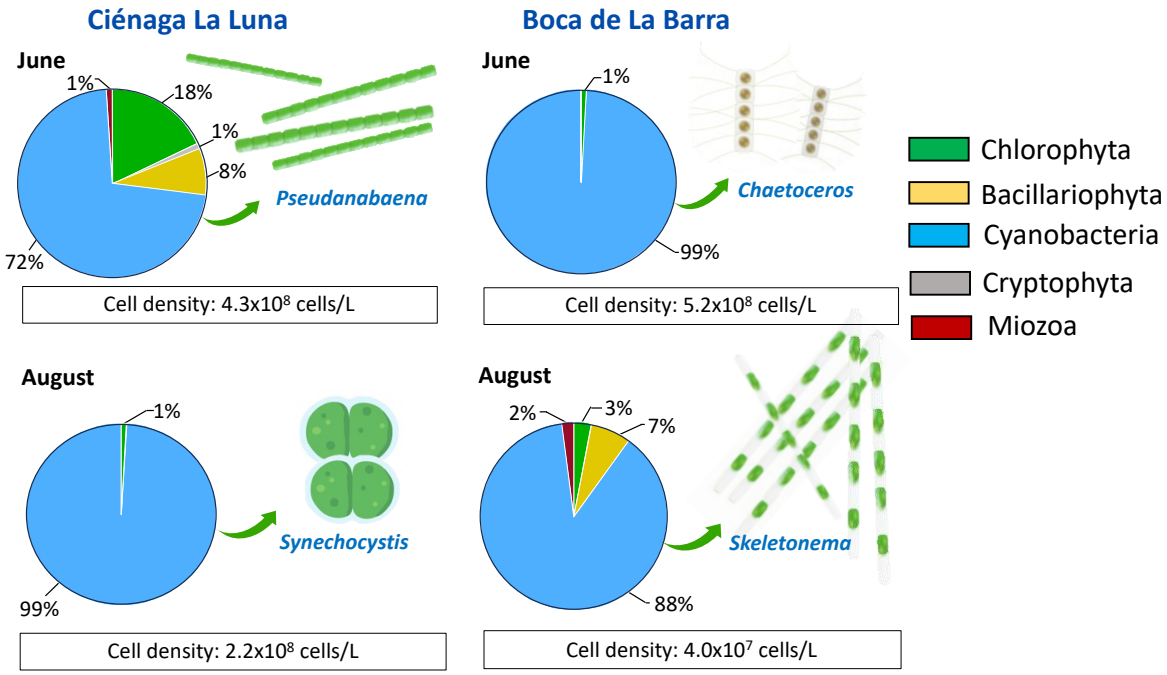

Figure 2. Relative abundance of the main taxonomic groups of phytoplankton at the sampling points Ciénaga La Luna and Boca de La Barra, CGSM, during June and August of 2022, along with cell density counts. Insets illustrate some of the most abundant potentially harmful microalgae species identified at each sampling point.

According to Figure 2, the phytoplankton cell density decreased significantly for the month of August compared to June in both sampling stations. These results fall within ranges previously reported by the INVEMAR during monitoring conducted from 2014 to 2021.[4] The highest average phytoplankton densities

were found in Ciénaga La Luna, the sampling point with the greatest influence of continental water contributions. While in June, a period of less rainfall, was the recorded the highest phytoplankton density at Boca de La Barra, the sampling point with inputs from the Caribbean Sea. Typically, the maximum value of total phytoplankton biomass occurs during the dry season.[2] Additionally, according to the literature, higher salinity values typically favor greater phytoplankton densities[51,52]. Here, we report that phytoplankton density values in August, high precipitation season, at Ciénaga La Luna and Boca de La Barra were significantly lower than in June, low precipitation season. Furthermore, cellular density values are closely related to phytoplankton concentration.

A total of five taxonomic groups (phyla) were identified in Ciénaga La Luna and Boca de La Barra, and no direct relationship was found between the diversity of identified taxonomic groups and the sampling month. This may be due to both sampling points presenting similar environmental parameters. Despite Boca de La Barra being directly connected to the Caribbean Sea, it exhibited low salinity compared to the Caribbean Sea due to the La Niña phenomenon, as mentioned earlier. Other authors have reported that climatic factors and environmental characteristics have a greater influence on changes in the phytoplankton community compared to spatial factors[53]. For example, low salinities and high nutrient concentrations can promote the growth of cyanobacteria, a taxonomic group identified at the sampling points[48]. These results coincide with those reported by different authors, who mention that variables such as salinity, transparency, nitrites, ammonia, and phosphates define the distribution, composition, and density of phytoplankton communities[52,54]. Additionally, low phytoplankton community diversity has been previously reported by other authors[4,55]. The authors suggest that aquatic ecosystems in a eutrophic state are characterized by low phytoplankton diversity and the predominance of certain species or groups, as observed in the CGSM with cyanobacteria. Systems showing a decrease in microalgae richness may be more vulnerable to intense or prolonged environmental alterations[4].

According to previous reports from the INVEMAR institute, a decrease in the number of taxonomic groups was observed compared to previous years[4]. This decreases, especially in the diatom group (Bacillariophyta), typically detected with higher abundance in stations with marine conditions like Boca de La Barra during the low precipitation season. The low detection of diatom group can possibly be attributed to the influence of the La Niña Event and the reported low salinities. For the same reason, marine species typically reported in previous years in the CGSM, such as dinoflagellates (e.g., *Ceratium* spp., *Gonyaulax* spp.)[4], were sporadic or absent in this study. It has been reported that salinity and transparency measured at the sampling point have a greater influence on the dynamics of the phytoplankton community in the CGSM[5,35,43]. Changes in salinity can lead to certain taxonomic groups dominating over others, as observed with cyanobacteria in this study. Salinity has also been identified as the variable that best explains the behavior of the phytoplankton community, with the salinity gradient linked to the distribution and variability of the species present[10]. Additionally, authors indicate that nutrient concentration (orthophosphates) influences the phytoplankton community behavior, possibly due to its significant influence on ecosystem eutrophication[56,57]. Ciénaga La Luna and Boca de La Barra exhibited low salinities during the monitored months (1.0 - 3.0 g/L), promoting the proliferation of cyanobacteria and even other characteristic freshwater groups such as chlorophytes.

For the relative proportion of different taxonomic groups, cyanobacteria always predominated, accounting for 72%–99%, consistent with historical behavior in the area[4]. Cyanobacteria benefit from freshwater influx and the availability of dissolved inorganic nutrients (e.g., nitrogen and phosphorus) from external inputs and remineralization processes, resulting in a highly productive ecosystem. Additionally, this taxonomic group exhibits extremely high morphological diversity, which likely increases its niche breadth and enhances its competitive advantage over other groups[58,59]. Nine genera of potentially

harmful microalgae were identified in Ciénaga La Luna and Boca de La Barra, belonging to cyanobacteria (*Synechocystis*, *Anabaena*, *Anabaenopsis*, *Pseudanabaena*, and *Microcystis*), and diatoms (*Skeletonema*, *Pseudo-nitzschia*, *Nitzschia*, and *Chaetoceros*), as reported by the INVEMAR.[4]. Cyanobacteria usually dominate phytoplankton communities in eutrophic freshwater sources worldwide.[10] The genus *Synechocystis*, a unicellular, non-nitrogen-fixing cyanobacterium with a diameter of 0.7–8.0 µm, was the most abundant in both sampling months in Ciénaga La Luna and Boca de La Barra, consistent with historical observations in the CGSM.[34,52,60,61] Interestingly, although the genus *Synechocystis* is not listed as a toxin producer in the UNESCO Intergovernmental Oceanographic Commission (IOC) list, its presence in high concentrations has been associated with massive fish kills in the CGSM, in previous INVEMAR reports.[4] Additionally, high abundances of the genera *Anabaenopsis*, *Skeletonema*, and *Nitzschia* were detected, which, although recognized as toxin producers, were not associated with organism mortality or other harmful effects related to their presence in the CGSM.[4] *Pseudanabaena* sp. is a common species in freshwater cyanobacteria blooms. Over the past few decades, *Pseudanabaena* sp. has been recorded nearly worldwide [62]. As early as 1984, *Pseudanabaena* sp. found in two different Southern California reservoirs were proven to produce 2-methylisoborneol (MIB). Subsequently, several authors have reported that besides producing MIB, *Pseudanabaena* sp. could also produce cyanotoxins, including hepatotoxins and neurotoxins[63,64]. Species of the genus *Microcystis* have the capacity to produce microcystins, a widely known cyanotoxin reported in the literature, thus being associated with harmful algal bloom production worldwide[65,66]. Massive fish kills caused by high cyanobacteria abundance and toxin production have been previously reported in the CGSM, e.g., July-August 1994, June 1995, 1996, 1997[4]. Authors associate the observed hypoxia and anoxia phenomena, causing fish kills, with the presence of high cyanobacteria densities in the CGSM[4]. This underscores the need for robust analytical methodologies for early toxin detection and expedited decision-making regarding aquatic ecosystems.

Pigment profile analysis by MALDI FT-ICR

The pigment profiles of phytoplankton extracts collected from Ciénaga La Luna and Boca de La Barra in June and August of 2022, analyzed using a 21 T FT-ICR mass spectrometer, are depicted in Figure 3. After the data filtration (see Materials and methods), 11,108 molecular formulas were assigned from 11,417 monoisotopic signals with relative abundances (RA) above 0.2% in Boca de La Barra, from a total of 42,745,183 evaluated molecular formulas. Similarly, 224 molecular formulas to 224 above 0.2% RA, with 220,011 molecular formulas evaluated in the phytoplankton samples collected in June and August 2022, respectively. Likewise, in Ciénaga La Luna, we assigned 2,808 molecular formulas to 2,995 above 0.2% RA, with 4,990,585 molecular formulas evaluated, and 2,187 molecular formulas to 2,610 above 0.2% RA, with 2,927,565 molecular formulas evaluated in the phytoplankton samples collected in June and August 2022, respectively. The analysis was conducted for signals within the mass range of *m/z* 200–1200, with peak resolving power exceeding 1.6×10^6 at *m/z* 400. Mass accuracy measurements were within the range of 1 to 250 ppb.[29] Molecular composition assignment was accomplished through automatic assignment of charged isotope clusters with single or mixed adducts, and van Krevelen diagrams, offering a multifaceted insight into class (heteroatom content) and DBE vs carbon number. The presented results only address the extractable and ionizable component in the phytoplankton samples. The mass spectrum provided a high-resolution view of the isotope fine structure of the peaks, closely aligned with spectra calculated for the same resolving power using the ChemCal molecular formula calculator algorithm[39].

Figure 3 and **Table 2** shows the diverse molecular composition observed among the samples collected in June and August 2022 at Ciénaga La Luna and Boca de La Barra, CGSM. We detected chlorophylls and their derivatives, carotenoids, and cyanobacteria's secondary metabolites as radical cations, protonated molecules, and sodium adducts. The chlorophyll derivatives were identified solely as radical cations due to successful charge-transfer reactions between the matrix primary ions (DCTB, E_i: 8.54 eV) and the

chlorine-based structures with characteristic low ionization energy (E_i) values.[17,30,69]. Carotenoids and secondary metabolites of cyanobacteria were detected as $[M]^{+\bullet}$, $[M + H]^+$, or $[M + Na]^+$ depending upon the molecule's structure, E_i, and cation/proton affinities, as discussed later. More compounds were identified in June than in August at both sampling sites, Ciénaga La Luna and Boca de La Barra. This correlates well with the cell density values recorded in June ($4.3x10^8$ and $5.2x10^8$ cells/L) and August ($2.2x10^8$ and $4.0x10^7$ cells/L) for both sampling sites, as discussed earlier.

The variation in molecular composition can be attributed to various environmental and temporal factors that affect phytoplankton communities in the CGSM. The presence of chlorophylls and carotenoids indicates the photosynthetic activity of the microorganisms in the samples, highlighting their importance in primary production and energy transfer in aquatic ecosystems[5]. Notably, intact chlorophyll a/b was not detected in any of the pigment extracts mass spectra, which aligns with the widely reported low survival yield of these compounds in MS.[70–73] Cholophyll degradation between sample colletion and analysis could be also possible. Nevertheless, the conditions used in this work allow for the detection of intact chlorophylls in the mass spectrum, as previously reported.[17,30]. Additionally, the chlorophyll concentration was measured by UV-Vis spectroscopy prior to MALDI MS analysis (**Table 1**). Chlorophyll a is commonly present in phytoplankton cells, and its degradation products are diagnostic indicators of the physiological condition and grazing processes affecting the phytoplankton community[71–73]. Here, we report the detection of radical cations of pheophytin a $[C_{55}H_{74}N_4O_5]^{+\bullet}$, pheophytin b $[C_{35}H_{34}N_4O_6]^{+\bullet}$, and pheophorbide b $[C_{35}H_{34}N_4O_6]^{+\bullet}$, at all sampling sites and months, with low mass accuracy values (∼20 ppb). Pheophytin a/b are considered markers of the phylum Chlorophyta and senescence/grazing, and pheophorbide a/b are associated with grazing among the microorganisms composing the phytoplankton[73]. Additionally, pyropheophorbide a $[C_{33}H_{34}N_4O_3]^{+\bullet}$, was detected at both sampling sites but only in the phytoplankton samples collected in August, a period of higher precipitation. These derivatives are formed during the breakdown of chlorophyll by herbivorous zooplankton or other phytoplankton microorganisms and senescent algae cells[10,74,75]. Chlorophyll decomposition products have been used as biomarkers of organic matter derived from phytoplankton in various environments, from oligotrophic open oceans to eutrophic inland lakes[8]. However, in shallow lagoons connected to various water sources, the application of chlorophyll decomposition products as biomarkers of the phytoplankton community is complicated by the fact that there are multiple sources that can contribute to the presence of chlorophyll and its decomposition products, such as terrestrial inputs, microalgae and macroalgae, seagrasses, among others[5]. Additionally, the mechanisms controlling chlorophyll transformation in aquatic environments remain under study.

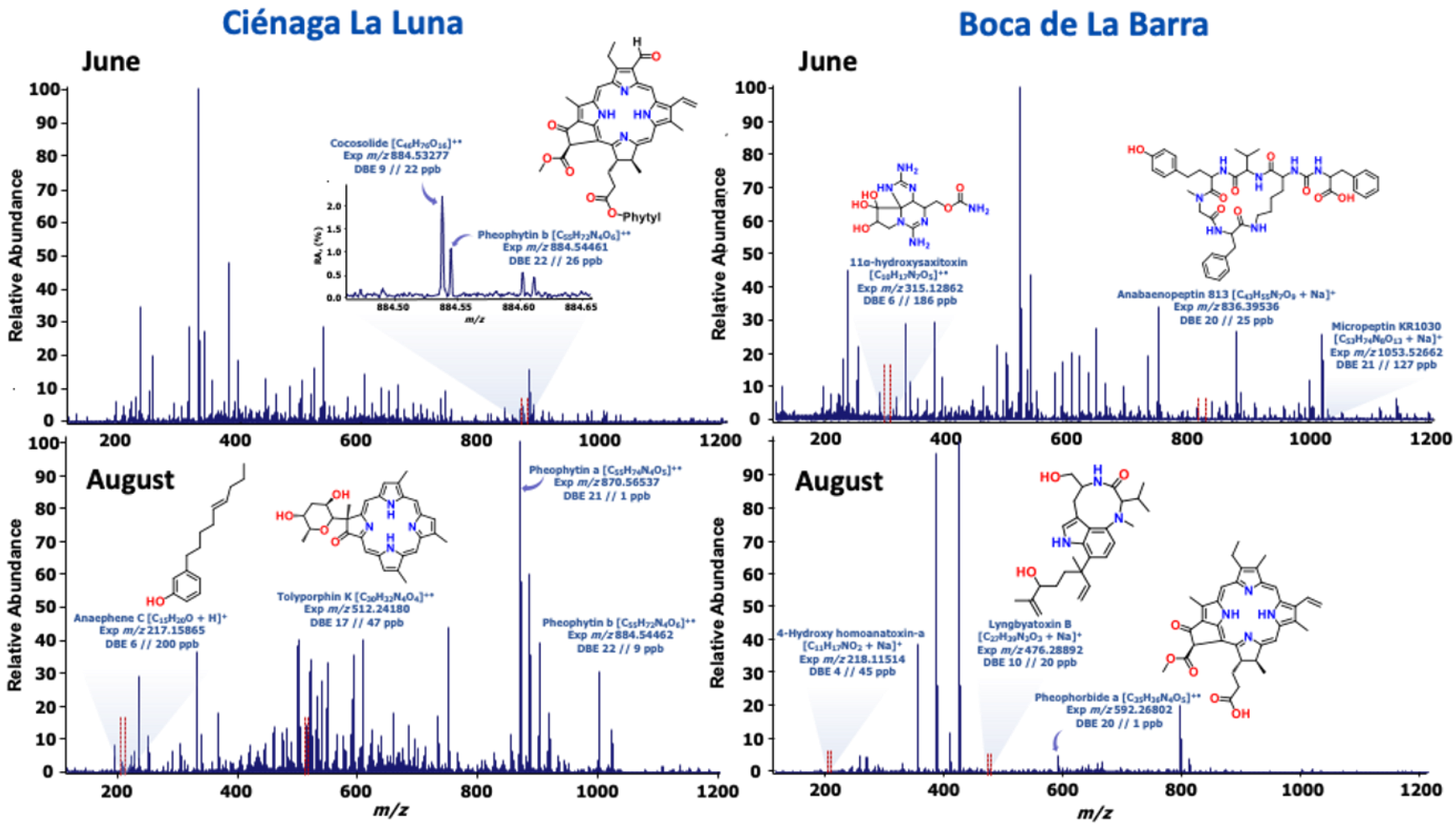

Figure 3. MALDI FT-ICR MS spectra of phytoplankton samples collected in June and August 2022 from Ciénaga La Luna and Boca de La Barra, CGSM. The resolving power at $m/\Delta m_{50\%}$ is ca., 1.6×10^6 (*m/z* 400). Insets offer details on the molecular formula, experimental mass, and mass accuracy for some of the identified compounds.

Table 2. Compounds detected in the phytoplankton samples collected in June and August 2022 in Ciénaga La Luna and Boca de La Barra, CGSM, by MALDI FT-ICR MS.

		MALDI FT-ICR MS												
		Ciénaga La Luna						Boca de La Barra						
		June			August			June			August			
Compound	**Detected ion**	***m/z* Exp**	**Mass accuracy (ppb)**	**RA (%)**	***m/z* Exp**	**Mass accuracy (ppb)**	**RA (%)**	***m/z* Exp**	**Mass accuracy (ppb)**	**RA (%)**	***m/z* Exp**	**Mass accuracy (ppb)**	**RA (%)**	**Marker for**
Chlorophyll pigments														
Pyropheophorbide a	$[C_{33}H_{34}N_4O_3]^{+\bullet}$				534.26253	18	18.82				534.26261	125	0.32	Senescence/grazing[10,12,68]
Pheophorbide a	$[C_{35}H_{36}N_4O_5]^{+\bullet}$				592.26804	40	29.87	592.26816	246	16.91	592.26802	1	4.99	Senescence/grazing[41]
Pheophorbide b	$[C_{35}H_{34}N_4O_6]^{+\bullet}$	606.24730	21	0.89	606.24731	41	6.84	606.24725	192	1.05	606.24727	32	1.54	Senescence/grazing[10,12,68]
Pheophytin a	$[C_{55}H_{74}N_4O_5]^{+\bullet}$	870.56537	1	5.93	870.56537	1	100.0	870.56537	1	0.91	870.56536	11	0.22	Chlorophyta[10,12,68] Bacillariophyta[10,12,68]
Pheophytin b	$[C_{55}H_{72}N_4O_6]^{+\bullet}$	884.54461	26	1.16	884.54462	9	19.68	884.54467	10	1.99	884.54461	33	0.23	Chlorophyta[10,12,68]
132-hydroxy-pheophytin a	$[C_{55}H_{74}N_4O_6]^{+\bullet}$	886.56028	1	3.74	886.56027	15	59.92	886.56027	10	0.73				Cyanobacteria *Cyanobium*[10,12,68]
Carotenoids														
4,4'-Diapocarotenoic acid	$[C_{30}H_{38}O_2 + Na]^+$							453.27633	162	0.33				Pseudomonadota[40]
Carotene	$[C_{40}H_{56}]^{+\bullet}$	536.43762	55	0.21	536.43764	19	0.93	536.43767	17	2.93				Not specific[10,12,68]
Alloxanthin	$[C_{40}H_{52}O_2]^{+\bullet}$				564.39620	43	0.46							Cryptophytes[10,12,68]
Zeaxanthin	$[C_{40}H_{56}O_2]^{+\bullet}$	568.42742	105	0.23	568.42745	52	0.36	568.42743	83	0.72	568.42744	18	0.29	Chlorophyta[10,12,68] Cyanobacteria[10,12,68]
1-Hydroxy-1,2-dihydrophytoene	$[C_{40}H_{66}O + Na]^+$							585.50064	84	0.37				*Rhodospirillum rubrum*[40]
Nonaprene	$[C_{45}H_{64}]^{+\bullet}$							604.50018	120	0.53				*Corynebacterium glutamicum*[40]
1-Methoxy-1'hydroxy-1,2,1',2'-tetrahydrophytofluene	$[C_{41}H_{68}O_2 + Na]^+$							615.51122	102	0.49				*Rhodospirillum rubrum*[40]
Cyanobacteria's secondary metabolites														
N-Acetyltryptamine	$[C_{12}H_{14}N_2O + H]^+$							203.11790	74	0.34				*Nostoc commune*[41]
Aphanorphine	$[C_{13}H_{17}NO]^{+\bullet}$	203.13041	188	0.22				203.13047	31	0.41				*Aphanizomenon flos-aquae*[41]
7-Formyl-3-methoxy-5-methylindanone	$[C_{12}H_{12}O_3]^{+\bullet}$	204.07804	207	0.20				204.07805	214	0.67				*Lyngbya* sp./*Moorea* sp.[41]
Geosmin	$[C_{12}H_{22}O + Na]^+$							205.15625	188	0.52				*Oscillatoria*[41]
3-Oxo-b-ionone	$[C_{13}H_{18}O_2]^{+\bullet}$							206.13013	41	0.52				*Nostoc commune*[41]
Carboxydihydroanatoxin-a	$[C_{11}H_{17}NO_3 + H]^+$	212.12814	122	0.21										*Cylindrosprmum stagnale*[41]
Anaephene C	$[C_{15}H_{20}O + H]^+$				217.15865	200	0.40	217.15868	49	0.37	217.15864	184	0.22	*Hormoscilla lyngbyaceus*[41]
4-Hydroxy homoanatoxin-a	$[C_{11}H_{17}NO_2 + Na]^+$	218.11516	91	0.20							218.11514	45	0.24	*Raphidiopsis mediterranea*[41]
Tetrahydroindol 2	$[C_{11}H_{15}NO_4]^{+\bullet}$	225.09950	229	0.28							225.09954	88	0.23	*Lyngbya/Moorea*[41]
Palythine	$[C_{10}H_{16}N_2O_5 + H]^+$				245.11321	82	0.84							*Nostoc commune*[41]
Anaephene B	$[C_{17}H_{22}O]^{+\bullet}$							242.16655	163	0.37				*Hormoscilla lyngbyaceus*[41]
12-Deoxydecarbamoylsaxitoxin	$[C_9H_{16}N_6O + Na]^+$							247.12777	17	0.56				*Lyngbya* sp.[41]
11,12-Didehydrospironostoic acid	$[C_{15}H_{20}O_3 + Na]^+$							271.13048	63	0.57				*Calothrix* sp.[41]
Malyngolide	$[C_{16}H_{30}O_3 + H]^+$							271.22675	88	0.82				*Lyngbya* sp./*Moorea* sp.[41]
4-Oxo-beta-apo-13-carotenone	$[C_{18}H_{24}O_2]^{+\bullet}$							272.17702	213	0.59				*Anabaena*[41]

Tumonoic acid D	$[C_{16}H_{29}NO_3 + H]^+$							284.22206	154	0.45				*Blennothrix cantharidosmum*
Palythene	$[C_{13}H_{20}N_2O_5 + H]^+$	285.14451	56	0.25										*Aphanothece* [41]
Hyellazone	$[C_{20}H_{17}NO + H]^+$	288.13827	43	0.25										*Hyella caespitosa* [41]
Deschloro 12-epi-fischerindole W nitrile	$[C_{21}H_{20}N_2 + H]^+$	301.16995	112	0.36										*Fischerella* [41]
Abietic acid	$[C_{20}H_{30}O_2]^{+\bullet}$							302.22404	37	0.58				*Nostoc commune* [41]
Deschloro 12-epi-fischerindole I nitrile	$[C_{21}H_{22}N_2 + H]^+$	303.18558	32	0.37										*Fischerella* [41]
N-(p-Coumaroyl)-tryptamine	$[C_{19}H_{18}N_2O_2 + H]^+$							307.14416	213	0.82				*Nostoc commune* [41]
15,16-dihydrosacrolide A	$[C_{18}H_{30}O_4 + H]^+$							311.22167	45	0.78				*Aphanothece* [41]
11α-hydroxysaxitoxin	$[C_{10}H_{17}N_7O_5]^{+\bullet}$							315.12862	186	0.37	315.12914	63	0.39	*Aphanizomenon flos-aquae* [41]
Takinolide seco-acid	$[C_{17}H_{34}O_4 + Na]^+$	325.23496	119	0.26										*Lyngbya sp./Moorea sp.* [41]
20-Nor-3α-acetoxy-12-hydroxy-abieta-5,7,9,11,13-pentaene	$[C_{21}H_{26}O_3]^{+\bullet}$							326.18767	86	0.49				*Microcoleus* [41]
Puna'auic acid	$[C_{18}H_{32}O_4 + Na]^+$	335.21933	168	0.24										*Anabaena* [41]
Ambiguine P	$[C_{25}H_{29}NO + H]^+$	360.23224	156	0.27										*Fischerella ambigua* [41]
Ethyl tumonoate A	$[C_{21}H_{37}NO_4]^{+\bullet}$							367.27167	99	0.30				*Oscillatoria/Planktothr*[41]
Ambiguine Q nitrile	$[C_{26}H_{28}N_2]^{+\bullet}$	368.22477	202	0.24				368.22477	214	0.69				*Fischerella ambigua* [41]
Tumonoic acid F	$[C_{21}H_{37}NO_5 + H]^+$	384.27453	214	0.22										*Blennothrix* [41]
Lyngbyatoxin B	$[C_{27}H_{39}N_3O_3 + Na]^+$							476.28834	36	0.41	476.28892	20	0.85	*Lyngbya sp./Moorea sp.* [41]
Tolyporphin K	$[C_{30}H_{32}N_4O_4]^{+\bullet}$				512.24180	47	0.60							*Tolypothrix* [41]
Muscoride B	$[C_{31}H_{41}N_5O_6 + H]^+$							580.31297	18	0.42				*Nostoc commune* [41]
Spumigin 638	$[C_{32}H_{42}N_6O_8 + H]^+$							639.31354	228	0.32				*Nostoc commune* [41]
Veraguamide H	$[C_{36}H_{58}N_4O_8]^{+\bullet}$							674.42486	73	0.30				*Oscillatoria/Planktothrix* [41]
Bacteriohopanetetrol	$[C_{41}H_{73}NO_8]^{+\bullet}$				707.53299	10	1.25							*Synechocystis* [41]
Almiramide C	$[C_{40}H_{66}N_6O_6 + H]^+$							727.51161	65	0.48				*Lyngbya sp./Moorea sp.* [41]
Galeapeptin GP729	$[C_{37}H_{59}N_7O_8 + Na]^+$							752.43173	1	0.33				*Pseudanabaena* [41]
[6(Z)-Adda[3]]NOD-R	$[C_{41}H_{60}N_8O_{10}]^{+\bullet}$							824.44262	86	0.39				*Nodularia* [41]
Anabaenopeptin AP806Ne	$[C_{41}H_{58}N_8O_9 + Na]^+$	829.42193	51	0.22										*Anabaena* [41]
[DMAdda[3]]NOD-R	$[C_{40}H_{58}N_8O_{10} + Na]^+$							833.41682	22	0.38				*Nodularia* [41]
Anabaenopeptin 813	$[C_{43}H_{55}N_7O_9 + Na]^+$							836.39536	25	0.44				*Anabaena* [41]
6-OH-scytophycin B	$[C_{45}H_{73}NO_{13} + H]^+$							836.51548	22	0.41				*Scytonema* [41]
Cocosolide	$[C_{46}H_{76}O_{16}]^{+\bullet}$	884.51277	22	0.29				884.51275	45	0.45				*Symploca* [41]
[D-Asp[3],Dha[7]]MC-FR	$[C_{50}H_{68}N_{10}O_{12}]^{+\bullet}$							1000.50118	89	0.57				*Anabaena* [41]
Micropeptin KR1030	$[C_{53}H_{74}N_8O_{13} + Na]^+$							1053.52662	127	0.43				*Microcystis aeruginosa* [41]
Micropeptin KB1046	$[C_{53}H_{74}N_8O_{14} + Na]^+$							1069.52189	212	0.47				*Microcystis* [41]

The presence of zeaxanthin $[C_{40}H_{56}O_2]^{+\bullet}$, in both June and August at Ciénaga La Luna and Boca de La Barra is consistent with the taxonomic identification performed, as this carotenoid is a biomarker of cyanobacteria presence [10,12,68]. 1-Hydroxy-1,2-dihydrophytoene $[C_{40}H_{66}O + Na]^+$, and 1-methoxy-1'hydroxy-1,2,1',2'-tetrahydrophytofluene $[C_{41}H_{68}O_2 + Na]^+$, detected in June in Boca de La Barra, are markers of *Rhodospirillum rubrum* [40], a bacterium widely distributed in aquatic environments such as ponds, lakes, streams, and standing water[40]. Another diagnostic carotenoid detected in phytoplankton samples was alloxanthin $[C_{40}H_{52}O_2]^{+\bullet}$, a biomarker for cryptophytes[40], previously reported through taxonomic identification. Variations in terms of carotenoid molecular composition could be related to differences in light intensity, temperature, and salinity between seasons and sampling sites.[76,77] Moreover, cyanobacteria's secondary metabolites were the compounds with the highest molecular diversity and were identified in both months and at both sampling sites. However, June had the highest number of identified compounds in both Ciénaga La Luna and Boca de La Barra. This could be related to a greater diversity of cyanobacteria in June at both sampling sites according to precipitation and salinity, as discussed previously. Among the cyanobacteria's secondary metabolites identified were cyclic peptides (e.g., veraguamide H, and cocosolide), cyclic non-peptides (tolyporphin K), linear peptides (almiramide C), linear non-peptides (aphanorphine), saxitoxin (11α-hydroxysaxitoxin), and anabaenopeptins (anabaenopeptin AP806Ne), typically detected as protonated molecules and sodium adducts. Additionally, the detection of these adducts may be due to preformed ions in the solution and desorbed due to the sublimation properties of the matrix used (DCTB, vapor pressure $9.09x10^{-7}$ mm Hg at 25 °C[78]). Interestingly, the relative abundance values of cyanobacteria's secondary metabolites were generally low and may be related to the efficiency in the ionization of these compounds, the extraction procedure employed, or the need for a pre-treatment process of the extract prior to analysis, as well as the MALDI matrix used. Here, a direct analysis of a mixture of phytoplankton extract and MALDI matrix was performed; some authors report prior purification of the analysis through Solid-Phase Extraction (SPE)[79,80]. That is, low relative abundance values would not mean that cyanobacteria's secondary metabolites are present in low concentrations in the phytoplankton samples. Additionally, there may be some cyanobacteria's secondary metabolites to which their molecular formula was assigned based on MALDI 21T FT-ICR data but are not previously reported in the consulted databases.

As discussed earlier, taxonomic ID revealed some potentially harmful microalgae genera in Ciénaga La Luna and Boca de La Barra. Interestingly, *Synechocystis*, the most abundant reported genus, is a producer of bacteriohopanetetrol[52], detected as $[C_{41}H_{73}NO_8]^{+\bullet}$, 10 ppb, in August at Ciénaga La Luna. Bacteriohopanetetrol is a linear non-peptide triterpenoid located in the membrane of cyanobacteria[34]. Some authors have reported the use of bacteriohopanetetrol isomers as markers of different species, e.g., in anaerobic ammonium oxidation (anammox) in marine paleo-environments[61]. Additionally, previously reported markers for cyanobacteria species belonging to the genera *Anabaena*, *Microcystis*, and *Pseudanabaena* detected through taxonomic ID, were detected through MALDI FT-ICR MS. Interestingly, other compounds detected, such as N-acetyltryptamine $[C_{12}H_{14}N_2O + H]^+$, 3-oxo-b-ionone $[C_{13}H_{18}O_2]^{+\bullet}$, palythine $[C_{10}H_{16}N_2O_5 + H]^+$, muscoride B $[C_{31}H_{41}N_5O_6 + H]^+$, and spumigin 638 $[C_{32}H_{42}N_6O_8 + H]^+$, refer to the presence of *Nostoc commune*[41], widely reported cyanobacteria whose colonies grow in moist soils, on mosses and herbs, and beside streams or pools as in the CGSM. Additionally, seven different compounds indicating the presence of cyanobacteria from the genera *Lyngbya* sp. and *Moorea* sp. were detected, which have a high morphological similarity but have been separated according to genetic information. Both genera include tropical marine and freshwater species and are known for their toxicity (they produce lyngbyatoxin-a and other compounds) that cause dermatitis by irritating human skin[81]. Ingestion of *Lyngbya* is potentially lethal. Most commonly, poisoning is caused by eating fish that have fed on *Lyngbya* or other fish that have consumed *Lyngbya*, this is called "ciguatera-like" poisoning, which has been widely reported in the literature[80]. Interestingly, a correlation can be observed between the phytoplankton

microorganisms derived from molecular composition analysis and those obtained from traditional analysis. This demonstrates the relevance of MALDI MS methodologies in the rapid and reliable detection of phytoplankton pigments that could provide relevant information about the status of marine ecosystems. Understanding the metabolite composition based on seasonal variability can assist in the management and conservation of these vulnerable ecosystems. Additionally, the detection of toxins, e.g., anatoxin-a, through MALDI MS highlights the importance of understanding potential risks to public health and water quality associated with the proliferation of toxic cyanobacteria and underscores the applicability of MALDI MS methodologies in the continuous monitoring of water quality in these environments to prevent human exposure to potentially harmful substances.

Fig 4 presents the compositional information derived from MALDI FT-ICR MS in the form of compound class histograms. Each class is divided into three sections showing the percentage of monoisotopic ions detected as radical cations ($[M]^{+\bullet}$), protonated molecules ($[M + H]^+$), and sodium adducts ($[M + Na]^+$).

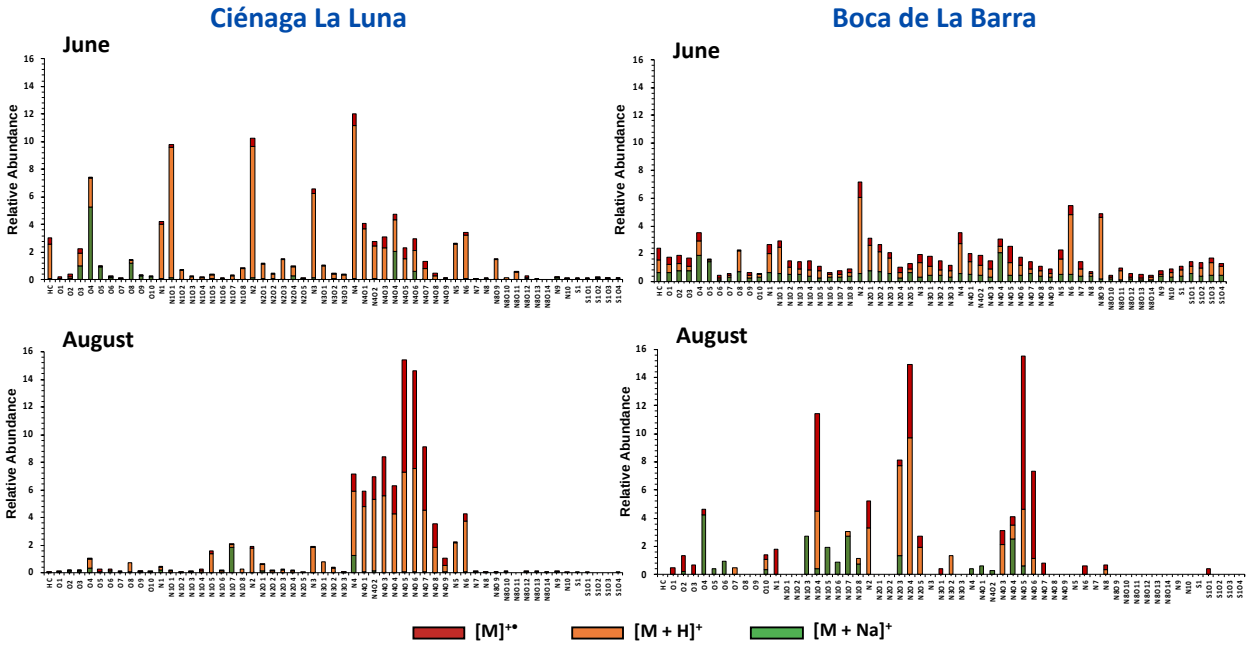

Figure 4. Comparative histograms showing compound classes detected in phytoplankton samples collected in June and August at Ciénaga La Luna and Boca de la Barra, CGSM. Each class is divided into three sections showing the percentage of monoisotopic ions detected as radical cations ($[M]^{+\bullet}$) in the red section, protonated molecules ($[M + H]^+$) in the orange section, and sodium adducts ($[M + Na]^+$) in the green section.

A total of 57 compound families were detected, of which 32 were common in both June and August at Ciénaga La Luna and Boca de Barra, e.g., O_1, O_2, O_3, O_4, O_5, O_6, O_7, N_1, N_1O_3, N_1O_4, N_1O_5, N_1O_6, N_1O_7, N_1O_8, N_2, N_2O_3, N_2O_4, N_2O_5, N_4, N_4O_1, N_4O_2, N_4O_3, N_4O_4, N_4O_5, N_4O_6, N_4O_7, N_6, N_8. These compound classes have been previously reported by other authors in analyses of Natural Organic Matter (NOM) from rivers and oceans[82,83]. Microbial degradation is one of the most important processes in regulating NOM composition in aquatic environments. Microorganisms are consistently involved in both supplying and depleting NOM, derived from detritus and secretions of aquatic microorganisms. Our observation of highly oxygenated

compound classes O_o (o=1, 2, 3, 4, 5, 6, 7, 8, 9, 10) in phytoplankton samples aligns with previous reports where O_o (o = 1, 2, 3, 4, 5, 6, 7) were detected in analyses of organic matter composition in rivers using APPI FT-ICR MS[82]. Within the oxygen-containing compound classes, O_4 was the most abundantly detected class in all samples, containing compounds such as puna'auic acid ($C_{18}H_{32}O_4$), and 15,16-dihydrosacrolide A ($C_{18}H_{30}O_4$), identified as $[M + Na]^+$ and $[M + H]^+$, respectively.

Species of class O_2 in negative ion mode analysis are typically assigned as naphthenic acids in samples from biodegraded petroleum reservoirs. However, petrogenic naphthenic acids exhibit a uniform carbon distribution, characteristic of the geochemical signatures of fossil organic matter formed via catagenetic processes occurring over geological timescales[84]. In contrast, the species of class O_2 detected in positive ion mode analysis in this work, exhibit short carbon distributions characteristic of recent organic matter[85]. Some authors have also reported class O_2 species with short carbon distributions in recently deposited organic matter in modern sedimentary environments[86]. Detected O_2 species are related to carotenoids, including compounds such as alloxanthin ($C_{40}H_{52}O_2$) and zeaxanthin ($C_{40}H_{56}O_2$), 4-oxo-beta-apo-13-carotenone ($C_{18}H_{24}O_2$), all detected as $[M]^{+\bullet}$. The latter, a marker of the cyanobacterium *Anabaena*, also reported through taxonomic ID. Additionally, toxins belonging to class O_2 were identified, e.g., 3-oxo-b-ionone ($C_{13}H_{18}O_2$), cyclic peptides previously reported in cyanobacteria *Nostoc commune* [41]. Furthermore, other authors have linked these oxygenated classes to long-chain diketones, i.e., diones, analogous to well-known alkynones and related to species C_{31}, C_{33}, and C_{35}, with low DBE values. Several authors [82,87,88] have reported the degradative oxidation of other organic species, both xenobiotics such as polycyclic aromatic hydrocarbons, and biogenic ones, such as triterpenoids, to their analogs.

Among nitrogen-containing compound classes, N_4O_o (o = 0, 1, 2, 3, 4, 5, 6, 7, 8, 9) were the most abundant in all samples, associated with tetrapyrrole derivatives (i.e., porphyrins) from chlorophyll pigments, as reported in previous studies by us and other authors[82]. These molecular characteristics have been extensively studied and reported in numerous FTI-CR MS investigations of petroleum porphyrins, the end products of the geochemical transformation of biogenic chlorophyll over geological timescales[84,89,90]. Here, we report the detection of chlorophyll derivatives as radical cations in all analyzed samples, indicative of senescence or grazing in the phytoplankton community [10,12,68]. Moreover, other studies corroborate N_4O_o species as representatives of primary producers in bacterial communities, linking the influx of phototroph-derived organic matter to sediments in high-salinity sites with increased abundance of specific Proteobacteria taxa efficient in consuming sedimented phototroph biomass[91]. The authors suggest that the detection of N_4O_3 species is an indicator of the transition to a marine-like environment from a freshwater-influenced environment within the estuary. Furthermore, classes like N_1O_o (o= 2, 3, 4, 5, 6) have been reported in marine sediments and associated with the presence of structural sphingolipids from marine phytoplankton[82]. Sphingolipids constitute a chemically and functionally diverse group of membrane lipids, many of which include N_1O_o linked to long alkyl chains. In our work, N_1O_o species were mostly detected as $[M + H]^+$ or $[M + Na]^+$. High abundances of N_1O_o species in sediment samples have been associated with increased bacterial activities at the water-sediment interface. Additionally, NOM components containing nitrogen stabilize in the water column through interactions with minerals[92]. Most cyanobacteria secondary metabolites consist of species from N_nO_o classes due to their cyclic peptide structures e.g. veraguamide H ($C_{36}H_{58}N_4O_8$) and anabaenopeptin 813 ($C_{43}H_{55}N_7O_9$), detected in CGSM phytoplankton samples, serving as markers for species of the genera *Oscillatoria* [41] and *Anabaena* [41], respectively. Additionally, non-cyclic peptides were assigned to N_6O_6 species, e.g., almiramide C ($C_{40}H_{66}N_6O_6$) and galeapeptin GP729 ($C_{37}H_{59}N_7O_8$), markers for species of the genera *Lyngbya* sp./*Moorea* sp. [41] and *Pseudanabaena* [41]. Cyanobacteria constituted the majority of the identified population in the phytoplankton samples collected at CGSM.

In contrast, classes like S_1O_o (o= 2, 3, 4) were mostly detected in June compared to August, at both sampling points. However, in June at Boca de La Barra, S_1O_o (o= 2, 3, 4) showed higher abundance. Sulfur species were detected as radical cations, protonated molecules, and sodium adducts. Previous studies have reported these species in FT-ICR MS analyses of river samples[82,93,94]. The increase in relative abundance of S_1O_o classes from June to August at both sampling points may be related to increased precipitation in August in the CGSM. Sulfur compounds may originate from anthropogenic activities near CGSM or algae production (containing sulfur-containing cysteine, methionine), and may also result from early diagenetic sulfurization of DOM[93,94]. The presence of sulfur compounds has been associated with the presence of thiophene compounds, as will be discussed later, with DBE values. Although the detection of thiophene compounds has not been previously reported in Ciénaga La Luna and Boca de La Barra, there are numerous reports in the literature showing anthropogenic interventions since the 1950s in CGSM[1,2,5,35], which may be related to the addition of polycyclic aromatic hydrocarbons, including related thiophene compounds. Previous studies on biodegraded crude oils have interpreted that the S_1O_2 compound class consists of acidic species, likely containing a sulfur and carboxyl functional group or a sulfur and two hydroxyl functional groups, which are degradation products of original species found in the S compound class[16]. Additionally, compositional differences at the sampling points may be related to differences in salinity, as previously reported by other authors[5,43].

Interestingly, in **Fig 4**, the relative abundances of the different detected species ($[M]^{+\bullet}$, $[M + H]^+$, $[M + Na]^+$) can be observed, providing information that ionization can occur through different pathways using an ET MALDI matrix such as DCTB. Although radical cations were detected for almost all compound classes, protonation was the ionization pathway with the highest relative abundance. Some authors, including our previous studies[17], have reported that DCTB can induce protonation of other molecules in MALDI ionization due to the presence of an acidic hydrogen in its structure. For this ionization to occur, the proton affinity of the analyte must be greater than the proton affinity of DCTB[20,95–97]. Compounds detected as $[M + H]^+$ or $[M + Na]^+$ (see **Table 2**) are compounds with high nitrogen or oxygen content, conferring high proton and cation affinities. Considering the origin of the analyzed samples, with high salt concentrations and minimal pretreatment before analysis, the formation of preformed ions in solution, requiring only MALDI matrix assistance for desorption in the MALDI ionization chamber, is possible. N_4O_o (o=1, 2, 3, 4, 5, 6, 7, 8, 9) were the predominant species detected as radical cations, possibly because they are related to chlorin derivatives, widely analyzed compounds as discussed earlier, with E_i lower than the E_i of the MALDI matrix DCTB (8.54 eV). In August, the highest percentage of radical cations was detected in both Ciénaga La Luna and Boca de La Barra, possibly due to increased precipitation reducing dissolved salt concentration and other nutrients on the water surface.

Fig. 5 provides a clearer picture of the distribution of different types of ions detected in MALDI, where overlapped van Krevelen diagrams of monoisotopic ions detected as radical cations, protonated molecules, and sodium adducts are shown for June and August at Ciénaga La Luna and Boca de La Barra, CGMS.

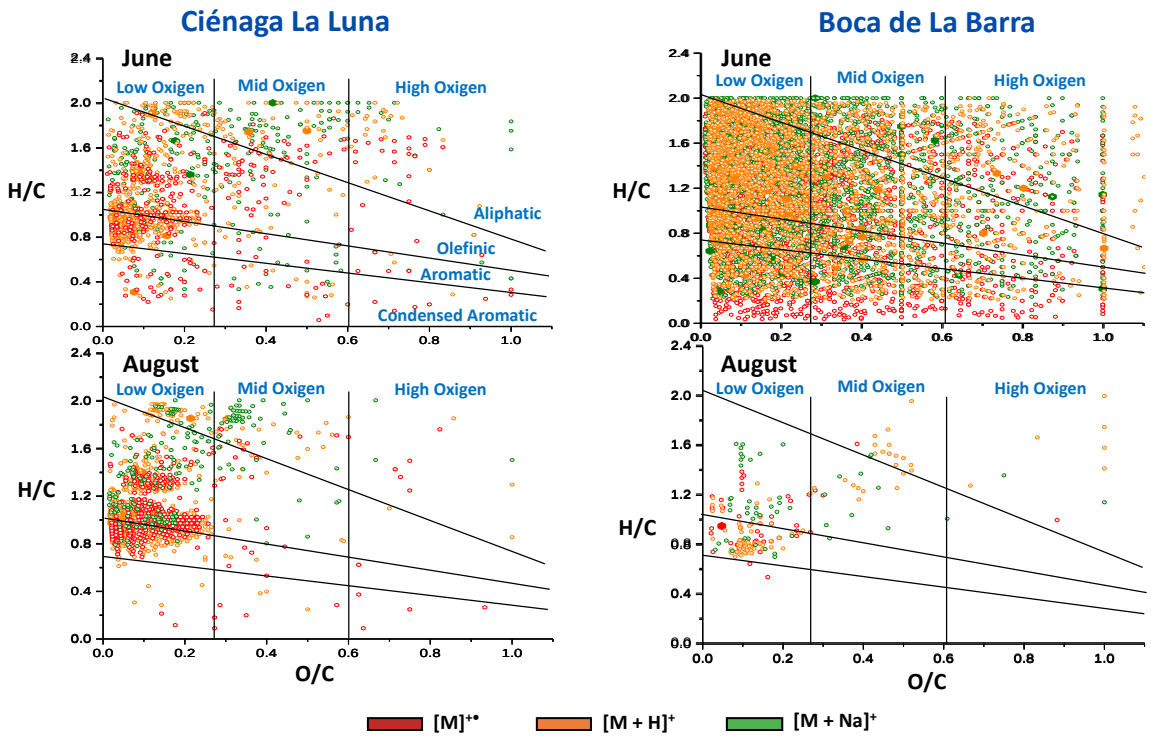

Figure 5. van Krevelen diagram overlapped for all O_o (o = 1, 10), N_nO_o (n= 1, 8, and o= 1, 14), and S_1O_o (o=1, 4) classes showing the H/C and O/C ratios of each assigned molecular formula as only radical cation, protonated molecule, or sodium adduct, in June and August at Cienaga La Luna and Boca de la Barra, CGSM.

The van Krevelen diagrams, plotting H/C versus O/C ratios, allow observation of compositional differences between sampling points and time. Overlaying different ion types allows determining their positions on the diagram and relating the preferred ionization pathway of compounds to their molecular properties. From the van Krevelen diagrams, evidence is obtained that although monoisotopic ions detected as protonated molecules showed the highest relative abundance (**Fig 4**), there is no marked difference between the number of monoisotopic ions detected as protonated molecules and the number of ions detected as sodium adducts (**Fig 5**). The oblique straight lines are related to the Aromaticity Indices (AI) and have been previously reported in the literature[28]. Highly saturated oxygenated compounds (1.2 < H/C < 2) such as aliphatic and some olefinic compounds were ionized through both proton and cation transfer; most of these ions are clustered at relatively low O/C ratios, meaning they have a high carbon content or are the heaviest within their class. Previous reports indicate that aliphatic compounds are typically produced from fatty acids inherent to phytoplankton[98].

Likewise, compounds with low H/C ratios, less saturated, possibly associated with condensed aromatic compounds, were generally ionized through electronic transfer in MALDI. This correlates perfectly with the molecular structures and E_i values of these compounds, lower than the E_i of the DCTB matrix (8.54 eV). Other authors report high amounts of phenolic acid-related compounds in macrophyte samples[12,45]. Furthermore, in the van Krevelen diagrams (**Fig 5**), compounds with low O/C ratios and high H/C ratios that may be related to lipids in the samples can be observed. According to previous reports, dissolved organic matter (DOM) derived from algae and analyzed using FT-ICR-MS contained greater proportions of lipids, followed by lignin[83,99]. Interestingly, in all analyzed samples, a set of compounds with low O/C ratios, potentially related to highly unsaturated compounds such as aromatic and some olefinic compounds,

were detected as radical cations, protonated molecules, and sodium adducts. Strikingly, for the month of June, the van Krevelen diagrams show that both in Ciénaga La Luna and Boca de La Barra, compounds with higher H/C values, i.e., aliphatic compounds with high and low O/C values, were detected compared to the analysis of samples collected in August. Likewise, in June, compounds with higher O/C ratios were detected at both sampling points. This observation likely reflects complex and seasonally variable hydrological and climatological patterns in the investigated region influencing the type and quantities of organic matter inputs from primary productivity in freshwater and marine ecosystems. Additionally, spatial (Ciénaga La Luna and Boca de La Barra) and seasonal variability (low and high precipitation, June and August, respectively) of nutrient concentrations, solar radiation, variable organic carbon fluxes, chlorophyll a concentration, and possible flooding events influence molecular composition in ecosystems. Previous reports indicate that the degree of oxidation of DOM would increase as salt lakes become saltier[83]. Our observations confirm the significant influence of seasonal patterns on molecular characteristics in aquatic ecosystems in CGSM in combination with precipitation impacts. Some authors have reported that eutrophication promotes the accumulation of autochthonous DOM (especially algal sources) in lakes[25]. In other words, compounds derived from algae, products of their metabolism, including aromatic, aliphatic, condensed aromatic, and olefinic compounds, would increase due to ecosystem eutrophication.

Fig 6 illustrates the distribution of homologous series detected through MALDI FT-ICR MS in June and August at Cienega La Luna and Boca de La Barra, CGSM. The plotted DBE values correspond to molecules detected in a neutral state, without distinguishing between odd-electron ions and even-electron ions. DBE vs carbon atom number plots are a useful tool for understanding molecular composition in complex mixtures, based on valence rules to differentiate ions containing a different total number of double bonds and/or rings.

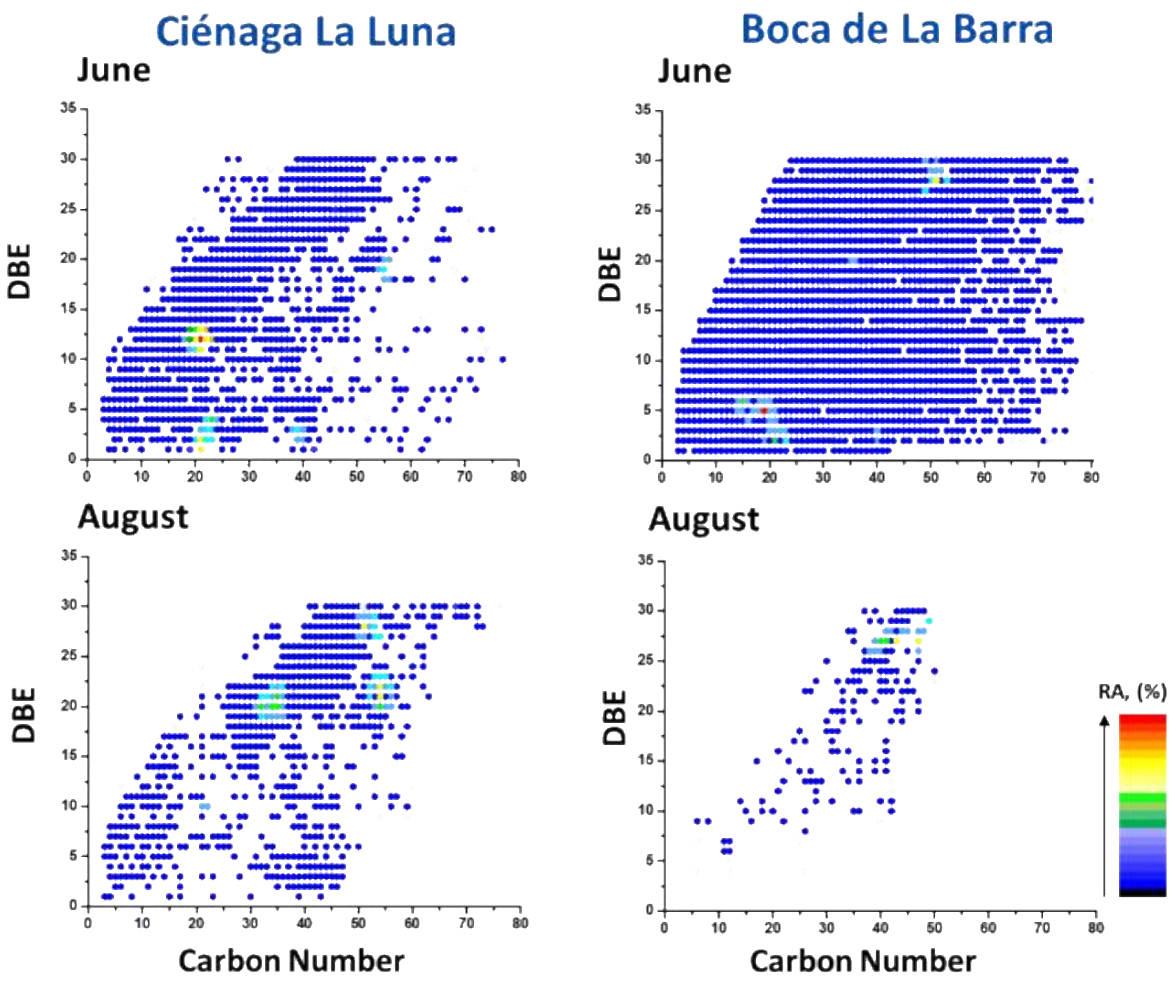

Figure 6. Neutral DBE versus carbon atom number plots for the molecular composition detected in June and August at Cienega La Luna and Boca de La Barra, CGSM, using MALDI FT-ICR MS.

These plots reveal evidence that compounds with higher relative abundance (**Fig 6**, points in red and yellow) vary by month, at both sampling points. While in June, compounds with maximum relative abundance (RA) had DBE values of 5 and 12, in August, compounds with maximum RA were between DBE 22 and 30. This may be related to the sampling month; some authors have reported that during rainy seasons, compounds with more rings and/or double bonds, i.e., higher DBE values, are detected more abundantly, less transformed from organic matter from marine (micro)organisms[82,87]. Nonetheless, the detected compounds mostly exhibited low RA values, as shown in **Fig 6** points in blue. Additionally, the detected compounds include aliphatic (DBE = 1), non-aromatic (DBE = 2, 3), and polyaromatic compounds with DBE values up to 30. Interestingly, the analyzed samples showed a distribution of some RA peaks, possibly related to different core structures. This is also related to the efficiency of ionization and the preferred ionization channel for different compounds, so some species of the same class may have a high RA. Similarly, homologous series with the highest number of compounds were found in June at Boca de La Barra with DBE 3 and 66 members. Overall, O_4 species have DBE values ranging from 1 to 30, with RA maxima peaks at 5 and 20, and carbon atom numbers between 9 and 80. Similarly, NO_2 species, including 4-hydroxy homoanatoxin-a ($C_{11}H_{17}NO_2$), anatoxin detected in this study, have DBE values ranging from 2 to 30, and carbon atom numbers between 12 and 79.

Moreover, it can be observed that in all analyzed samples, compound classes containing N_4O_o (o= 1, 2, 3, 4, 5, 6) shift towards higher DBE values compared to the O_o compound class (o = 1, 2, 3, 4, 5). This indicates that N_4O_o species are present in the form of conjugated structures, e.g., chlorin derivatives in chlorophylls. Additionally, N_8O_o species (o=10, 11, 12, 13, 14, 15) exhibit high DBE values, possibly related to cyclic peptides with multiple amino acid residues, e.g., micropeptins assigned in this study. Conversely, analogs containing S mostly exhibit lower DBE values, suggesting that these heteroatoms probably do not form part of aromatic units in the structures. Among the detected S-containing species are DBE 3 and 12, a possible indication of the presence of thiophene derivatives, and benzothiophene, respectively, of petrogenic origin[82,100], suggesting the contribution of petroleum-derived contamination mainly from communities near Boca de La Barra in CGSM. **Fig 7** illustrates an expanded region from the neutral DBE versus carbon atom number plots related to homologous series of some cyanobacteria's secondary metabolites detected in the phytoplankton sample collected in June at Boca de La Barra, CGSM.

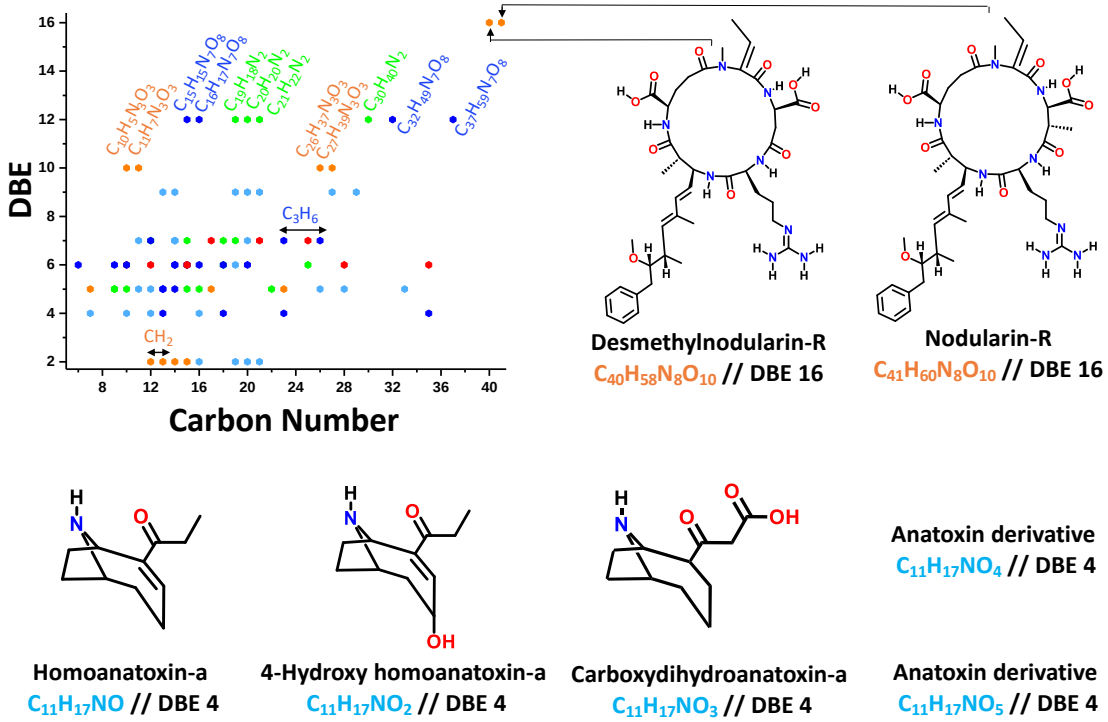

Figure 7. Filtered and enlarged region from the neutral DBE versus carbon atom number plot for homologous series of some cyanobacteria's secondary metabolites detected in the phytoplankton sample collected in June at Boca de La Barra, using MALDI FT-ICR MS. Colors indicate different compound classes. Inset shows two toxins that vary in -CH_2 in their structures and derivatives of anatoxin ($C_{11}H_{17}NO$) that vary by one oxygen atom.

The use of homologous series in HR MS analysis enables understanding molecular diversity and compositional distribution in complex mixtures, identifying key structural and functional patterns. In **Fig 7**, various homologous series detected in the samples related to cyanobacterial metabolites can be observed, with molecular formulas differing in -CH_2 units. Overall, series with few members were detected, contrasting with the analysis of petroleum samples where abundant series of different molecular derivatives are obtained due to diagenesis and catagenesis processes. Additionally, **Fig 7** shows the position of two nodularin derivatives in the DBE versus carbon atom number plot. In this study, we report a short series composed of $C_{40}H_{58}N_8O_{10}$ and $C_{41}H_{60}N_8O_{10}$, desmethylnodularin-R or [DMAdda^3]NOD-R and nodularin-R or [6(Z)-Adda^3]NOD-R, respectively. Nodularins (NOD) are cyclic pentapeptide

hepatotoxins produced by the planktonic cyanobacteria *Nodularia spumigena*[41], typically found in brackish waters[101], salinity conditions encountered in June and August at Ciénaga La Luna and Boca de La Barra, CGSM. Furthermore, these hepatotoxins (nodularin, LD50 ¼ 50 mg kg^{-1})[65,101] have been reported in coastal areas and have been associated with animal poisonings, where, in liver cells, these toxins inhibit the activity of protein phosphatase 1 and 2A7 and act as potent tumor promoters and initiators.

The structure of nodularin is cyclo[-D-erythro-b-methylAsp(iso-link)-L-Arg-Adda-D-Glu(iso-link)-2-(methylamino)-2(Z)-dehydrobutyric acid], where Adda is the amino acid C20b, (2S,3S,8S,9S)-3-amino-9-methoxy-2,6,8,-trimethyl-10-phenyldeca-4(E),6(E)-dienoic acid[65]. The amino acid Adda is exclusive to cyanobacterial hepatotoxins like nodularins and structurally and functionally similar microcystins[65]. The configuration of the Adda-Glu part of the toxins is crucial for their activity. Structure-activity relationship studies have shown that the formation of the stereoisomer [6(Z)Adda], saturation of the diene in Adda, methylation of glutamic acid, or linearization render the compounds non-toxic or lead to a significant decrease in toxicity[65]. On the other hand, the formation of demethylated derivatives in amino acid residues in nodularins and microcystins has little effect on their toxicity. Furthermore, previous mass spectrometry studies of nodularins and microcystins using fast atom bombardment (FAB), electrospray (ESI), MALDI, and tandem analysis have allowed the identification of over 50 structural derivatives of microcystins and five derivatives of nodularins from more than 80 cyanobacterial hepatotoxin analogs currently reported[65,102,103]. Additionally, some compounds detected in this study vary in the number of oxygen atoms in their structures while keeping the number of carbon atoms constant, e.g., anatoxin-a and its derivatives, potent neurotoxins produced by cyanobacteria[104], including *Anabaena*, *Microcystis*, identified through taxonomic ID in this study and in previous works in CGSM[4]. Interestingly, in this study, we report homoanatoxin-a ($C_{11}H_{17}NO$), 4-hydroxy homoanatoxin-a ($C_{11}H_{17}NO_2$), carboxydihydroanatoxin-a ($C_{11}H_{17}NO_3$), along with two possible analogs $C_{11}H_{17}NO_4$ and $C_{11}H_{17}NO_5$. Anatoxin-a derivatives are one of the smallest bioactive groups from cyanobacteria, with seven known compounds[104]. Structurally, they consist of a bicyclic secondary amine with a ketone functional group. The first report of intoxication by anatoxin-a was published in 1961, and its structural elucidation was reported in 1977 using an extract of cyanobacteria from the NRC 44 clone of *Dolichospermum flosaquae* from freshwater[63,64,104]. Anatoxin-a and its analogs affect both muscular and neuronal acetylcholine receptors, block the activity of acetylcholinesterase, resulting in paralysis, exaggerated abdominal respiration, cyanosis, convulsions, and ultimately asphyxiation and death [104]. However, anatoxin-a can easily degrade in the presence of N_2 and O_2. Several studies have determined that sunlight accompanied by a pH change can hydrolyze anatoxin-a into dihydroanatoxin-a and anatoxin-a epoxide, non-toxic derivatives[65,104]. Additionally, it has been reported that benthic microorganisms have the ability to biodegrade anatoxin-a [65,104].

The detected analogs $C_{11}H_{17}NO_4$ and $C_{11}H_{17}NO_5$ may be products of oxidative processes, as oxidation plays a significant role in anatoxin biosynthesis, which begins with the adenylation of proline by anac, forming a prolil-anaD complex, and then the complex is oxidized by the enzyme encoded in anaB[104]. The remaining biosynthetic steps are based on colineality, where anaE adds two reduced carbons, anaF adds two partially reduced carbons, anaJ then cyclizes the compound to form anatoxin-a. Furthermore, some authors have reported oxidation processes in other toxins e.g., microcystins[65,103,105]. Based on this, we can speculate that these compounds are being reported for the first time, and these toxin groups may contain more analog structures than those reported so far, perhaps with different levels of neurotoxicity. The use of ultra-high-resolution mass spectrometry allows the identification of toxin homologous series that can enable the detection of new toxins, enrich existing databases, and improve our understanding of aquatic ecosystems.

Conclusions

The analysis of phytoplankton samples collected from Ciénaga La Luna and Boca de La Barra in June and August 2022 revealed significant variations in molecular composition. These differences are attributed to environmental factors such as light intensity, temperature, salinity, and precipitation, which influence phytoplankton community composition and abundance. Biomarker analysis, particularly through MALDI FT-ICR MS, identified specific phytoplankton taxa and associated metabolites, offering insights into taxonomic compositions. Cyanobacteria's secondary metabolites displayed the highest molecular diversity, including cyclic peptides, cyclic non-peptides, linear peptides, and linear non-peptides. The presence of toxins like anatoxin-a emphasizes the importance of water quality monitoring to mitigate potential risks to ecosystem and public health. The correlation between molecular composition analysis and traditional taxonomic methods highlights the reliability of MALDI MS methodologies in environmental monitoring.

The utilization of MALDI FT-ICR MS provided comprehensive insights into the diverse array of compound classes present in phytoplankton samples. Thirty-two compound classes were consistently detected in samples from both June and August, reflecting their ubiquitous presence and potential significance as environmental markers. Highly oxygenated compound classes aligned with microbial degradation processes, while nitrogen-containing compound classes were associated with chlorophyll pigments, indicating the importance of primary producers in organic matter dynamics. Variations in sulfur compound abundance suggested environmental influences, including precipitation and anthropogenic activities. The observed ion distribution patterns and homologous series characteristics revealed insights into molecular diversity influenced by seasonal and spatial factors. The detection of cyanobacterial toxins underscored the importance of advanced mass spectrometry techniques in identifying and characterizing bioactive compounds, contributing to our understanding of aquatic ecosystem health and facilitating management strategies.

Acknowledgements

The authors acknowledge the Guatiguará Technology Park and the Central Research Laboratory Facility at Universidad Industrial de Santander (UIS) for infrastructural support. The authors acknowledge funding from MINCIENCIAS (Grant 2019000100020). A portion of this work was performed at the National High Magnetic Field Laboratory, which is supported by the National Science Foundation Cooperative Agreement No. DMR-2128556 and the State of Florida. The authors thank the staff of the INVEMAR research institute, for carrying out the fieldwork to collect the phytoplankton samples and carry out laboratory analysis, especially Julián Franco-Angulo and Edgar Arteaga.

References

1 L. F. Espinosa-Díaz, Y. T. Zapata-Rey, K. Ibarra-Gutierrez and C. A. Bernal, *Science of the Total Environment*, 2021, **785**, 147203.

2 K. Gocke, C. Hernández, H. Giesenhagen and H. G. Hoppe, *J Plankton Res*, 2004, **26**, 1429–1439.

3 C. A. Hernández-Jiménez, *Rev. Intropica*, 2017, **12**, 117–130.

4 INVEMAR, *Monitoreo de las condiciones ambientales y los cambios estructurales y funcionales de las comunidades vegetales y de los recursos pesqueros durante la rehabilitación de la Ciénaga Grande de Santa Marta*, 2022.

5 M. V Delahoz, *Bol. Invest. Mar. Cost.*, 2004, **33**, 157–177.

6 N. Rangel-Buitrago and J. Idarraga-García, in *Biodiversidad del margen continental del Caribe colombiano*, 2010, vol. 1, pp. 29–51.

7 M. Krajewska, M. Szymczak-Żyła and G. Kowalewska, *Current Chemistry Letters*, 2017, **6**, 91–104.

8 J. Chen, O. Oseji, M. Mitra, Y. Waguespack and N. Chen, *J Coast Res*, 2016, **32**, 768–775.

9 J. J. Pierella Karlusich, F. M. Ibarbalz and C. Bowler, *J Plankton Res*, 2020, 42, 595–612.

10 S. Roy, C. Llewellyn, E. Skarstad and G. Johnsen, *Phytoplankton Pigments: Characterization, Chemotaxonomy and Applications in Oceanography*, 2011.

11 J. Capblancq and J. Catalan, *Phytoplankton: which, and how much?*, N.Y., 1994.

12 S. Wright and S. Jeffrey, *Hdb. Env. Chem.*, 2006, **2**, 71–104.

13 N. Sanz, A. García-Blanco, A. Gavalás-Olea, P. Loures and J. L. Garrido, *Methods Ecol Evol*, 2015, **6**, 1199–1209.

14 L. Heukelem and C. Thomas, *J Chromatogr A*, 2001, **910**, 31–49.

15 L. Mackenzie, P. Holland, P. Mcnabb, V. Beuzenberg, A. Selwood and T. Suzuki, *Toxicon*, 2002, **40**, 1321–1330.

16 V. Mangal, N. L. Stock and C. Guéguen, *Anal Bioanal Chem*, 2016, **408**, 1891–1900.

17 L. M. Díaz-Sánchez, C. Blanco-Tirado and M. Y. Combariza, *MethodsX*, 2023, **10**, 102140.

18 J. Gross, *Mass Spectrometry*, Springer, Heidelberg, Germany, Third Edition., 2017.

19 T. Mccarley, R. L. Mccarley and P. A. Limbach, *Anal Chem*, 1998, **70**, 4376–4379.

20 Y. Vasil'ev, O. Khvostenko, A. Streletskii, O. Boltalina, S. Kotsiris and T. Drewello, *Journal of Physical Chemistry A*, 2006, **110**, 5967–5972.

21 A. J. Hoteling, W. F. Nichols, D. J. Giesen, J. R. Lenhard and R. Knochenmuss, *European Journal of Mass Spectrometry*, 2006, **12**, 345–358.

22 R. Knochenmuss and R. Zenobi, *Chem Rev*, 2003, **103**, 441–452.

23 M. Karas and R. Krüger, *Chem Rev*, 2003, **103**, 427–439.

24 R. Knochenmuss, A. Stortelder, K. Breuker and R. Zenobi, *Journal of Mass Spectrometry*, 2000, **35**, 1237–1245.

25 S. Liu, Z. He, Z. Tang, L. Liu, J. Hou, T. Li, Y. Zhang, Q. Shi, J. P. Giesy and F. Wu, *Science of the Total Environment*, 2020, **703**, 134764.

26 D. F. Smith, D. C. Podgorski, R. P. Rodgers, G. T. Blakney and C. L. Hendrickson, *Anal Chem*, 2018, **90**, 2041–2047.

27 Y. Liu, C. Ma and J. Sun, *iScience*.

28 W. F. R. Bare, E. Struhs, A. Mirkouei, K. Overturf, M. L. Chacón-Patiño, A. M. McKenna, H. Chen and K. S. Raja, *Processes*.

29 W. Bahureksa, T. Borch, R. B. Young, C. R. Weisbrod, G. T. Blakney and A. M. McKenna, *Anal Chem*, 2022, **94**, 11382–11389.

30 L. Calderón-Vergara, L. M. Díaz-Sánchez, C. Blanco-Tirado and M. Combariza, *Analytical Methods, Submitted*.

31 G. M. Hallegraeff, D. M. Anderson and A. D. Cembella, *Intergovernmental Oceanographic Commission Manuals and Guides 33 MANUAL ON HARMFUL MARINE MICROALGAE*, 1995.

32 H. Utermöhl, *Methods of collecting plankton for various purposes are discussed.*, 1958.

33 C. D'Agrosa, O. Vidal and W. Graham, *Reports-international whal comm spec issues*, 1995, **94**, 283–294.

34 A. M. Collins, M. Liberton, H. D. T. Jones, O. F. Garcia, H. B. Pakrasi and J. A. Timlin, *Plant Physiol*, 2012, **158**, 1600–1609.

35 M. González-Arteaga and C. Ricaurte-Villota, *Boletin de Investigaciones Marinas y Costeras*, 2023, **52**, 45–65.

36 S. Chakraborty, M. K. Paidi, K. S. Udata, A. Veeruraj, M. Moovendhan and S. K. Mandal, *Biomass Convers Biorefin*.

37 *Standard Methods for the Examination of Water and Wastewater - 20th edition. 10200 H. Spectrophotometric Determination of Chlorophyll*, 2018.

38 H. K. LICHTENTHALER and A. R. WELLBURN, *Biochem Soc Trans*, 1983, **11**, 591–592.

39 L. Patiny and A. Borel, *J Chem Inf Model*, 2013, **53**, 1223–1250.

40 Carotenoids Database, available at: http://carotenoiddb.jp Consultation date: May 7, 2024.

41 M. R. Jones, E. Pinto, M. A. Torres, F. Dörr, H. Mazur-Marzec, K. Szubert, L. Tartaglione, C. Dell'Aversano, C. O. Miles, D. G. Beach, P. McCarron, K. Sivonen, D. P. Fewer, J. Jokela and E. M. L. Janssen, *Water Res*.

42 Parques Nacionales Naturales de Colombia, *Plan de manejo Santuario de Flora y Fauna de la Ciénaga Grande de Santa Marta*, 2020.

43 Y. S. Tuchkovenko Luis Alfredo Calero, *MODELO MATEMÁTICO DEL ECOSISTEMA DE LA CIÉNAGA GRANDE DE SANTA MARTA*, 2003, vol. 32.

44 I. Cristina, T. Potosi and D. C. Urrego-Rubio, *Análisis espacial de las propiedades fisicoquímicas y biológicas de la Ciénaga Grande de Santa Marta Spatial analysis of physic-chemical and biologic properties of Cienega Grande de Santa Marta.*

45 R. Wetzel and G. Likens, *Composition and Biomass of Phytoplankton*, N.Y., Primera., 2000, vol. First Edit.

46 Ministerio de Ambiente y Desarrollo Sostenible, Colombia, Decreto 1076 del 2015.

47 S. Liu, J. Hou, C. Suo, J. Chen, X. Liu, R. Fu and F. Wu, *Water Res*.

48 R. Sirota, G. Winters, O. Levy, J. Marques, A. Paytan, J. Silverman, G. Sisma-Ventura, E. Rahav, G. Antler and E. Bar-Zeev, *Environ Sci Technol*, 2024, 58, 5631–5645.

49 A. Vonshak, *Photosynthesis and Production in a Changing Environment*, 1993, 337–355.

50 M. M. Maroneze, L. Q. Zepka, E. J. Lopes, A. Pérez-Gálvez and M. Roca, *Antioxidants*, 2019, **8**, 1–15.

51 M. F. Al Dayel and F. El Sherif, *Saudi J Biol Sci*, 2021, **28**, 1687–1696.

52 H. Lee, Y. J. Noh, S. J. Hong, H. Lee, D. M. Kim, B. K. Cho, C. G. Lee and H. K. Choi, *J Appl Phycol*, 2021, **33**, 197–209.

53 G. Zhang, Z. Liu, Z. Zhang, C. Ding and J. Sun, *Front Mar Sci*.

54 W. Xu, H. Zhu, L. Zhang, D. J. S. Montagnes and Z. Yang, *Environ Sci Technol*, 2023, **57**, 10331–10338.

55 F. M. Ibarbalz, J. José and P. Karlusich, *Diversity of global marine plankton*.

56 X. Yan, X. Xu, M. Ji, Z. Zhang, M. Wang, S. Wu, G. Wang, C. Zhang and H. Liu, *Science of the Total Environment*, 2019, **651**, 466–474.

57 K. M. Stroski, D. L. Roelke, C. M. Kieley, R. Park, K. L. Campbell, N. H. Klobusnik, J. R. Walker, S. E. Cagle, J. M. Labonté and B. W. Brooks, *Environ Sci Technol*, 2024, **58**, 1473–1483.

58 H. Li, B. Bhattarai, M. Barber and R. Goel, *Environ Sci Technol*, 2023, **57**, 16016–16032.

59 L. T. Tan, in *Studies in Natural Products Chemistry*, Elsevier B.V., 2012, vol. 36, pp. 67–110.

60 D. Lagarde, L. Beuf and W. Vermaas, *Increased Production of Zeaxanthin and Other Pigments by Application of Genetic Engineering Techniques to Synechocystis sp. Strain PCC 6803*, 2000, vol. 66.

61 Y. Noh, H. Lee, M. Kim, S. J. Hong, H. Lee, D. M. Kim, B. K. Cho, C. G. Lee and H. K. Choi, *Biomolecules*, 2021, **11**, 1–17.

62 J. Gao, J. Zhu, M. Wang and W. Dong, *Sustainability (Switzerland)*.

63 A. Zaccaroni and D. Scaravelli, in *NATO Security through Science Series C: Environmental Security*, 2008, pp. 45–89.

64 V. Vasconcelos, *CYANOBACTERIA TOXINS: DIVERSITY AND ECOLOGICAL EFFECTS*.

65 L. Pearson, T. Mihali, M. Moffitt, R. Kellmann and B. Neilan, *Mar Drugs*, 2010, 8, 1650–1680.

66 F. Lepillanca, G. Martínez de la Escalera, F. Bordet, I. O'Farrell and C. Piccini, *INNOTEC*.

67 R. J. Strife, S. Campbell, J. M. Price and S. Motlagh, *J Am Soc Mass Spectrom*, 2021, **32**, 989–995.

68 S. Jeffrey, R. Mantoura and S. Wright, *Phytoplankton pigments in oceanography: guidelines to modern methods*, Paris, Primera., 1997, vol. 48.

69 C. Padilla-Jaramillo, L. M. Díaz-Sánchez, M. Combariza, C. Blanco-Tirado and A. Combariza, *Orinoquia*, 2021, **25**, 13–23.

70 J. Wei, H. Li, M. P. Barrow and P. B. O'Connor, *J Am Soc Mass Spectrom*, 2013, **24**, 753–760.

71 M. O. Senge, A. A. Ryan, K. A. Letchford, S. A. MacGowan and T. Mielke, *Symmetry (Basel)*, 2014, **6**, 781–843.

72 K. I. Takamiya, T. Tsuchiya and H. Ohta, *Trends Plant Sci*, 2000, **5**, 426–431.

73 S. Hörtensteiner, *Annu Rev Plant Biol*, 2006, **57**, 55–77.

74 Y. Saga and H. Tamiaki, *Chem Biodivers*, 2012, **9**, 1659–1683.

75 M. Roca and A. Pérez-Gálvez, *Antioxidants*, 2021, **10**, 1622–1645.

76 A. Sánchez, L. Flores, E. Langley, R. Martín, G. Maldonado and S. Sánchez, *Rev Latinoam Microbiol (1958)*, 1999, **41**, 175–191.

77 I. Generalić Mekinić, V. Šimat, N. B. Rathod, I. Hamed and M. Čagalj, *Foods*, 2023, 12.

78 US EPA. 2023. Estimation Programs Interface Suite™ for Microsoft® Windows, v 4.11. United States Environmental Protection Agency, Washington, DC, USA.

79 F. Pagels, R. N. Pereira, A. A. Vicente and A. C. Guedes, *Applied Sciences (Switzerland)*, 2021, **11**, 2–20.

80 I. Sanseverino, D. Conduto, R. Loos and T. Lettieri, *Cyanotoxins: methods and approaches for their analysis and detection*, 2017.

81 P. Rzymski and B. Poniedziałek, *Post Dermatol Alergol*, 2012, **XXIX**, 47–50.

82 J. Radović, W. Xie, R. Silva, T. Oldenburg, S. Larter and C. Zhang, *Org Geochem*, 2022, **173**, 1–12.

83 W. Xu, Q. Gao, C. He, Q. Shi, Z. Q. Hou and H. Z. Zhao, *Environ Sci Technol*, 2020, **54**, 12929–12937.

84 J. S. Ramírez-Pradilla, C. Blanco-Tirado, M. Hubert-Roux, P. Giusti, C. Afonso and M. Y. Combariza, *Energy and Fuels*, 2019, **33**, 3899–3907.

85 Z. Wen, Y. Shang, K. Song, G. Liu, J. Hou, L. Lyu, H. Tao, S. Li, C. He, Q. Shi and D. He, *Water Res*, 2022, **224**, 1–17.

86 N. Reuss, D. Conley and T. Bianchi, *Mar Chem*, 2005, **95**, 283–302.

87 M. P. Ávila, L. P. M. Brandão, L. S. Brighenti, D. Tonetta, M. P. Reis, P. A. Stæhr, E. Asmala, A. M. Amado, F. A. R. Barbosa, J. F. Bezerra-Neto and A. M. A. Nascimento, *Science of the Total Environment*, 2019, **672**, 990–1003.

88 D. Marchand, J. C. Marty, J. C. Miquel and J. F. Rontani, *Mar Chem*, 2005, **95**, 129–147.

89 Y. Lu, X. Li, R. Mesfioui, J. Bauer, R. Chambers, E. Canuel and P. Hatcher, *PLoS One*, 2015, **10**, 10–16.

90 J. M. Jarvis, J. M. Billing, R. T. Hallen, A. J. Schmidt and T. M. Schaub, *Energy and Fuels*, 2017, **31**, 2896–2906.

91 J. Lee, S. Kim, J. Jung, B. Oh, I. Kim and S. Hong, *Environmental Engineering Research*, 2009, **14**, 19–25.

92 M. Ruan, F. Wu, F. Sun, F. Song, T. Li, C. He and J. Jiang, *Crit Rev Environ Sci Technol*, 2023, 53, 1534–1562.

93 S. Li, L. Meng, C. Zhao, Y. Gu, R. Spencer, X. Álvarez–Salgado, A. Kellerman, A. McKenna, T. Huang, H. Yang and C. Huang, *Water Res*, 2023, **234**, 119812.

94 Q. Liu, Y. Tian, Y. Liu, M. Yu, Z. Hou, K. He, H. Xu, B. Cui and Y. Jiang, *J Clean Prod*, 2021, **289**, 125144.

95 J. S. Ramírez-Pradilla, C. Blanco-Tirado and M. Y. Combariza, *ACS Appl Mater Interfaces*, 2019, **11**, 10975–10987.

96 D. Giraldo-Dávila, M. L. Chacón-Patiño, J. S. Ramirez-Pradilla, C. Blanco-Tirado and M. Y. Combariza, *Fuel*, 2018, **226**, 103–111.

97 J. A. Oñate-Gutiérrez, L. M. Díaz-Sánchez, D. L. Urbina, J. R. Pinzón, C. Blanco-Tirado and M. Y. Combariza, *RSC Adv*, 2023, **13**, 12712–12722.

98 I. Tolosa, I. Vescovali, N. LeBlond, J. C. Marty, S. De Mora and L. Prieur, *Mar Chem*, 2004, **88**, 103–125.

99 C. He, Y. Zhang, Y. Li, X. Zhuo, Y. Li, C. Zhang and Q. Shi, *ACS Omega*, 2020, **5**, 11730–11736.

100 J. R. Radovic, R. C. Silva, R. W. Snowdon, M. Brown, S. Larter and T. B. P. Oldenburg, *Rapid Communications in Mass Spectrometry*, 2016, **30**, 1273–1282.

101 H. Mazur-Marzec, J. Meriluoto, M. Pliński and J. Szafranek, *Rapid Communications in Mass Spectrometry*, 2006, **20**, 2023–2032.

102 Y. Huang, H. Li, X. Wei, D. Wang, Y. Liu and L. Li, *Chemical Engineering Journal*, 2020, **383**, 123141.

103 K. Mcdonald, *Mass-spectrometry based metabolomics to decipher strain specific Microcystis cyanopeptine profiles*, 2020.

104 D. G. Beach, L. Zamlynny, M. MacArthur and C. O. Miles, *Anal Bioanal Chem*, 2023, **415**, 5281–5296.

105 P. Bouteiller, E. Lance, T. Guérin and R. Biré, *Toxins (Basel)*, 2022, **2022**, 550.

Chapter 5

General conclusions

The use of ET MALDI-MS for pigment analysis in microalgae/phytoplankton allows for the ionization of labile and thermally unstable species. Additionally, ET MALDI-MS offers several advantages: speed, sensitivity, and precision, making it a highly promising tool for advancing research in this field, especially when compared to traditional techniques like High-Performance Liquid Chromatography (HPLC).

ET MALDI-MS's ability to selectively ionize compound families with similar architectures below the matrix ionization energy allows for a rapid and accurate analysis of pigment extracts, addressing challenges like sample handling and low-abundance compound detection. This selectivity, combined with its high tolerance to contaminants, positions ET MALDI-MS as a robust strategy for pigment analysis and phytoplankton chemotaxonomic identification, aligning with the broader goals of ecological comprehension and sustainable stewardship practices.

The direct MALDI-ET analysis of intact cells and isolated chloroplasts from *C. vulgaris* unveils critical chemotaxonomic markers such as chlorophylls, carotenoids, and lipids distributed across distinct cell membranes. The use of effective extraction methods like ultrasonic-assisted and supercritical CO_2 extraction enhances access to pigments, revealing a diverse array of chemical species. Despite its primary role as an electron transfer (ET) matrix, DCTB (8.54 eV) also allowed the detection of protonated molecules and sodium adducts, possibly preformed ions in solution. Likewise, the pigment profiles of the microalgae *C. vulgaris* measured using MALDI MS highlight the impacts of the extraction protocol used.

The MALDI 21-T FT-ICR MS analysis enabled the identification of the molecular composition, increasing from ca., 20 compounds identified using MALDI TOF to 1,418 compounds identified using MALDI FT-ICR. Even so, and based on the information collected with either analyzer, more molecular information is obtained with MALDI MS than in traditional analyses such as HPLC/UV-Vis. Experiments using FT-ICR MS allow the assignment of compounds with low relative abundance, which could contribute to precise chemotaxonomic identification and provide important information about marine ecosystems.

Additionally, the use of Kendrick mass defects (KMD) and van Krevelen diagrams in the detailed analysis of pigments from MALDI 21-T FT-ICR MS data contributes to rapid and accurate molecular information about phytoplankton and could enhance biomonitoring efforts. Integrating these advanced mass spectrometry methodologies with traditional taxonomic approaches amplifies our ability to monitor and manage aquatic ecosystems effectively, providing nuanced insights into environmental influences on phytoplankton communities, essential for informed conservation strategies.

The implementation of biomarker analysis, notably utilizing MALDI FT-ICR MS, has been pivotal in unveiling specific phytoplankton taxa and their associated metabolites, providing crucial insights into taxonomic compositions. The extensive molecular diversity within microalgae/cyanobacteria's secondary metabolites, encompassing chlorophylls, carotenoids, and cyclic and linear peptides toxins, underscores the ongoing necessity for water quality monitoring to safeguard both ecosystems and public health. The revealed ion distribution patterns and homologous series characteristics offer valuable perspectives on seasonal and spatial factors that shape molecular diversity. Additionally, the clear identification of cyanobacterial toxins using MALDI FT-ICR MS emphasizes their critical importance in characterizing bioactive compounds and enhancing our understanding of aquatic ecosystem health in a comprehensive manner.

Chapter 6

Recommendations for future work.

1. Integrating Ion Mobility Spectrometry (IMS) into pigment analysis holds promise for enhancing isomer differentiation e.g., carotenoids. The capability of IMS to segregate molecules based on ion mobility offers enhanced specificity, which would complement MALDI-MS experiments, particularly in discerning pigment isomers with greater precision.

2. Exploring the potential of quantifying pigments using MALDI-MS is a promising avenue. While challenges persist in achieving precise quantification, further exploration into calibration methods and sample preparation techniques could advance the quantification capabilities of MALDI-MS for pigments, thereby providing valuable insights to pigment analysis methodologies.

3. Recognizing the influence of microorganism growth states on pigment composition is paramount. Understanding how the relative abundances of pigments fluctuate with different growth stages of microorganisms is essential for obtaining comprehensive and accurate pigment profiles, necessitating comparative analyses across varied growth conditions.

4. Enhancing ionization selectivity through the utilization of 100% Electron Transfer (ET) matrices can significantly improve specificity in pigment identification. Employing matrices exclusively based on ET mechanisms enhances ionization selectivity, contributing to more precise identification and characterization of pigments, especially within complex samples.

5. Exploring automation possibilities for High Resolution (HR) analysis presents an opportunity for streamlining workflows. Automating HRMS analysis can standardize procedures, enhance reproducibility, and improve efficiency in pigment analysis workflows, thereby facilitating researchers in obtaining reliable and consistent results.

6. Analyzing isolated microorganism cultures by HRMS provides detailed insights into pigment profiles. Establishing individual cultures allows for precise and focused analysis of pigment compositions for each microorganism, aiding in database enrichment and facilitating rapid detection of specific microalgae and cyanobacteria.

7. Considering negative mode analysis for detecting specific compounds in phytoplankton samples offers valuable insights. Negative ion mode detection provides complementary information about compounds like carboxylic acids, broadening the scope of molecular composition analysis in phytoplankton samples.

8. Delving deeper into the study of cyanotoxins, with a focus on extraction and pretreatment techniques, is essential for comprehensive toxin detection. Investigating optimized methods for extracting and pretreating samples can significantly enhance cyanotoxin detection, contributing to effective risk assessment and management strategies in aquatic ecosystems.

Chapter 7

Appendix

Appendix 1. Papers published as first author.

1) Luis M. Díaz-Sánchez, Cristian Blanco-Tirado, Marianny Y. Combariza, Electron-transfer MALDI MS methodology for microalgae/phytoplankton pigments análisis, MethodsX, 10 (2023) 102140. (https://doi.org/10.1016/j.mex.2023.102140).
2) Luz A. Calderón-Vergara*, Luis M. Díaz-Sánchez*, Cristian Blanco-Tirado, Marianny Y. Combariza, Comparative Profiling of *Chlorella vulgaris* Cells, Extracts, and Intact Chloroplasts Using Electron Transfer Matrix-Assisted Laser Desorption/Ionization Mass Spectrometry (ET MALDI-MS), Analytical Methods, 2024, Submitted.
   *These authors contributed equally. (https://doi.org/10.1039/D4AY00846D)

Appendix 2. Papers under review as first author.

1) Luis M. Díaz-Sánchez, Martha L. Chacón-Patiño, Chad R. Weisbrod, Cristian Blanco-Tirado, Marianny Y. Combariza, Insights into the compositional space and molecular signatures of microalgae pigment extracts from MALDI 21T-FT-ICR mass spectrometry, Algal Research.
2) Luis M. Díaz-Sánchez, Martha L. Chacón-Patiño, Chad R. Weisbrod, Lizbeth J. Vivas-Aguas, David Stranz, Scott Campbell, Cristian Blanco-Tirado, Marianny Y. Combariza, Linking MALDI FT-ICR MS pigment profiles with phytoplankton community to study aquatic ecosystems., Algal Research.
3) Luis M. Díaz-Sánchez, Guillermo Montoya, Cristian Blanco-Tirado, Marianny Y. Combariza, Comparative Analysis of Pentacyclic Triterpenes in Wild and *in Vitro* Cultivated Plant Roots Using ESI 21-T FT-ICR MS, Chemical Communications.

Appendix 3. Papers published as second author.

1) Carlos Padilla, Luis M. Díaz-Sánchez, Marianny Y. Combariza, Cristian Blanco-Tirado, Aldo F. Combariza, Photon harvesting molecules: ionization potential from quantum chemical calculations of phytoplanktonic pigments for MALDI-MS analysis, Orinoquia 25, 1, 2021, 13-23. (https://doi.org/10.22579/20112629.676)
2) Jesús A. Oñate-Gutiérrez, Luis M. Díaz-Sánchez, Diana L. Urbina, Julio R. Pinzón, Cristian Blanco-Tirado, Marianny Y. Combariza, Exploring the chemical composition and coloring qualities of cacao fruit epicarp extracts, RSC Adv., 2023, 13, 12712. (https://doi.org/10.1039/D3RA01049J)
3) Carlos Padilla, Luis M. Díaz-Sánchez, Cristian Blanco-Tirado, Aldo F. Combariza, Marianny Y. Combariza, AI-Guided Design of MALDI Matrices: Exploring the Electron Transfer Chemical Space for Mass Spectrometric Analysis of Low Molecular Weight Compounds, JASMS, 2025, 35, 12, 2836–2848. (https://doi.org/10.1021/jasms.4c00186)

Appendix 4. Papers under review as second author.

1) Juan E León-Jaimes, Luis M. Díaz-Sánchez, Cristian Blanco-Tirado, Marianny Y. Combariza, Gas-phase behavior of *cis*-bixin under MALDI MS conditions, Dyes and Pigments.

Appendix 5. Co-advisor undergraduate students in Chemistry and Biology.

1) Evaluación de las propiedades emulsificantes de mezclas de fosfolípidos aislados de *Theobroma cacao* L. Author: Laura Alejandra Paiba. BSc in Chemistry. **2024.** (https://noesis.uis.edu.co/handle/20.500.14071/43697)
2) Gas Phase Charge Transfer in MALDI-MS: An *in silico* Perspective. Author: María José Álvarez. BSc in Biology. Universidad de Sucre, Colombia. **2023.**
3) Monitoreo de biomarcadores como indicadores de crecimiento de *Chlorella vulgaris* utilizando MALDI MS. Author: Maicol Andrés Avellaneda. BSc in Chemistry. **2023.** (https://noesis.uis.edu.co/handle/20.500.14071/12502)
4) Caracterización de pigmentos lipofílicos en *Chlorella vulgaris* utilizando espectrometría de masas MALDI TOF. Author: Stefanny Yajaive Claro. BSc in Chemistry. **2023**. (https://noesis.uis.edu.co/handle/20.500.14071/14439)
5) Reactividad en fase gaseosa de sistemas orgánicos Donor-Aceptor basados en trifenilamina en MALDI MS. Author: Bryan Hernández Baca. BSc in Chemistry. **2023.** (https://noesis.uis.edu.co/handle/20.500.14071/12509)
6) Síntesis de nuevas matrices MALDI ET basadas en un núcleo de trifenilamina para el análisis de compuestos lábiles y termoinestables. Author: Anderson Rodríguez Mantilla. BSc in Chemistry. **2022**. (https://noesis.uis.edu.co/handle/20.500.14071/12126)
7) Evaluación de la bixina como matriz MALDI para el análisis de pigmentos naturales. Author: Juan Esteban León Jaimes. BSc in Chemistry. **2022**. (https://noesis.uis.edu.co/handle/20.500.14071/9916)
8) Estudio de la evolución de pigmentos y lípidos en células intactas de *Chlorella vulgaris.* Author: Cristian Alejandro Blanco Combariza. BSc in Chemistry. **2021**. (https://noesis.uis.edu.co/handle/20.500.14071/11261)
9) Theoretical calculations of Ionization Potentials in Phytoplanktonic photosensible biomolecular species for MALDI assays. Author: Carlos Andrés Padilla Jaramillo. BSc in Biology. Universidad de Sucre, Colombia. **2020.**
10) Caracterización de las fracciones resultantes del proceso de purificación de xilo-oligosacáridos obtenidos a partir de raquis de palma de aceite africana. Author: Cristian Jair Martínez Beltrán. BSc in Chemistry. **2020**. (https://noesis.uis.edu.co/handle/20.500.14071/40495)

Appendix 6. Project submitted to the National High Magnetic Field Laboratory-MagLab, Tallahassee, Florida, USA, approved.

1. **Characterization of biomarkers in microalgae**. 2022. Proposal number: P19920. Facility Requested: ICR. Principal Investigator: Dr. Marianny Combariza.
2. **Spatial distribution of pentacyclic triterpenes in root systems from *Cecropia* spp. using MALDI IMS**. 2023. Proposal number: P20198. Facility Requested: ICR. Principal Investigator: Dr. Marianny Combariza.

Appendix 7. Funded research projects.

1. **Convocatoria del Fondo de Ciencia, Tecnología e Innovación del Sistema General de Regalías para la conformación de una lista de proyectos elegibles para ser viabilizados, priorizados y aprobados por el OCAD en el marco del programa de Becas de Excelencia Doctoral del Bicentenario**, 2020, Título: "Análisis de pigmentos fotosintéticos y fotoprotectores en fitoplancton utilizando reacciones de transferencia electrónica en fase gaseosa". Centro de Estudios e Investigaciones Ambientales-CEIAM. Estudiante de Doctorado en Química. 2020-2024.

2. **Convocatoria Interna de Investigación Libre con Aporte en Efectivo – Vicerrectoria de Investigación y Extensión**, 2021, Código interno: 2815. Título: "Evaluación de Sistemas Orgánicos Donor-Aceptor como matrices MALDI libres de interferencias". Grupo de Investigación en Fisicoquímica Teórica y Experimental-GIFTEX. Coinvestigador no planta, inicio: 20/08/2021, fin: 20/04/2023.

3. **Convocatoria Pacto para la Generación de Nuevo Conocimiento a Través de Proyectos de Investigación, Programa Nacional de Ciencia, Tecnología e Innovación en Salud**, Título: "Extracto estandarizado de triterpenos nano-vehiculizados que modulan la hiperglucemia y resistencia a la insulina en biomodelos de pre-diabetes tipo 2 asociada con obesidad". Universidad Icesi, Profesional, 2024.

Appendix 8. Posters presented at international and national conferences.

72th Annual ASMS American Society for Mass Spectrometry Conference. June 02 to 06, 2024, Anaheim, California, EE.UU.

1. Unraveling Phytoplankton Communities in a Marine Ecosystem through MALDI-FT-ICR Profiling.

II International Congress on Technological Innovation and Circular Processes. October 04 to 06, 2023, EcoCampus UPB Montería, Colombia.

2. Análisis de fotoreactividad en sistemas orgánicos Donor-Aceptor como matrices UV-MALDI: Una perspectiva *in silico.*

71th Annual ASMS American Society for Mass Spectrometry Conference. June 04 to 08, 2023, Houston, Texas, EE.UU.

3. Pigment profiles in microalgae extracts by electron-transfer MALDI: the analyzer's influence.
4. Linking MALDI-FT-ICR phytoplankton pigment profiles with community taxonomy in a marine ecosystem.
5. Spatial Distribution of Pentacyclic Triterpenes in *Cecropia* app roots using MALDI Imaging MS.

XIX Congreso Colombiano de Química: "Alianza por un desarrollo sostenible", October 02 to 06, 2023, Bogotá, Colombia.

6. Exploring Strange New MALDI matrix Worlds: An AI System for Chemical Space Navigation.

Congreso Internacional de Semilleros de Investigación-Educación-Tecnología CISIET. October 04 to 06, 2023, Penafiel, Portugal.

7. Quantum secrets of phytoplankton pigments analysis by MALDI-MS.

70th Annual ASMS American Society for Mass Spectrometry Conference. June 05 to 09, 2022, Minneapolis, Minnesota, EE.UU.

8. Gas-phase charge exchange reactions using Donor-Acceptor systems.
9. Gas-phase behavior of *cis*-bixin under MALDI conditions.

III Encuentro Internacional de Ciencias de la Salud y I Congreso Internacional Vida, Salud y Bienestar. November 03 to 05, 2022, Bucaramanga, Colombia.

10. Monitoreo de biomarcadores como indicadores de crecimiento de *Chlorella vulgaris* utilizando MALDI MS.

LVII Congreso Nacional y VIII Internacional de Ciencias Biológicas. October 11 to 14, 2022, Sincelejo, Colombia.

11. Bioquímica cuántica para el análisis de biomarcadores fotosensibles vía MALDI-MS.

69th Annual ASMS American Society for Mass Spectrometry Conference. October 31 to November 04, 2021, Filadelfia, Pensilvania, EE.UU.

12. Relative quantification from pigment profiles of phytoplankton samples from the Caribbean Ocean using MALDI MS.
13. Monitoring the compositional dynamics of microalgae cultures with MALDI-TOF MS.

34° Congreso Latinoamericano de Química. October 11 to 15, 2021, Cartagena, Colombia.

14. Depth-dependent pigment profiles in phytoplankton samples from the Caribbean Ocean using MALDI MS.
15. Rational Design of novel Matrices for MALDI MS assays: an *in- silico* perspective.
16. Cocoa Pod Husk Epicarp: A source of natural pigments.
17. Caracterización del pigmento bixina aislado a partir de semillas de *Bixa orellana.*
18. Caracterización de pigmentos lipofílicos en *Chlorella vulgaris* utilizando espectrometría.

LatinXChem Conference, September 24, 2021, Colombia.

19. Rational Design of novel MALDI MS Matrices from Empirical and Theoretical Data.
20. Anomalías en el proceso de ionización de analitos en MALDI: Transferencia Electrónica vs. Transferencia Protónica vía Química Cuántica.
21. Caracterización de pigmentos lipofílicos en *Chlorella vulgaris* utilizado espectrometría de masas MALDI TOF.

LatinXChem Conference, September 07, 2020, Colombia.

22. Theoretical Calculation of the Ionization Potential of Molecules Derived from Fluorene as MALDI Electron Transfer Matrices.

23. Ionization Potential from Quantum Chemical Calculations of Photosensible Phytoplanktonic Pigments for MALDI Analysis.
24. Caracterización de las fracciones resultantes del proceso de purificación de xilo-oligosacáridos obtenidos a partir de raquis de palma de aceite Africana.
25. Flavonoids Profiling of Cacao Pod Husk Epicarp using MALDI-TOF Mass Spectrometry.
26. Characterization of Phytoplanktonic Pigments Using Electron Transfer MALDI MS.

III Congreso Internacional de Ciencias Básicas e Ingeniería – CICI, August 11 to 13, 2020, Villavicencio, Colombia.

27. Photon Harvesting Molecules: Ionization Potential from Quantum Chemical Calculations of Phytoplanktonic Pigments for MALDI Analysis.